Lithogeochemical vectors for hydrothermal processes in the Strange Lake peralkaline granitic REE-Zr-Nb deposit

Alexander P. Gysi*[1], Anthony E. Williams-Jones[2] and Patrick Collins[3]

[1]Department of Geology and Geological Engineering, Colorado School of Mines, 1516 Illinois Street, Golden, CO 80401

[2]Department of Earth and Planetary Sciences, McGill University, 3450 University Street, Montreal, Quebec, Canada, H3A 2A7

[3]Vulcan Minerals Incorporated, 333 Duckworth Street, St. John's, Newfoundland & Labrador, Canada, A1C 1G9

* Corresponding author: e-mail, agysi@mines.edu

Tel: +1 303 273 3828

Revised manuscript submitted to Economic Geology

Gysi, A.P., Williams-Jones, A.E., Collins, P., 2016b. Lithogeochemical Vectors for Hydrothermal Processes in the Strange Lake Peralkaline Granitic REE-Zr-Nb Deposit. Econ Geol 111, 1241-1276. DOI:10.2113/econgeo.111.5.1241.

ABSTRACT

Extreme enrichment and post-magmatic hydrothermal mobilization of the rare earth elements (REE), Zr and Nb have been reported for a number of anorogenic peralkaline intrusions, including the world-class REE-Zr-Nb deposit at Strange Lake, Quebec, Canada. Establishing lithogeochemical vectors for these types of deposits is a challenging task because the effects of hydrothermal processes on element distribution are poorly known and the relationships of alteration types to mineralization stages have not been well documented. Here, we present results of a detailed mineralogical and geochemical investigation involving a dataset of over 500 mineral and bulk rock analyses of a NE-SW section through the potential ore zone at Strange Lake. Based on these data, we develop a model that explains the role of hydrothermal processes in concentrating metals in peralkaline granitic systems, and identify lithogeochemical vectors for their exploration.

The B Zone, located along the northwestern margin of the Strange Lake pluton, contains a lens-shaped pegmatite-rich domain comprising sub-horizontal sheets of pegmatites hosted by granites with a total indicated resource of 278 Mt grading 0.93 wt.% total rare earth oxides (TREO), of which 39 % are heavy (H)REE. Within this resource, there is an enriched zone containing 20 Mt of ore grading 1.44 wt.% TREO, of which 50 % are HREE. The pegmatites are characterized by a core enriched in quartz, fluorite and light (L)REE fluorocarbonates, and a granitic border enriched in zirconosilicates and granitic minerals. The pegmatite sheets and surrounding granites evolved in three essential stages: I) a magmatic stage, II) a near neutral hydrothermal stage involving their interaction with NaCl-bearing orthomagmatic fluids, and III) an acidic hydrothermal stage (comprising high (IIIa) and low (IIIb) temperature substages) that resulted from their interaction with pegmatite-sourced HCl-HF-bearing fluids. Stage IIIa led to pseudomorphic mineral replacement reactions (e.g., Na-Ca exchange during replacement of zirconosilicates) and formation of an aegirinization/hematization halo around the pegmatites. In contrast, Stage IIIb, which was responsible for the hydrothermal mobilization of Zr and REE, is manifested by fluorite and quartz veins, zircon spherules, gadolinite-group minerals, gittinsite and ferriallanite-(Ce) and a pervasive replacement of the granite by these minerals. The distribution of REE, Zr, Nb and Ti was controlled by the competition between hydrothermal fluids and the stability of

Gysi, A.P., Williams-Jones, A.E., Collins, P., 2016b. Lithogeochemical Vectors for Hydrothermal Processes in the Strange Lake Peralkaline Granitic REE-Zr-Nb Deposit. Econ Geol 111, 1241-1276.
DOI:10.2113/econgeo.111.5.1241.

primary REE-F-(CO_2) minerals [e.g., bastnäsite-(Ce) host to LREE], zirconosilicates (i.e., Na-zirconosilicates and zircon host to HREE and Zr), Nb-Ti-minerals (i.e., pyrochlore host to Nb, and narsarsukite host to Ti) and the stability of secondary LREE-silicates [i.e., ferriallanite-(Ce)], HREE-silicates [i.e., gadolinite-(Y)], zirconosilicates (i.e., gittinsite and zircon) and Nb-Ti-minerals (i.e., titanite and pyrochlore).

Lithogeochemical vectors were identified to distinguish between the high temperature acidic alteration (IIIa) using CaO/Na_2O (indicator of Ca-metasomatism) and Fe_2O_3/Na_2O ratios (indicator of aegirinization/hematization), and the low temperature acidic alteration (IIIb) using the CaO/Al_2O_3 ratio (indicator of Ca-F-metasomatism). Bulk rock compositional data show that alteration was accompanied by an enrichment of HREO and ZrO_2 at the deposit scale, whereas the LREO were not selectively enriched. A 2-D geochemical model of the deposit indicates that the LREO are more dispersed, whereas HREO and ZrO_2 are selectively distributed. These variations in LREE/HREE are also reflected in the mineral chemistry, especially in hydrothermal zircon crystals showing an unusual LREE enrichment and HREE depletion, contrasting with pseudomorphs, which are enriched in HREE. Hydrothermal ferriallanite-(Ce) and gadolinite-group minerals also show a clear trend of REE depletion with Ca enrichment. Controlling factors for the hydrothermal mobilization of LREE, HREE and Zr were temperature, pH and the availability of fluoride ions (F^-) in the fluid for the dissolution of zircon, and chloride ions (Cl^-) for the complexation of the REE. The study of rare hydrothermal minerals in conjunction with field observations and the evaluation of variations in bulk rock composition, allowed us to develop a new model for the hydrothermal evolution stage of Strange Lake.

Introduction

Recent advances in high technology industries have created a large increase in demand for the "critical" metals and a need to develop robust models of ore genesis to facilitate their successful exploration. Peralkaline and alkaline igneous complexes are highly enriched in some of these metals, including the REE (in particular the HREE) and other high-field strength elements (HFSE), notably Zr, Ti and Nb. The high alkali and fluorine content of the corresponding melts leads to depolymerization, a decrease in the solidus temperature and a lowering of the viscosity of these melts, all of which combine to facilitate incorporation of the above metals in these magmas (Manning, 1981; Linnen and Keppler, 2002; Thomas et al., 2012; Bartels et al., 2013). Minerals that host the REE and other HFSE in these deposits include fluorocarbonates [e.g., bastnäsite-(Ce) and parisite-(Ce)], phosphates [e.g., xenotime-(Y) and monazite-(Ce)], silicates [e.g., allanite-(Ce) and gadolinite-group minerals] and zirconosilicates (e.g., zircon, eudyalite, gittinsite). Some intrusive complexes are sufficiently enriched in these elements to host potential mineral resources for exploitation, such as the peralkaline granitic pluton at Strange Lake (Salvi and Williams-Jones, 2006; Gysi and Williams-Jones, 2013) and the nepheline-aegirine syenite at Nechalacho both in Canada. Even though these igneous complexes are of magmatic origin, subsolidus re-equilibration and alteration make it difficult to separate igneous processes of critical metal enrichment from those involving hydrothermal fluids.

At Strange Lake, critical metal enrichment was initially attributed to igneous fractionation (Miller, 1986, 1990; Boily and Williams-Jones, 1994). However, Salvi and Williams-Jones (1990, 1996, 2006) subsequently provided evidence for significant mobilization of the metals by hydrothermal fluids. These studies identified a high

Gysi, A.P., Williams-Jones, A.E., Collins, P., 2016b. Lithogeochemical Vectors for Hydrothermal Processes in the Strange Lake Peralkaline Granitic REE-Zr-Nb Deposit. Econ Geol 111, 1241-1276.
DOI:10.2113/econgeo.111.5.1241.

temperature saline orthomagmatic fluid (~20-25 wt.% NaCl equivalent; homogenization temperatures Th of 300 to 360 °C) accompanied by an immiscible hydrocarbon-bearing fluid, and a low temperature Ca-bearing fluid (~10-25 wt.% NaCl equivalent; Th of 90 to 225 °C). Recently, Gysi and Williams-Jones (2013), have built on this work by using mineralogical observations and thermodynamic calculations to develop a quantitative model, in which fluid exsolution from the magma and acidic alteration, led to hydrothermal mobilization of the REE and other HFSE within and beyond the host pegmatites. Most recently, Vasyukova and Williams-Jones (2014, and 2016) have shown that separation of an immiscible fluoride melt from the silicate magma, and preferential concentration of the REE in the fluoride melt also may have played an important, previously unrecognized, role in the magmatic concentration of the REE. It is therefore becoming increasingly clear that the extraordinary concentration of critical metals at Strange Lake was due to a complex interplay of igneous and hydrothermal processes.

In this study, we focus on the hydrothermal stage of the evolution of the peralkaline granites and pegmatites and the associated metal mobilization. Our purpose was to determine: (1) the mineral assemblages related to the different alteration stages; (2) how the changes in bulk rock and mineral chemistry are related to the chemistry of the hydrothermal fluids, and (3) the scale and mechanism of REE, Zr and Nb mobilization and concentration. Using this information, we developed lithogeochemical vectors, which we believe will aid in the exploration for similar granite-hosted REE/HFSE ore deposits in anorogenic settings.

Geological setting and lithology

Gysi, A.P., Williams-Jones, A.E., Collins, P., 2016b. Lithogeochemical Vectors for Hydrothermal Processes in the Strange Lake Peralkaline Granitic REE-Zr-Nb Deposit. Econ Geol 111, 1241-1276.
DOI:10.2113/econgeo.111.5.1241.

The Strange Lake pluton

Strange Lake is ~6 kilometer wide mid-Proterozoic (1240 Ma; Pillet et al., 1989; Miller et al., 1997) peralkaline granitic pluton located in northeastern Canada along the border between Quebec and Labrador. The pluton consists of anorogenic (A-type) granites surrounded by a fluorite/hematite breccia, and is hosted in Aphebian gneiss and Elsonian monzonite (Fig. 1A). The presence of roof pendants of gneiss and monzonite in the Strange Lake granite and low trapping pressures estimated from orthomagmatic fluid inclusions (Salvi and Williams-Jones, 1992) indicate a shallow level of emplacement. Two different granite types have been recognized based on their feldspar mineralogy (Nassif, 1993). In the central and southern part of the pluton, the rocks consist of hypersolvus granite (perthitic K-feldspar). These rocks are surrounded by a later subsolvus granite (two feldspars, albite and microcline), which is host to two pegmatite-rich ore zones. This reverse zoning of the granites has been ascribed to feldspar fractionation and fluid saturation during crystallization (Nassif, 1993). However, a similar reverse zoning could result from a later batch of melt forcing its way to the margins during multiphase intrusion cycles (Vigneresse, 2007). The latter hypothesis is supported by field observations, which indicate that the first batch of melt was less hydrous as evidenced by the occurrence of late interstitial amphibole, and the second batch of melt was saturated with H_2O at an early stage of crystallization, with amphibole occurring as early phenocrysts (Siegel and Williams-Jones, 2015). This indicates that successive intrusions of variably evolved melts likely affected H_2O saturation, alkali content and HFSE enrichment (i.e., REE, Zr, Nb and Ti).

Gysi, A.P., Williams-Jones, A.E., Collins, P., 2016b. Lithogeochemical Vectors for Hydrothermal Processes in the Strange Lake Peralkaline Granitic REE-Zr-Nb Deposit. Econ Geol 111, 1241-1276.
DOI:10.2113/econgeo.111.5.1241.

Potential ore zones

Two potential ore zones have been recognized, the Main Zone located in the central part of the pluton and the B Zone located in the northwest (Fig. 1A). The B Zone, which is the target of current exploration, consists of a lens-shaped pegmatite spine hosted by subsolvus granite, and covers an area of ~400,000 m^2 (Fig. 1B). The pegmatites consist of a series of flat-lying sheets dipping gently to the northeast (Fig. 1C). The total indicated mineral resource is 278 Mt ore grading 0.93 wt.% total rare earth oxide (TREO), 1.92 wt.% ZrO_2 and 0.18 wt.% Nb_2O_5 (www.questrareminerals.com). The highest grades are within the pegmatite spine where there is an indicated resource of 20 Mt ore grading 1.44 wt.% TREO, 2.59 wt.% ZrO_2 and 0.34 wt.% Nb_2O_5. This zone also has the highest proportion of heavy (H)REO (50%, versus 39% for the entire deposit). A list of REE-, Nb- and Zr-bearing ore minerals and their occurrences is given in Table 1.

This study is based on a detailed sampling of four drill cores (Fig. 1B: BZ11176; BZ10027; BZ10078; BZ11109) across a NE-SW section of the pegmatite spine. Four additional samples containing hydrothermal veins were also considered (see the Supplementary Online Material Tables for a list of samples). The detailed geological map (Fig. 1B) and element distribution of the deposit (Fig. 2) are based on data made available by Quest Rare Minerals Ltd for over 23,000 drill core samples. As exemplified in Figure 2, the spatial distribution of LREO, HREO and ZrO_2 concentrations is related primarily to the distribution of the pegmatites, which contain the highest concentrations of these elements; concentrations are significant in the surrounding subsolvus granite but generally lower. Five domains displaying variable relative metal concentrations can be recognized (Fig. 2). Zone 1 (pegmatite spine) is highly enriched in LREO, HREO and

ZrO_2, whereas zones 2 to 5 (granite) have highly variable relative LREO, HREO and ZrO_2 concentrations. The overall enrichment of the REE and Zr in the granite (Zones 2 to 4) below the pegmatite sheets, and the presence of irregular patches in the granite that are enriched/depleted in metals to depths of >150 m below them, suggests a post-magmatic hydrothermal metal mobilization on a scale of hundreds of meters.

Petrography

The granite in the B Zone is pervasively altered to a depth of >150 m (Fig. 3). However, the primary magmatic textures are relatively well preserved. Thus, it is possible to observe amphibole cumulate layers up to 20 cm thick and ellipsoidal inclusions of fine-grained granite with a diameter of ~5-10 cm. The least altered granite is porphyritic with euhedral to subhedral arfvedsonite phenocrysts (~0.5-0.8 cm) or nearly equigranular with smaller (<0.4 cm) arfvedsonite crystals. The matrix consists of fine-grained (<0.2 cm) anhedral albite, K-feldspar and quartz (Fig. 3A). Zirconosilicate minerals can be observed in hand samples with an estimated modal proportion ranging between 5 and 10 vol.% of the rock. They commonly occur as rectangular pale yellow subhedral phenocrysts (0.5-1 cm) of vlasovite ($Na_2ZrSi_4O_{11}$) with poikilitic inclusions of feldspar and arfvedsonite. White to pinkish gagarinite-(Y) [$NaCa(Y,Ce)F_6$] crystals occur interstitially and in patches with a modal proportion of <5 vol.%. Fine-grained (50-100 µm) euhedral pyrochlore [$(Na,Ca)_2Nb_2O_6(OH,F)$], <1 vol. %, is only distinguishable in thin section. Titanium-bearing minerals comprise dark brown rectangular primary narsarsukite [$Na_2(Ti,Fe^{3+})Si_4O_{10}(O,F)$] phenocrysts (1-2 cm) and, more rarely, patches of radially grown dark brown-orange astrophyllite crystals; these minerals comprise <5 vol.% of the

Gysi, A.P., Williams-Jones, A.E., Collins, P., 2016b. Lithogeochemical Vectors for Hydrothermal Processes in the Strange Lake Peralkaline Granitic REE-Zr-Nb Deposit. Econ Geol 111, 1241-1276.
DOI:10.2113/econgeo.111.5.1241.

rock.

The pegmatites form sheets that range from a few centimeters up to 10 meters in thickness that are mineralogically zoned into border and core zones (Fig. 4), hereafter referred to as border and core pegmatite, respectively (Gysi and Williams-Jones, 2013). Most of the pegmatite sheets are highly altered and primary features are rarely preserved. The least altered border pegmatites, however, are similar in mineralogy to the granite, whereas the core pegmatite consists of quartz, variable proportions of zircon and fluorite and REE-F-(CO_2) minerals. Thin pegmatite dikes (~3 to 5 cm thick) are unzoned and have a mineralogy similar to the border pegmatite, albeit with a higher modal proportion of quartz. The border pegmatites contain large (>1 to 5 cm) to medium (~1 cm) size subhedral K-feldspar crystals (between ~40 and 60 vol. %). Quartz forms subhedral to interstitial crystals (>40 vol. %). Rarely preserved euhedral arfvedsonite crystals (2 to >3 cm in length) make up <10 vol.% of the rock. Large boat-shaped pseudomorphs (up to 3 cm in diameter), consisting of zircon/quartz or gittinsite/quartz (10-40 vol.%), occur among the K-feldspar and quartz crystals. Previous studies of the Main Zone pegmatites have determined that the pseudomorphs represent former elpidite ($Na_2ZrSi_6O_{15} \cdot 3H_2O$) crystals (Salvi and Williams-Jones, 1995). Only pseudomorphs, (i.e., no relicts of primary zirconosilicates), however, have been found in the B Zone. Pseudomorphs after narsarsukite (now consisting of titanite and quartz; Salvi and Williams-Jones, 1995), of 1 to >3 cm in diameter, locally form cumulate-like textures (Fig. 4B). In addition to the main rock-forming minerals, referred to above, there are large numbers of fine-grained REE and HFSE minerals (Table 1), many of which are of hydrothermal origin, including members of the gadolinite-group, which are accompanied by fluorite and quartz (Fig.

4E). Finer grained aplites form layers varying between ~20 and 30 cm in thickness around some of the borders of the pegmatite sheets.

Analytical and sampling methods

Bulk rock samples were collected from drill cores following geological core logging. Mineralized samples and pegmatites were marked out with a nominal length of 0.5 to 1.0 m, while the remaining core was usually sampled at 2 m interval lengths; each drill hole was sampled from top to bottom. Sample intervals typically do not cross alteration boundaries or lithological contacts where either of these features is sharp; where gradational contacts occur, samples were divided so as to minimize the mixing of lithological or alteration types. Bulk rock samples were analyzed by Actlabs Ltd. using several techniques described in their Code-8 REE Assay + F, the Code-4 Litho-Quant (11+) Major elements fusion and the Code-4E XRF for Nb protocols. The REE were analyzed in fused lithium meta- and tetraborate pellets dissolved in dilute nitric acid followed by inductively coupled plasma mass spectrometry (ICP-MS). Fluorine concentrations were determined using a fluoride ion sensitive electrode and other major elements were analyzed in digested samples using ICP optical emission spectrometry (OES). Niobium was analyzed separately by X-ray fluorescence (XRF) in pressed powder pellets.

Mineral compositions were determined in 30 µm-thick carbon-coated thin sections using a JEOL JXA-8900L electron microprobe (EMP). The beam current was 30 nA and the acceleration voltage was 20 kV. The beam diameter was 1-5 µm for zircon and 10 µm for ferriallanite-(Ce), gadolinite-group minerals, vlasovite, gittinsite,

Gysi, A.P., Williams-Jones, A.E., Collins, P., 2016b. Lithogeochemical Vectors for Hydrothermal Processes in the Strange Lake Peralkaline Granitic REE-Zr-Nb Deposit. Econ Geol 111, 1241-1276.
DOI:10.2113/econgeo.111.5.1241.

pyrochlore and titanite. Counting times and standards employed in the analyses are given in Appendix Table A1, together with detection limits based on repeated analyses of standards. Backscattered electron photomicrographs (BSE) were taken using a 1 µm beam diameter and 20 nA acceleration voltage. Element X-ray maps were produced using wavelength dispersive spectrometers (WDS) with a beam current of 50 nA, an acceleration voltage of 20 kV and a dwell time of 60 ms. A list of all samples, and a compilation of bulk rock and mineral chemical data can be found in the Supplementary Online Material Tables.

Metasomatic Processes

The evolution of the Strange Lake B-Zone granites and pegmatites can be subdivided into three different stages related to different rock textures and mineral assemblages. These are: I) a magmatic stage, II) a near neutral hydrothermal stage (alkali metasomatism) and III) an acidic hydrothermal stage.

Alkali metasomatism

The alkali metasomatism comprises: i) Na-metasomatism with albitization of the granite in which primary K-feldspar was replaced by albite (Fig. 5A) and ii) K-metasomatism (potassic alteration) of the pegmatites in which albite lamellae were replaced by microcline (Fig. 5B). The albitization is interpreted to have been earlier than the potassic alteration because it occurred pervasively in the granite, even in the less altered subsolvus granite of the central part of the pluton, whereas the potassic alteration was restricted to the borders of the pegmatite sheets. The alteration of the K-feldspar can be described by

Gysi, A.P., Williams-Jones, A.E., Collins, P., 2016b. Lithogeochemical Vectors for Hydrothermal Processes in the Strange Lake Peralkaline Granitic REE-Zr-Nb Deposit. Econ Geol 111, 1241-1276.
DOI:10.2113/econgeo.111.5.1241.

the reaction:

$$(Kfs)\ KAlSi_3O_8 + Na^+ = (Ab)\ NaAlSi_3O_8 + K^+ \qquad (1)$$

As is evident from the distribution of K and Na in the large crystal illustrated in Figures 5C and D, the replacement of albite by K-feldspar in the pegmatites proceeded with the development of large heterogeneous microcline crystals having highly variable domains with respect to their K/Na ratios.

A possible explanation for the sodic metasomatism of the granite and the potassic metasomatism of the pegmatites is that the former occurred at higher temperature. This would be consistent with the observation that the equilibrium constant for Reaction 1 is given by the activity ratio of the cations (aK^+/aNa^+), and increases with increasing temperature. Thus, for a given K^+/Na^+ ratio in the fluid, the right hand side of Reaction (1) or formation of albite would be favored by higher temperature and the left hand side of this reaction or formation of K-feldspar by lower temperature. This does not rule out the possibility that the K/Na ratio of the fluid evolved to higher values in the pegmatites, thereby promoting potassic alteration of the latter.

Acidic alteration

The acidic alteration was part of the evolution of the pegmatites, as shown previously by Gysi and Williams-Jones (2013), and involved pegmatite-sourced low pH fluids that produced complex alteration assemblages, which varied with temperature and the extent to which the rock buffered pH. These fluids were responsible for the hydrothermal mobilization of REE/HFSE in the late stage development of the pegmatite spine and infiltrated the surrounding granites. The acidic alteration is characterized by the following

Gysi, A.P., Williams-Jones, A.E., Collins, P., 2016b. Lithogeochemical Vectors for Hydrothermal Processes in the Strange Lake Peralkaline Granitic REE-Zr-Nb Deposit. Econ Geol 111, 1241-1276.
DOI:10.2113/econgeo.111.5.1241.

alteration textures/types: i) the pseudomorphic replacement of Na- by Ca-zirconosilicates (Ca-metasomatism), ii) aegirinization/hematization, iii) the formation of late stage quartz and fluorite veins (Ca-F-metasomatism), iv) phyllic alteration and v) brecciation. These alteration textures/types have been subdivided according to whether they occurred at high temperature (e.g., pseudomorphic replacement reactions), and low temperature (e.g., quartz/fluorite vein formation).

Aegirinization/hematization is manifested by the variable replacement of arfvedsonite by aegirine and/or hematite in both the granite and the pegmatites (Figs. 3 and 4). The original igneous porphyritic textures are preserved in this alteration type, which is manifested by a distinctive alteration halo around the pegmatite spine. The reaction of arfvedsonite to aegirine leads to the release of Si, Na and Fe as follows:

$$\text{(Arf) } Na_3Fe^{2+}{}_4Fe^{3+}Si_8O_{22}(OH)_2 + 10H^+ + 6H_2O = \text{(Aeg) } NaFe^{3+}Si_2O_6 + 6H_4SiO_4^0 + 2Na^+ + 4Fe^{2+} \quad (2)$$

which leads to the formation of hydrothermal quartz and hematite (if oxidized) or magnetite. Three modes of occurrences of aegirinization/hematization have been distinguished in the granite, namely hematite replacement of arfvedsonite in crystal cores (Fig. 3B), pervasive replacement of arfvedsonite by aegirine (Fig. 3C) and replacement of arfvedsonite rims by aegirine ± hematite. Aegirinization is particularly intense around the pegmatite spine, suggesting that the pegmatites were the cause of alteration, and that acidic alteration and aegirinization/hematization are closely related. Hematization is more widespread than aegirinization, and also occurs pervasively in the granite (after aegirine and arfvedsonite) and as hematite veins.

Calcium-metasomatism is interpreted to have occurred pervasively along the

Gysi, A.P., Williams-Jones, A.E., Collins, P., 2016b. Lithogeochemical Vectors for Hydrothermal Processes in the Strange Lake Peralkaline Granitic REE-Zr-Nb Deposit. Econ Geol 111, 1241-1276.
DOI:10.2113/econgeo.111.5.1241.

borders of the pegmatites and patchily in the granite, and is manifested by Ca-zirconosilicate (gittinsite and armstrongite) pseudomorphs, which formed after Na-zirconosilicates (i.e., vlasovite and elpidite) according to the reaction:

$$\text{(Elp) } Na_2ZrSi_6O_{15}\bullet 3H_2O + Ca^{2+} + 5H_2O = \text{(Git) } CaZrSi_2O_7 + 4H_4SiO_4^0 + 2Na^+ \qquad (3)$$

and Na-Ti-bearing minerals (narsarsukite) by titanite and quartz according to the reaction:

$$\text{(Nar) } Na_2(Ti_xFe^{3+}_{1-x})Si_4O_{10}(OH,F) + xCa^{2+} = \text{(Ttn) } xCaTiSiO_5 + \text{(Qtz) } (4-x)SiO_2 + 2Na^+ + 1\text{-}xFe^{3+} \qquad (4)$$

Reactions (3) and (4) indicate that quartz may form, depending on temperature and the activity of Na^+.

Calcium-F-metasomatism is manifested by the assemblage ferriallanite-(Ce) ±gittinsite ±zircon ±fluorite ±quartz (Fig. 3D), and macroscopically in the granite by the white-purple color of the rock matrix. The presence of quartz/fluorite veins (Fig. 6), which crosscut aegirinized arfvedsonite and pseudomorphs (see further below), indicates that Ca-F-metasomatism postdated aegirinization/hematization and Ca-metasomatism. Moreover, whereas the latter two alteration types involved pervasive replacement and were restricted to the pegmatite spine, Ca-F-metasomatism extended well into the surrounding granite and involved the formation of veins and the filling of vugs by REE-Zr mineralization. Most of the veins are subvertical, ~0.5 to 2.5 cm thick, and can be subdivided into quartz-, quartz-fluorite-, fluorite- and hematite-types. They are

Gysi, A.P., Williams-Jones, A.E., Collins, P., 2016b. Lithogeochemical Vectors for Hydrothermal Processes in the Strange Lake Peralkaline Granitic REE-Zr-Nb Deposit. Econ Geol 111, 1241-1276.
DOI:10.2113/econgeo.111.5.1241.

interpreted to represent one of the latest hydrothermal event that affected the B Zone. Colloform fluorite layers in quartz-fluorite veins indicate a progressive growth of the mineral from a low temperature hydrothermal fluid (Fig. 6C). The quartz-fluorite- and quartz-veins are either barren or mineralized, with the latter containing ferriallanite-(Ce) ± titanite ± gadolinite-group minerals ± chlorite. A sample from a drill core to the NE of the B Zone (Figs. 1, 6D) contains a contact between pegmatite/granite that is both micro-brecciated and filled with fluorite. The formation of quartz/fluorite/hematite veins was accompanied by the late formation of breccias and micro-breccias (Figs. 6D and E).

Acidic hydrothermal activity also gave rise to phyllic alteration textures with the late stage replacement of primary silicate minerals (i.e., K-feldspar and arfvedsonite) by K-, Fe- and Al- phyllosilicates. Phyllic alteration is generally restricted to the border pegmatite where it is extensive, but also is observed locally in the adjacent granite, commonly as phyllosilicate-filled micro-fractures in K-feldspar and arfvedsonite. The phyllosilicates comprise Al varieties (compositions ranging between donbassite and dickite-halloysite-kaolinite, and pyrophyllite), Fe-rich varieties (chamosite and ferrosudoite) and K-bearing varieties (muscovite and ferroceladonite) (Gysi and Williams-Jones, 2013). Excess cations for some analyzed crystals may indicate the presence of Li as polylithionite (Gysi and Williams-Jones, 2013).

Mineral paragenesis

The mineral paragenesis in the B Zone was reconstructed from textural relationships involving the different minerals, using a combination of optical microscopy, scanning electron microscopy and element maps prepared using the EMP. These are illustrated in

Gysi, A.P., Williams-Jones, A.E., Collins, P., 2016b. Lithogeochemical Vectors for Hydrothermal Processes in the Strange Lake Peralkaline Granitic REE-Zr-Nb Deposit. Econ Geol 111, 1241-1276.
DOI:10.2113/econgeo.111.5.1241.

Figures 7–11. Minerals were interpreted as magmatic based on textural relationships, for example if they occur as phenocrysts (e.g., arfvedsonite) or as isolated relict crystals displaying dissolution/corrosion textures [e.g., bastnäsite-(Ce) and pyrochlore]. The latter was especially the case for minerals in the pegmatites where it is more difficult to distinguish between magmatic and hydrothermal minerals. Hydrothermal minerals were recognized on the basis of replacement and dissolution textures and their presence in veins and breccia cement.

Magmatic REE/HFSE minerals

The REE/HFSE minerals interpreted as magmatic are the Na-zirconosilicates, pyrochlore, the REE-F-CO_2-minerals [gagarinite-(Y), bastnäsite-(Ce) and fluocerite-(Ce)] and the Na-Ti-bearing minerals (Fig. 8). The dominant Na-zirconosilicate in the granite is vlasovite (Figs. 7A and 8A), which forms interstitial intergrowths with feldspar and quartz, and contains inclusions of euhedral albite and fragmented albitized K-feldspar and arfvedsonite. Vlasovite also displays evidence of post-magmatic exsolution of zircon+quartz and a patchy Ca-F metasomatic overprint by gittinsite and quartz or fluorite and zircon. The dominant zirconosilicate (elpidite) in the pegmatites is boat-shaped and is represented by pseudomorphs of either zircon and quartz or gittinsite and quartz (Fig. 8D). Gagarinite-(Y) formed interstitially to the primary silicate minerals, and is the dominant REE-F-mineral in the granite. In the cores of the pegmatites, bastnäsite-(Ce) and fluocerite-(Ce) relicts were replaced by hydrothermal fluorite and/or quartz. The occurrence of REE-F-CO_2-minerals that have been replaced in both the granites and pegmatites has therefore been interpreted to indicate a magmatic or late magmatic-

Gysi, A.P., Williams-Jones, A.E., Collins, P., 2016b. Lithogeochemical Vectors for Hydrothermal Processes in the Strange Lake Peralkaline Granitic REE-Zr-Nb Deposit. Econ Geol 111, 1241-1276.
DOI:10.2113/econgeo.111.5.1241.

hydrothermal origin for these minerals (Gysi and Williams-Jones, 2013). The main magmatic Ti- and Nb-bearing minerals are narsarsukite and pyrochlore, respectively. The latter is also host to significant concentrations of LREE. Pyrochlore forms euhedral crystals on the surface of K-feldspar or arfvedsonite, and occurs as aggregates in quartz. The crystals must have been relatively resistant to corrosion during alteration as pyrochlore relicts are found throughout the B Zone. Some of the pyrochlore may also be of hydrothermal origin as its crystals occur as clusters in hydrothermal quartz. Narsarsukite was identified by Birkett et al. (1996) in several localities in the pluton, but only occurs as rectangular prismatic pseudomorphs replaced by titanite and quartz (Figs. 4B and 8F) in the B Zone. Other REE minerals that occur in pseudomorphs are cerite-(Ce) [$Ce_9Fe(SiO_4)_6(SiO_3)(OH)_4$] in the granite and kainosite-(Y) [$Ca_2Y_2(SiO_3)_4(CO_3)\cdot H_2O$] in the pegmatite. Relicts of these minerals, however, are rare in the B Zone.

Hydrothermal REE/HFSE minerals

Secondary zirconosilicates and REE-bearing silicates occur as early alteration and late stage vein assemblages in both the granite and the pegmatite sheets (Figs. 7 and 9). Based on the common occurrence of hydrothermal minerals in the B Zone, we estimate that >90% of primary REE- and Zr-minerals were replaced by hydrothermal equivalents.

The secondary LREE-bearing silicate is ferriallanite-(Ce), which occurs as elongated crystal intergrowths that formed by replacement of albite and arfvedsonite during chemical dissolution-precipitation reactions, or filled micro-fractures and pores in the rock matrix. The micro-fractures occur in K-feldspar and arfvedsonite/aegirine, with

Gysi, A.P., Williams-Jones, A.E., Collins, P., 2016b. Lithogeochemical Vectors for Hydrothermal Processes in the Strange Lake Peralkaline Granitic REE-Zr-Nb Deposit. Econ Geol 111, 1241-1276.
DOI:10.2113/econgeo.111.5.1241.

ferriallanite-(Ce) being accompanied by fluorite and quartz. These microtextures preserve evidence of dissolution of primary minerals but do not involve secondary phyllosilicates. The ferriallanite-(Ce) crystals are chemically zoned, as illustrated by backscattered electron images and element maps; La and Ce are concentrated in micro-domains, whereas the Nd distribution is more homogeneous (Fig. 10A). On a micron scale, Y is enriched in small domains. Ferriallanite-(Ce) also occurs in late stage quartz veins, as intergrowths with quartz and fluorite. (Fig. 9D and F)

The HREE-bearing silicates are dominantly gadolinite-group minerals that form concentrically zoned spherules. In the granite, these minerals occur interstitially as a replacement of feldspars and arfvedsonite, as pore fillings and as crystal aggregates in secondary quartz and quartz veins. By contrast, in the pegmatite sheets, they form dispersed crystal aggregates in late veins or are concentrated in strongly altered HREE layers (Fig. 4E). In the latter, the gadolinite-group minerals display a colloform growth texture that is characteristic of low temperature hydrothermal minerals (Fig. 10B). Significantly, the cores of the colloform domains are enriched in Gd and Dy, whereas the rims are enriched in the heavier Yb and Y, indicating that LREE and HREE partitioned differently between the hydrothermal fluid and the precipitating minerals.

The hydrothermal zirconosilicates are either zircon, gittinsite, or in few cases armstrongite. Several types of zircon crystals were observed in the pegmatites and granites. Gysi and Williams-Jones (2013) recognized two generations of euhedral zircon crystals in the pegmatites. Zircon I occurs as a pseudomorphic replacement of elpidite and zircon II occurs as hydrothermal crystal clusters intergrown with quartz and/or fluorite. Zircon II displays strong chemical zoning. In the granite, a third zircon type was

Gysi, A.P., Williams-Jones, A.E., Collins, P., 2016b. Lithogeochemical Vectors for Hydrothermal Processes in the Strange Lake Peralkaline Granitic REE-Zr-Nb Deposit. Econ Geol 111, 1241-1276.
DOI:10.2113/econgeo.111.5.1241.

recognized. Zircon III forms spherules of radial aggregates intergrown with fluorite and minor proportions of quartz. This type of zircon accompanied Ca-F-metasomatism, filled pores and replaced primary silicate minerals in the granite. In a few samples, anhedral zircons seemingly replaced vlasovite in the granite, and are interpreted to have formed by a process similar to that of zircon I, which occurs in pseudomorphs in the pegmatites. This interpretation is also consistent with the observed mineral chemistry (see below). Early gittinsite and quartz occur as pseudomorphs after elpidite in the pegmatites, whereas interstitial elongated feathery gittinsite crystals formed in pores with quartz or replaced primary silicate minerals (in both the granite and pegmatites). Zircon also has been observed in veinlet networks within a fluorite vein in a pegmatite sheet (Fig. 11). Element maps show that one of the zircon veinlets cuts an assemblage of aegirine + quartz in a pseudomorph after arfvedsonite, indicating that Zr was mobilized after aegirinization (Fig. 11).

Hydrothermal titanite forms small euhedral crystals intergrown with quartz, gadolinite-group minerals and/or ferriallanite-(Ce) in the granite and pegmatite sheets (it also occurs as pseudomorphs after narsarsukite as discussed above). This type of titanite filled pores and replaced primary silicate minerals. Late titanite occurs as euhedral crystals in quartz veins together with either gadolinite-(Y) and/or ferriallanite-(Ce) (Fig. 9E).

Interpretation of alteration events

A mineral paragenesis tied to the different alteration types and textural changes is presented in Figure 12. The magmatic crystallization of subsolvus granite and pegmatite

Gysi, A.P., Williams-Jones, A.E., Collins, P., 2016b. Lithogeochemical Vectors for Hydrothermal Processes in the Strange Lake Peralkaline Granitic REE-Zr-Nb Deposit. Econ Geol 111, 1241-1276. DOI:10.2113/econgeo.111.5.1241.

sheets (stage I) led to the concentration of the REE in REE-F-(CO_2)-minerals (Figs. 8B and E), Zr in Na-zirconosilicates (Figs. 7A, 8A and D), Ti in Na-Ti-bearing minerals (Fig. 8F) and Nb in pyrochlore (it also contains significant amounts of LREE). Initially, alteration was dominated by alkali metasomatism (stage II) with the replacement of K-feldspar by albite in the granite (Fig. 5A) and the replacement of albite by K-feldspar in the border pegmatite (Fig. 5B).

Once the pegmatite border developed further, exsolution of fluids from the pegmatites led to acidic alteration (stage III), which was important for element mobilization and the formation of hydrothermal REE- and Zr- bearing minerals. As discussed earlier, the acidic alteration comprised a high temperature substage (IIIa) dominated by Ca-metasomatism and a low temperature substage (IIIb) dominated by Ca-F-metasomatism (IIIb).

Stage IIIa was characterized by the pseudomorphic replacement of magmatic minerals (i.e., Ca-metasomatism of zirconosilicates and titanosilicates and the aegirinization/hematization of arfvedsonite) and crystallization of Ca-bearing REE minerals such as ferriallanite-(Ce) and gadolinite-group minerals. Restriction of aegirinization/hematization to a halo around the pegmatite spine is interpreted to indicate that the acidic fluids responsible for Ca-pseudomorphic replacement of primary zircon- and titano-silicates were neutralized on coming in contact with the granite.

Stage IIIb involved the formation of quartz/fluorite veins in the granite, followed by phyllic alteration in the border pegmatites and finally brecciation. Mobilization of the REE and other HFSE (Zr, Nb and Ti) during this stage is evident in the pegmatite sheets and granite where dissolution/precipitation and open-space filling textures are common

Gysi, A.P., Williams-Jones, A.E., Collins, P., 2016b. Lithogeochemical Vectors for Hydrothermal Processes in the Strange Lake Peralkaline Granitic REE-Zr-Nb Deposit. Econ Geol 111, 1241-1276. DOI:10.2113/econgeo.111.5.1241.

(Figs. 7B-D, 9A-C, 10A-B and 11). The presence of abundant fluorite accompanying zircon in veins cutting aegirine+quartz in a pseudomorph after arfvedsonite (Fig. 11) is strong evidence that Ca-F-metasomatism (substage IIIb) overprinted aegirinization/hematization (substage IIIa). Late stage hydrothermal quartz and fluorite veins containing Ca-bearing REE, Zr and Ti minerals, further indicate that Ca-F-metasomatism continued until the termination of hydrothermal activity. The alteration of amphibole and aegirine led to a continuous Fe supply for hematization until late stage brecciation. The source of F that led to Ca-F-metasomatism was undoubtedly the pegmatitic magma, whereas the source of Ca in the system is more difficult to explain as peralkaline magmas are relatively depleted in Ca (see discussion section).

Bulk rock and mineral chemistry

Bulk rock compositions

A comparison of the bulk rock compositions of the four drill cores along the NE-SW profile of the B Zone shows that the highest concentrations of REE (LREO and HREO), Zr and Nb occur in domains dominated by pegmatites (Fig. 13). The background concentrations are close to those of the indicated mineral resource, with the granites having concentrations of 0.55 wt.% LREO, 0.33 wt.% HREO, 1.87 wt.% ZrO_2 and 0.16 wt.% Nb_2O_5, and the pegmatites having concentrations of 0.72 wt.% LREO, 0.72 wt.% HREO, 2.59 wt.% ZrO_2 and 0.34 wt.% Nb_2O_5 (http://www.questrareminerals.com). Concentrations of ZrO_2 vary considerably in the granite but generally increase towards the pegmatite-rich domains at the top of BZ10027 and BZ11176, and the center of BZ10078 and BZ11109 (see also Fig. 2C). In the case of the LREO and HREO, there are

Gysi, A.P., Williams-Jones, A.E., Collins, P., 2016b. Lithogeochemical Vectors for Hydrothermal Processes in the Strange Lake Peralkaline Granitic REE-Zr-Nb Deposit. Econ Geol 111, 1241-1276.
DOI:10.2113/econgeo.111.5.1241.

a few spikes of increased concentration in the granite, most of which can be related to the presence of hydrothermal ferriallanite-(Ce) and the gadolinite-group minerals, as discussed earlier. The overall distribution of the REE and HFSE suggests that ore metal concentrations were controlled primarily by the location of the pegmatites. However, the detailed mineralogical observations reported above, indicate that most of the REE- and Zr-bearing minerals are of hydrothermal origin. Therefore, hydrothermal mobilization and concentration processes may explain the large variations in ZrO_2 and the spikes for REE, which are observed in both the granites and the pegmatites. Furthermore, the REE profiles indicate that some pegmatites and granites may have been enriched by factors of 2-3 over distances of less than 10 m by this process.

Compositions of allanite group minerals (LREE)

The general mineral formula of epidote-group minerals is $A_2M_3Si_3O_{12}(OH,F)$, with the A-site containing Ca^{2+} and the M-site Al^{3+} and Fe^{3+} in the epidote subgroup ($Ca_2Al_2Fe^{3+}Si_3O_{12}(OH)$), and with the A-site containing Ca^{2+} and REE^{3+} and the M-site Al^{3+} and Fe^{2+} in the allanite subgroup ($CaREEAl_2Fe^{2+}Si_3O_{12}(OH)$). The main control on the chemistry of these subgroups is a heterovalent coupled substitution of the type $[REE^{3+}+Fe^{2+}]=[Ca^{2+}+Fe^{3+}]_{-1}$. There is also a homovalent substitution of the type $[Fe^{3+}]=[Al^{3+}]_{-1}$ between ferriallanite-allanite and ferriepidote-epidote. As shown in Figure 14A adopted from Petrík et al., (1995) and Poitrasson (2002), these coupled substitutions can be depicted on an Al vs. REE diagram and Fe^{3+}/Fe^{2+} ratios can be estimated using the equation:

$$Fe^{3+}/(Fe^{3+}+Fe^{2+})=(REE^{3+}/Al^{3+})+1 \qquad (5)$$

Gysi, A.P., Williams-Jones, A.E., Collins, P., 2016b. Lithogeochemical Vectors for Hydrothermal Processes in the Strange Lake Peralkaline Granitic REE-Zr-Nb Deposit. Econ Geol 111, 1241-1276.
DOI:10.2113/econgeo.111.5.1241.

Structural formulae were calculated based on 3 Si due to possible vacancies on the A-site and a charge deficit from our EMP data (Armbruster et al., 2006). The A-site generally has >0.5 apfu REE, and the M-site >0.5 apfu Fe^{3+}, classifying the mineral in the allanite-subgroup, with the "ferri" in ferriallanite-(Ce) indicating that the Fe^{3+}-rich variety is dominant. Compositional data for hydrothermal ferriallanite-(Ce) are listed in Table 2 for granites, pegmatites and quartz/fluorite veins, and have been further subdivided, based on textural relationships, into phases occurring as mineral replacements, as pore fillings (Fig. 9A), in micro-fractures (Fig. 9B), and as veins (Figs. 9D and F). The ferriallanite-(Ce) in hydrothermal veins and micro-fractured rocks generally has higher Al^{3+}, REE^{3+} and lower Fe^{3+} contents than ferriallanite-(Ce) from the mineral replacement and pore space filling stage (Fig. 14A). The overall result is a mixed ferriallanite-ferriepidote-epidote composition, in which the REE concentration increases with decreasing Ca concentration (Fig. 14B). We therefore consider that the ferriallanite-(Ce) composition can be used to relate stages of Ca-metasomatism to the redox condition (Fe^{3+}/Fe^{2+}), and the Al and REE concentrations of the hydrothermal fluid. As shown in Figure 14C, the data plot on a linear trend of Ca vs. $Fe^{3+}/(Fe^{3+}+Fe^{2+})$, with ferriallanite-(Ce) from micro-fractures and late stage veins departing from the general trend towards lower $Fe^{3+}/Fe^{3+}+Fe^{2+}$ ratios with decreasing Ca concentration. For comparison, we have added data for epidote-group minerals from the Corupá pluton in Brazil (Vlach, 2012) to Figure 14. These are for hydrothermal ferriallanite-(Ce) and epidote from a peralkaline granitic pluton similar to Strange Lake. Our data for Strange Lake plot within the trends observed for the Corupá pluton, with deviations related to ferriallanite-(Ce) in fractures and veins. On a Ca vs. total REE diagram (not shown here), both datasets yield the same

Gysi, A.P., Williams-Jones, A.E., Collins, P., 2016b. Lithogeochemical Vectors for Hydrothermal Processes in the Strange Lake Peralkaline Granitic REE-Zr-Nb Deposit. Econ Geol 111, 1241-1276.
DOI:10.2113/econgeo.111.5.1241.

linear trend representing a substitution range of up to 1 apfu REE for Ca, indicating a near perfect substitution of the REE for Ca without other elements being involved, except Fe for the coupled substitution with Al.

Compositions of gadolinite-group minerals (HREE)

The general formula for the gadolinite-group minerals is $A_2Z_2XSi_2O_8(O,OH,F)_2$, with the A-site being filled with Y [e.g., gadolinite-(Y) and hingganite-(Y)] or Ce [e.g., gadolinite-(Ce) and hingganite-(Ce)] and other lanthanides, Z being filled with Be, and X filled with Fe^{2+} (gadolinite end member), Ca^{2+} (minasgeraisite end member) or being vacant (hingganite end member) (DeMartin et al., 2001). Gerenite-(Y) was first described from Strange Lake as a new gadolinite-group mineral, containing significant proportions of Ca and Na with the general formula $(Ca,Na)_2(Y,REE)_3Si_6O_{18}x2H_2O$ (Jambor et al., 1998). Chemical analyses of the gadolinite-group minerals are given in Table 3. A ternary plot showing the different end members and analyzed gadolinite-group minerals occurring in the granite and pegmatites of the B Zone, indicates that these minerals have compositions ranging among gadolinite, hingganite, gerenite and a not yet IMA approved mineral, "calciogadolinite" ($CaYBe_2FeSi_2O_8O_2$) (Fig. 15A). The data indicate a possible solid solution with a general trend of Ca-REE substitution (Fig. 15C) similar to that observed for ferriallanite-(Ce). This suggests strongly that a major change in fluid chemistry occurred during the hydrothermal evolution of the system, particularly as epidote group minerals display evidence of a similar substitution mechanism. The chondrite-normalized REE profiles observed for gadolinite-group minerals in the granite and pegmatites can be subdivided into LREE-, MREE- and HREE-enriched varieties

(Fig. 16). The gadolinite-group minerals in the pegmatite are more enriched in LREE, MREE and HREE compared to those in the granite; the HREE-enriched variety is restricted to the pegmatites. We interpret the observed variations in REE chemistry of gadolinite-group minerals to partly reflect the sources of HREE, MREE and LREE during alteration (i.e., pegmatite enriched in HREE and granite with variable distributions of HREE, MREE and LREE). In part, the variations also reflect the evolution of the chemical composition of the hydrothermal fluids during cooling and the timing of mineral saturation. The latter is evident in the growth textures of colloform and zoned gadolinite-group minerals (i.e., rims enriched in HREE and cores enriched in MREE; Fig. 10B). Comparison of our REE profiles with those for gadolinite-group minerals observed in pegmatites from other localities (Fig. 16C) allows us to classify our LREE-enriched variety as being between hingganite-(Ce) and gadolinite-(Ce), the MREE-rich variety as being between gadolinite-(Y)/hingganite-Y) and the HREE-rich variety as gerenite-(Y). This indicates several possible complex solid solutions of the gadolinite-group minerals at Strange Lake.

Compositions of Zr-bearing minerals

The average compositions of the zirconosilicate minerals (gittinsite, armstrongite, vlasovite and zircon) are reported in Tables 4 and 5 and illustrated in Figure 17. The composition of the Na-zirconosilicates in the granite plots close to that of the vlasovite endmember (Fig. 17A). Gittinsite has a Ca concentration that correlates negatively with those of the REE (not shown here), as is the case for ferriallanite-(Ce) and the gadolinite-group minerals. In contrast, zircon shows a systematic increase in HREE concentration

Gysi, A.P., Williams-Jones, A.E., Collins, P., 2016b. Lithogeochemical Vectors for Hydrothermal Processes in the Strange Lake Peralkaline Granitic REE-Zr-Nb Deposit. Econ Geol 111, 1241-1276.
DOI:10.2113/econgeo.111.5.1241.

with F concentration in the pegmatites, but in the granites the HREE concentration varies independently of F concentration (Fig. 17C). The opposite is observed for Ca concentration, which correlates positively with HREE concentration in the granites but not in the pegmatites (Fig. 17D). This separation of Ca and F trends suggests that the source of Ca in the granites during growth of the hydrothermal zircon spherules was different from that of F during growth of the zircon crystals in the pegmatites.

Zircon displays two distinctly different types of chondrite-normalized REE profile, one that is strongly enriched in the HREE and depleted in the LREE (especially in zircon I), and another that is relatively flat (Fig. 18). This is true for both the zircon spherules in the granite and the zircon euhedra in the pegmatites. Profiles with intermediate slopes (i.e., HREE-depleted profiles in the pegmatites and LREE-enriched profiles in the granite) are also observed. In principle, the HREE should be preferentially incorporated in the zircon crystal structure because their ionic radii are closer to that of Zr^{4+} than those of the LREE. The flat and intermediate REE profiles are therefore very unusual. The steep HREE-enriched profiles in euhedral zircon crystals, correspond to pseudomorphs after elpidite in the pegmatites and to zircon relicts (after vlasovite) in the granite. Both of these zircon generations therefore formed early in the overall hydrothermal evolution of the system (zircon I). In contrast, zircon spherules in the granite (zircon III) usually show a flat REE profile, with the zircon rims enriched in LREE compared to their cores. In the pegmatites, some euhedral zircon crystals occurring as clusters in hydrothermal quartz and fluorite (zircon II), display a flat REE profile similar to that of the zircon spherules (zircon III), but the core and rim compositions have no distinguishable LREE zoning. These unusual REE variations may be interpreted to reflect the alteration of zircon during fluid-mineral interaction and the crystallization of hydrothermal zircon from a fluid with variable LREE/HREE ratios. To distinguish and understand the origin for each of these variations, the zircon chemistry needs to be considered in the context of the associated alteration stage and the behavior of the REE in hydrothermal fluids as a function of temperature and fluid composition (see discussion section).

Compositions of Nb- and Ti-bearing minerals

The average chemical compositions of titanite and pyrochlore are reported in Tables 6 and 7. Titanite shows clear trends of increasing Ti concentration with decreasing concentrations of Fe and F; titanite in the hydrothermal veins is enriched in Ti (and depleted in Fe and F) compared to titanite in the pegmatites (Fig. 19A and B). Pyrochlore shows a negative correlation of Ca concentration with REE concentration and a positive correlation between Na and F (Fig. 19C and D). The same correlation of Ca with REE is observed with ferriallanite-(Ce) and the gadolinite-group minerals, possibly indicating the occurrence of pyrochlore with a hydrothermal signature; the highest REE concentrations are in pyrochlore from the granite. The chondrite-normalized REE profiles (not shown) are LREE-enriched for pyrochlore, as is the case for the other LREE-silicates in the deposit. This mineral may also represent an important source for the LREE during alteration.

Lithogeochemical vectors of hydrothermal alteration

Introduction

The first step in identifying lithogeochemical vectors is to relate geochemical changes at

Gysi, A.P., Williams-Jones, A.E., Collins, P., 2016b. Lithogeochemical Vectors for Hydrothermal Processes in the Strange Lake Peralkaline Granitic REE-Zr-Nb Deposit. Econ Geol 111, 1241-1276.
DOI:10.2113/econgeo.111.5.1241.

the mineral, rock and deposit scale to changes in specific processes leading to element mobilization/mineralization. In the case of hydrothermal-magmatic systems, for which the alteration types and their relations to mineralization are not well known, this requires: a) separation of magmatic from hydrothermal processes based on reaction textures; b) classification of alteration types and delineation of temporal relationships; c) documentation of the mineral chemistry and changes in this chemistry with alteration stages and mineralization in the deposit; d) thermodynamic modeling of fluid-rock interaction to determine element mobility as a function of physico-chemical parameters of the fluids (e.g. pH, temperature, ligand activity); e) identifying key alteration reactions by linking mineral textures, mineral chemistry and thermodynamic modeling of fluid-mineral equilibria; f) recognizing bulk rock element ratios based on e) and separating these data by trends; g) relating the trends in f) to alteration stage and element mobilization; h) establishing the spatial geochemical manifestation of alteration at the deposit scale based on f) and g).

High and low temperature acidic alteration vectors

Using the bulk rock chemical data, we have identified several lithogeochemical vectors that permit us to distinguish among the different alteration types. These vectors are predicted by the chemical reactions that explain the mineralogical textures produced by the different types of hydrothermal alteration (Table 8). Changes in the Fe_2O_3/Na_2O ratio are due to aegirinization/hematization, whereas changes in the CaO/Na_2O ratio reflect the pseudomorphic replacement of zirconosilicates (Ca-metasomatism) during high temperature acidic alteration (IIIa). The CaO/Na_2O ratio also reflects the formation of

Gysi, A.P., Williams-Jones, A.E., Collins, P., 2016b. Lithogeochemical Vectors for Hydrothermal Processes in the Strange Lake Peralkaline Granitic REE-Zr-Nb Deposit. Econ Geol 111, 1241-1276. DOI:10.2113/econgeo.111.5.1241.

zircon, fluorite and quartz after aegirine in the granite during low temperature acidic alteration (IIIb, Ca-F metasomatism). An independent signature of Ca-F metasomatism, is provided by changes in the CaO/K_2O and CaO/Al_2O_3 ratios, due to the formation of gittinsite and quartz after K-feldspar. The formation of zircon+fluorite+quartz (replacement of aegirine) and quartz+gittinsite (replacement of K-feldspar) was common in the granite (Fig. 7B), and is satisfactorily explained by replacement reactions related to Ca-F-metasomatism (Table 8). If Al is available for complexation with F in the fluid (alteration of K-feldspar), fluorite will not form but gittinsite and quartz will be stable, whereas if Al is not available (alteration of aegirine), fluorite will form and zircon will be stable instead of gittinsite. We emphasize this finding here, as it indicates the importance of the availability of Al for the mobilization of Zr in F-rich crustal fluids.

In order to distinguish the different alteration types based on bulk rock chemistry, it was essential to first filter out the magmatic signature. To do so, we compared the data for the least altered granite in the B Zone with the data for the altered granites and pegmatites (Fig. 20). Outliers were eliminated and the data points for pegmatites and strongly altered granite were subdivided based on the distribution of Fe_2O_3/Na_2O and CaO/Al_2O_3 values. Classification of the data based on these parameters is also supported by other lithogeochemical parameters such as CaO/Na_2O. The data indicate that, with increasing intensity of alteration, the Fe_2O_3/Na_2O ratio increases systematically for aegirinized/hematized samples, which are mainly from border pegmatites, whereas the CaO/Al_2O_3 ratio increases systematically for samples of core pegmatites and granites subjected to Ca-F-metasomatism. From a plot of Fe_2O_3/Na_2O vs. CaO/Na_2O (Fig. 20B), it is evident that the aegirinized/hematized samples follow a trend that may be related to

Gysi, A.P., Williams-Jones, A.E., Collins, P., 2016b. Lithogeochemical Vectors for Hydrothermal Processes in the Strange Lake Peralkaline Granitic REE-Zr-Nb Deposit. Econ Geol 111, 1241-1276. DOI:10.2113/econgeo.111.5.1241.

either Ca-metasomatism (IIIa, high temperature pseudomorphs) or late stage Ca-F-metasomatism (IIIb, low temperature alteration of aegirine to zircon+fluorite+quartz). This ambiguity can be resolved, however, with a plot of CaO/Al_2O_3 vs. CaO/Na_2O (Fig. 20C), from which it can be seen that aegirinized/hematized samples follow the high temperature acidic alteration trend related to Ca-metasomatism. This is consistent with the observation that late stage fluorite and zircon veinlets crosscut aegirinized arfvedsonite (Fig. 11), and that Ca-F-metasomatism occurred later.

Density plots for LREO, HREO and ZrO_2 using CaO/Al_2O_3 as a vector for separating the high temperature acidic alteration (IIIa) from the low temperature acidic alteration (IIIb) show that, overall, the LREO concentrations were relatively constant during acidic alteration (i.e., both high and low temperature acidic alteration) with some samples depleted and others enriched. In contrast, HREO and ZrO_2 display clear trends of enrichment with increased Ca-F-metasomatism. Samples subjected to high temperature acidic alteration (IIIa) also display a significant enrichment in ZrO_2, which is similar to that for samples subjected to strong Ca-F-metasomatism (high CaO/Al_2O_3 ratio). The observed trends can be explained by the fact that the pegmatite sheets are zoned into a border enriched in a granitic component (K-feldspar +quartz +arfvedsonite ±aegirine ±zirconosilicates ±Ti-bearing minerals) and a core enriched in hydrothermal quartz, fluorite and LREE minerals such as REE fluorocarbonates (Gysi and Williams-Jones, 2013). Owing to this zonation, border pegmatites are enriched in Zr, HREE, Al, Fe, K and Si, and core pegmatites are enriched in LREE and F. Aegirinized/hematized samples of the border zone therefore should record the mobility of Zr and HREE. The Ca-F-metasomatic samples should likewise record the remobilization of Ca, F and LREE in

Gysi, A.P., Williams-Jones, A.E., Collins, P., 2016b. Lithogeochemical Vectors for Hydrothermal Processes in the Strange Lake Peralkaline Granitic REE-Zr-Nb Deposit. Econ Geol 111, 1241-1276. DOI:10.2113/econgeo.111.5.1241.

core pegmatite. The reason for the more homogeneous distribution of LREE may be the higher mobility of LREE during the early higher temperature alteration stages (Gysi and Williams-Jones, 2013), whereas the mobility of Zr and HREE was “activated” only during the later stages of alteration. The distinct enrichment of ZrO_2 and a less distinct enrichment of HREO of samples subject to high T alteration (IIIa) suggest that, whereas Zr was enriched during alteration of the border pegmatite, the HREE were more mobile and thus more dispersed. In addition, the observation that Ca-F-metasomatism was able to enrich the rocks considerably, in both Zr and HREE, may indicate a high mobility of Zr and HREE at low temperature. In order to understand the factors controlling this element partitioning, it is necessary to determine the behavior of the LREE, HREE and Zr in the hydrothermal fluids. This was done using available thermodynamic models of fluid-mineral equilibria.

Discussion

Mechanisms of hydrothermal REE and Zr mobilization

The controlling factors for the mobilization of the LREE relative to the HREE and Zr are temperature and fluid composition. This is best illustrated using available mineral stability data. Previous numerical modeling of hydrothermal processes in the pegmatites (Gysi and Williams-Jones, 2013), showed that the key to the observed REE mobilization was the formation of chloride complexes ($REECl^{2+}$, $REECl_2^{+}$), whereas the mobility of Zr depended on the formation of hydroxyfluoride complexes such as $ZrF(OH)_3^0$ and $ZrF_2(OH)_2^0$; for further information on the speciation of these metals refer to Migdisov et al. (2009, 2011). This modeling emphasized the role of pH, which depends on the initial

Gysi, A.P., Williams-Jones, A.E., Collins, P., 2016b. Lithogeochemical Vectors for Hydrothermal Processes in the Strange Lake Peralkaline Granitic REE-Zr-Nb Deposit. Econ Geol 111, 1241-1276.
DOI:10.2113/econgeo.111.5.1241.

acid supply (i.e., the concentrations of HCl and HF), temperature (decreasing temperature increases the dissociation of acids and thus the supply of H^+) and the degree of fluid-rock interaction. Changing temperature also affects metal mobility by promoting dissolution of minerals. For many minerals, including REE minerals like bastnäsite-(Ce), solubility increases with increasing temperature (prograde solubility), whereas some minerals, e.g., zircon, undergo retrograde solubility, i.e., their solubility increases with decreasing temperature (Migdisov et al., 2011; Gysi and Williams-Jones, 2015). In addition, temperature affects the relative mobility of the LREE and HREE, with the former being more mobile at high temperature and the latter at low temperature (Gysi and Williams-Jones, 2013). This is due to the increased stability of LREE chloride complexes with increasing temperature (Migdisov et al., 2009).

In principle, it should be possible to transport the REE as fluoride complexes in hydrothermal solutions with elevated fluorine concentration because of the very high stability of REE-fluoride species (Migdisov et al., 2009). Recent numerical simulations (Migdisov and Williams-Jones, 2014; Williams-Jones et al., 2012), however, have shown that the REE are unlikely to be transported as REE fluoride complexes (e.g., $REEF^{2+}$) due to the association of H^+ and F^- to form HF at mildly acidic conditions. Furthermore, the low solubility of REE fluoride minerals (i.e., $REEF_3$ - fluocerite) at the mildly acidic to neutral pH values, for which F^- would be available for complexation, inhibits the formation of REE fluoride complexes. Hydrothermal fluids with elevated fluorine concentrations, by contrast, should be capable of transporting significant Zr as hydroxyfluoride complexes provided either that pH is high enough to release F^- ions bound in HF, or the concentration of F is high enough that at low pH, sufficient numbers

Gysi, A.P., Williams-Jones, A.E., Collins, P., 2016b. Lithogeochemical Vectors for Hydrothermal Processes in the Strange Lake Peralkaline Granitic REE-Zr-Nb Deposit. Econ Geol 111, 1241-1276.
DOI:10.2113/econgeo.111.5.1241.

of F^- ions not bound to HF are available for complexation. The availability of F^- ions also can be limited by the release of cations, such as Al^{3+}, during alteration of minerals like feldspar, which may lead to the formation of complexes like AlF_2^+. On the other hand, as shown by Gysi and Williams-Jones (2013), AlF_2^+ will breakdown in the presence of very acidic fluids, releasing F^- in concentrations sufficient to promote Zr solubility as hydroxyfluoride complexes at very low pH.

The paucity of thermodynamic data for REE minerals and to a lesser extent REE aqueous species is an important limitation on our ability to reliably evaluate the mobility of the REE and associated metals. Recent experiments designed to determine the thermodynamic properties of the REE fluorocarbonates and HREE phosphates (Gysi and Williams-Jones, 2015; Gysi et al., 2015) represent important steps to alleviate this problem. Unfortunately, however, as discussed earlier, LREE mobility at Strange Lake was largely controlled by the stability of ferriallanite-(Ce), for which there are no thermodynamic data. The same problem applies in evaluating HREE mobility, which, as also discussed earlier, was controlled by gadolinite-group minerals, for which there are no thermodynamic data, and zircon for which partitioning of the HREE into hydrothermal fluids is very poorly constrained.

Considering the thermodynamic models and the observed lithogeochemical vectors described above, the more homogeneous distribution of the LREO during alteration may be due to the higher mobility of the LREE compared to Zr and HREE in hydrothermal fluids; LREE complexes would have been more stable than HREE complexes in the early chloride-rich fluids known to have circulated in the Strange-Lake pluton (see introduction). The HREE mobility (and that of Zr) was controlled by the solubility of

Gysi, A.P., Williams-Jones, A.E., Collins, P., 2016b. Lithogeochemical Vectors for Hydrothermal Processes in the Strange Lake Peralkaline Granitic REE-Zr-Nb Deposit. Econ Geol 111, 1241-1276. DOI:10.2113/econgeo.111.5.1241.

zircon, which is promoted by low temperature and pH, and high F concentration, conditions that likely prevailed during the Ca-F-metasomatic alteration stage. The precipitation of gadolinite-group minerals also must have occurred at low temperature, as displayed by their colloform textures (Fig. 10B), and therefore controlled the mobility of HREE in pegmatites, granites and veins. The same applies to zircon veinlets, zircon spherules and gittinsite, which display low temperature alteration textures (Figs. 9 and 11) and controlled the precipitation of Zr after aegirinization. Once this hydrothermal fluid reacted with feldspar, the release of Al^{3+} led to destabilization of Zr hydroxyfluoride species due to the formation of Al fluoride species, which may have enhanced precipitation of the hydrothermal zircon spherules in the granite. The fluid must have had either a very low pH, as indicated by the absence of phyllosilicates related to the alteration of feldspar in the granite (Figs. 9A and B), or was strongly undersaturated with respect to Al (due to complexation of Al with F). The LREE mobility was controlled by the solubility of bastnäsite-(Ce) and fluocerite-(Ce) and the precipitation of ferriallanite-(Ce), with the latter occurring in the granites, pegmatites and hydrothermal veins. This is consistent with the pervasive LREE mobilization on the deposit scale and the observed relatively constant LREE concentrations during Ca-F-metasomatism (Fig. 20D). Previous thermodynamic modeling of the B Zone, suggests that REE chloride complexes played an important role in the mobilization of the REE, and that this mobilization must have commenced at relatively higher temperature (Gysi and Williams-Jones, 2013).

The Links between zircon REE chemistry and fluid evolution during acidic alteration

The different chondrite-normalized REE profiles for zircon correspond to the different acidic alteration stages (Fig. 21). During high temperature acidic alteration (Fig. 21a), euhedral zircon formed as pseudomorphs after elpidite (Ca-metasomatism) in the pegmatite borders and replaced vlasovite in the granite (zircon I). This early zircon is characterized by steep HREE enriched profiles, and evolved in a nearly closed system without much disturbance by the hydrothermal fluid, except for an internal Na-Ca exchange in the pegmatites, for which the source of Ca was likely the fluorite in the core pegmatites. Continued cooling and exsolution of fluids from the pegmatite cores led to the formation of zones of increased fluid-rock reaction (Fig. 21b). Acidic hydrothermal activity initiated in these zones and mobilized LREE during alteration of LREE-bearing minerals (i.e., pyrochlore, bastnäsite-(Ce) and fluocerite-(Ce)). This stage is marked by euhedral zircon crystals (zircon II) with REE profiles that are either similar to those observed for zircon in the pseudomorphs (i.e., steep, HREE enriched) or LREE enriched and HREE depleted (i.e., flat REE profiles). The latter profiles, likely reflect the beginning of open-system behavior and interaction with a fluid having a high LREE/HREE ratio at high temperature. During the low temperature acidic alteration (Fig. 21c), the pegmatite system opened with the formation of veins and more intense acidic alteration by a much cooler fluid. This low temperature stage was favorable for the transport of Zr and HREE. This led to leaching of Zr, HREE and LREE in the pegmatites, interaction of the acidic F-bearing metal-enriched fluid with the surrounding granite, mixing with a Ca-bearing fluid (see further below), and precipitation of zircon spherules (zircon III) with flat chondrite-normalized REE profiles. The zircon III spherules and their flat REE profiles is one of the signatures of the Ca-F-metasomatic event.

Gysi, A.P., Williams-Jones, A.E., Collins, P., 2016b. Lithogeochemical Vectors for Hydrothermal Processes in the Strange Lake Peralkaline Granitic REE-Zr-Nb Deposit. Econ Geol 111, 1241-1276.
DOI:10.2113/econgeo.111.5.1241.

The source of Ca and its role in Zr/REE mobility

In many peralkaline and alkaline igneous systems, there is evidence that interaction of fluids from the parent pluton with the surrounding rock units (e.g., carbonates) or mixing of these fluids with externally derived meteoric waters added Ca to the system and led to a corresponding decrease of metal mobility. For example, in the Tamazeght complex, Morocco, pegmatites are interpreted to have contained H_2O-HF-rich fluids, which transported Zr and interacted with the surrounding limestones, leading to deposition of HFSE (Salvi et al., 2000). In the case of Anjanabonoina, Madagascar, it was proposed that fluids released from the pegmatites circulated through the country rock, interacted with plagioclase to release Ca and cycled back through the pegmatite body (Martin and De Vito, 2014). For Strange Lake, it was initially proposed, based on studies of fluid inclusions, that high salinity NaCl-rich (~20-25 wt.% NaCl) orthomagmatic fluids exsolved from pegmatites and mixed with low temperature (<200 °C), lower salinity, Ca-rich fluids to produce the observed Ca-metasomatism and Ca-bearing REE/HFSE phases (Salvi and Williams-Jones, 1990, 1992, 1996, 1997). Recently, however, Vasyukova and Williams-Jones (2014; 2016) provided melt inclusion evidence for the presence of immiscible Ca-F-bearing melts, and proposed that these melts may have accumulated in the pegmatites and been later dissolved by magmatic hydrothermal fluids. This proposal is supported by observation of hydrothermal fluorite vugs and fluorite-fluocerite solid solutions in the pegmatites (Gysi and Williams-Jones, 2013). Indeed, there is considerable evidence for two separate sources of Ca, one that was responsible for the Ca-metasomatism at high temperature (represented by early Ca-zirconosilicate pseudomorphs in the pegmatites) when the pegmatite system was closed, and one

Gysi, A.P., Williams-Jones, A.E., Collins, P., 2016b. Lithogeochemical Vectors for Hydrothermal Processes in the Strange Lake Peralkaline Granitic REE-Zr-Nb Deposit. Econ Geol 111, 1241-1276. DOI:10.2113/econgeo.111.5.1241.

responsible for the low temperature Ca-F-metasomatic event (represented by late zircon, gittinsite and fluorite in the granite), when the pegmatite system was open. Furthermore, the presence of a large fluorite breccia surrounding the pluton in the northwest, south and northeast (Fig. 1A), suggest strongly that most of the F and Ca did not originate from the same source and were not transported together on any significant scale. It thus seems likely that the fluids exsolved from the pegmatites were enriched in F but not Ca during the low temperature acidic hydrothermal event, thereby enabling them to transport Zr and REE as described previously. A possible explanation for this is that during the high temperature acidic hydrothermal event, fluorite in the core pegmatites was more soluble, as predicted by experiments (e.g. Tropper and Manning, 2007), which permitted a closed system Ca-Na exchange during the formation of pseudomorphs in the border pegmatites. This explanation is also supported by the reaction path model of Gysi and Williams-Jones (2013), which predicts that during acidic alteration, fluorite from the core zone pegmatites may have dissolved at very low pH. This Ca-Na exchange would have led to a selective enrichment of the pegmatitic fluid in HF, whereas Ca was lost during the formation of the pseudomorphs. The availability of F to complex with Zr on cooling would explain the mobilization of Zr from the border pegmatites to the granites, as indicated by the occurrence of hydrothermal zircon spherules in the latter (the presence of Ca would have inhibited mobilization of Zr by destabilizing Zr hydroxyfluoride species and crystallizing fluorite+zircon or gittinsite, Table 8). Support for this interpretation is provided by the observation that the HREE content of zircon in the pegmatites correlates positively with its F content and is independent of its Ca content (which is very low), whereas the opposite is true for zircon in the granite, i.e., Ca and F were decoupled from

Gysi, A.P., Williams-Jones, A.E., Collins, P., 2016b. Lithogeochemical Vectors for Hydrothermal Processes in the Strange Lake Peralkaline Granitic REE-Zr-Nb Deposit. Econ Geol 111, 1241-1276.
DOI:10.2113/econgeo.111.5.1241.

the HREE (Fig. 17 C-D). The high content of Ca in zircon in the granite but not in the pegmatite suggests that the Ca was supplied by external fluids, whereas the high content of F in zircon in the pegmatites and not in zircon in the granite suggests that F was supplied by fluids exsolving from the pegmatites.

Genetic model for the deposit

Based on field observations, the mineral paragenesis, and mineral and bulk rock chemistry, we conclude with a genetic model for the formation of the Strange Lake REE-Zr-Nb deposit (Figure 22). After intrusion of the hypersolvus granite, fractionation of feldspar in the parental magma chamber led to the saturation of H_2O and an increase in the concentration of volatiles and incompatible elements in the melt. This was followed by intrusion of the subsolvus granite along zones of structural weakness between the gneisses and monzonite that had previously been exploited by the hypersolvus granite magma (Fig. 22A). This magmatic stage (stage I) was accompanied by a continuous release of volatiles from the magma chamber and their accumulation along the walls (manifested by a large fluorite/hematite breccia) and roof of the intrusion, leading to conditions favorable for the formation of pegmatites. This fluid accumulation caused repetitive fracturing, and may also explain the occurrence of pegmatites in the B Zone and Main Zone (west and central parts of the pluton) and the overall horizontal sheet like distribution of the pegmatites at the roof of the intrusion. Crystallization of border pegmatites led to the formation of zones enriched in Zr and HREE due to the crystallization of zirconosilicates, whereas in the pegmatite cores, the addition of immiscible Ca-F-rich melts (Vasyukova and Williams-Jones, 2014), and/or the

Gysi, A.P., Williams-Jones, A.E., Collins, P., 2016b. Lithogeochemical Vectors for Hydrothermal Processes in the Strange Lake Peralkaline Granitic REE-Zr-Nb Deposit. Econ Geol 111, 1241-1276.
DOI:10.2113/econgeo.111.5.1241.

exsolution of a fluid enriched in F and LREE may have led to the separation and crystallization of REE-F-CO_2-rich minerals [i.e., bastnäsite-(Ce) and fluocerite-(Ce)]. The hydrothermal activity can be subdivided based on the fluid sources and evolution stages into: (II) alkali metasomatism; (IIIa) high temperature acidic alteration; and (IIIb) low temperature acidic alteration (Fig. 22B-D). During alkali metasomatism, which was unrelated to the rare metal mineralization, a high temperature orthomagmatic fluid, most likely derived from either the parental magma chamber or from the crystallizing melt of the subsolvus granite, replaced K-feldspar rims with albite pervasively in the granite via a Na-K exchange reaction. This was followed by K-metasomatism, which was restricted to the border pegmatite. The composition of this orthomagmatic fluid is constrained by fluid inclusion studies showing that it was a brine (NaCl-KCl) (Salvi and Williams-Jones, 1992, 1997, 2006). Once the pegmatite border had crystallized, but prior to complete crystallization of the core, the magma exsolved an aqueous-carbonic fluid. This coincided with the onset of high temperature acidic alteration and the development of a closed system with a fluid-buffered acidic pH in the pegmatites cores (Fig. 22C). Alteration of the REE-F-CO_2-rich minerals and fluorite in the core pegmatite ensued, and there was local pseudomorphic replacement of zirconosilicates in the border pegmatite due to the availability of Ca from the core pegmatite leading to Ca-Na exchange (Ca-metasomatism). The latter process led to an increase of F over Ca in the hydrothermal fluid. Interaction of this fluid with the border pegmatite and the adjacent granite, which had a rock-buffered pH, also caused aegirinization/hematization of arfvedsonite forming an alteration halo restricted to the pegmatite spine. Upon cooling, the pegmatitic fluids became more acidic (due to dissociation of the acids) leading to the formation of the HF-

HCl-rich fluid 1. The formation of quartz/fluorite veins (both barren and mineralized), extending into the granite (Fig. 22 D), indicates an opening of the fluid-pegmatite system and the release of the acidic HF-HCl-bearing fluids, which was accompanied by porosity creation through mineral dissolution. During this process, low temperature, low pH and availability of F^- to complex with Zr, led to destabilization of zirconosilicates in the pegmatites (Gysi and Williams-Jones, 2013). This highly acidic fluid mobilized HREE and Zr from the zirconosilicates and LREE from the REE-F-CO_2-rich minerals of the pegmatite into the granite. Once the fluid mixed with the low temperature Ca-bearing external meteoric fluid (fluid 2) on a large scale, gittinsite, zircon spherules, fluorite, gadolinite-(Y) and ferriallanite-(Ce) precipitated and the hydrothermal breccia formed along a zone of structural weakness. The essential ingredient for REE and Zr mobilization was the formation of a pegmatite-rich zone in the roof of the intrusion where fluids accumulated and pH was buffered to low values as temperature decreased.

Conclusions

The B Zone in the Strange Lake peralkaline granitic pluton underwent intense hydrothermal alteration during complex post-magmatic hydrothermal processes. Although primary REE and Zr enrichment was due to the fractionation of the subsolvus granitic melt in a deep magma chamber and to the formation of pegmatites at the roof of the intrusion, most of the primary mineralogy was not preserved. The remobilization of REE and Zr resulted from the presence of HF- and HCl-bearing fluids capable of forming aqueous complexes with Zr and REE, respectively. This led to their transport on a scale of tens to hundreds of meters until termination of hydrothermal activity at low

Gysi, A.P., Williams-Jones, A.E., Collins, P., 2016b. Lithogeochemical Vectors for Hydrothermal Processes in the Strange Lake Peralkaline Granitic REE-Zr-Nb Deposit. Econ Geol 111, 1241-1276.
DOI:10.2113/econgeo.111.5.1241.

temperature. Detailed mineralogical observations, in combination with the bulk rock chemistry, made it possible to retrieve useful lithogeochemical vectors for the different stages of fluid-rock interaction in the system, and showed how the corresponding parameters affected the mobility of the REE and Zr. Thus, mobilization of HREE and Zr was related to a change in the CaO/Al_2O_3 ratio, which yielded a vector for the low temperature Ca-F-metasomatism; the higher temperature aegirinization and hematization were traceable using the Fe_2O_3/Na_2O ratio. This study emphasizes the importance of relating field studies to thermodynamic models of fluid-rock reaction, and shows how such linkage can lead to practical lithogeochemical tools that can guide the exploration of critical metals in peralkaline and alkaline igneous settings.

Acknowledgements

This project was funded by a fellowship from the Swiss National Science Foundation to AG (SNSF grant PBSKP2_134329) and by NSERC Discovery and Industry Collaborative grants and a grant from Quest Rare Minerals Ltd to AEW-J. Essential logistical support was provided by P. Cashin and P. Guay and help in EMP analysis by L. Shi. The manuscript benefited greatly from numerous discussions with N.C. Hurtig, R. Martin, A. Migdisov, V. Moeller, K. Siegel and O. Vasyukova. We also appreciate the support from P. Cashin and P. Guay and collaboration with Quest Rare Minerals Ltd.

REFERENCES

Armbruster, T., Bonazzi, P., Akasaka, M., Bermanec, V., Chopin, C., Gieré, R., Heuss-Assbichler, S., Liebscher, A., Menchetti, S., Pan, Y., Pasero, M., 2006. Recommended nomenclature of epidote-group minerals. European Journal of Mineralogy 18, 551–567.

Bartels, A., Behrens, H., Holtz, F., Schmidt, B.C., Fechtelkord, M., Knipping, J., Crede, L., Baasner, A., Pukallus, N., 2013. The effect of fluorine, boron and phosphorus on the viscosity of pegmatite forming melts. Chemical Geology 346,184-198.

Birkett, T.C., Trzcienski, W.E.Jr., Stirling, J.A.R., 1996. Occurrence and compositions of some Ti-bearing minerals in the Strange Lake intrusive complex, Quebec-Labrador boundary. The Canadian Mineralogist 34, 779-801.

Boily, M., Williams-Jones, A.E., 1994. The role of magmatic and hydrothermal processes in the chemical evolution of the Strange Lake plutonic complex, Québec-Labrador. Contributions to Mineralogy and Petrology 118, 33-47.

Chakrabarty, A., Mitchell, R.H., Ren, M., Sen, A.K., Pruseth, K.L., 2013. Rinkite, cerianite-(Ce), and hingganite-(Ce) in syenite gneisses from the Sushina Hill Complex, India: occurrence, compositional data and petrogenetic significance. Mineralogical Magazine 77, 3137-3153.

DeMartin, F., Minaglia, A., Gramaccioli, C.M., 2001. Characterization of gadolinite-group minerals using crystallographic data only : the case of hingganite-(Y) from Cuasso Al Monte, Italy. Canadian Mineralogist 39, 1105–1114.

Gysi, A.P., Williams-Jones, A.E., 2013. Hydrothermal mobilization of pegmatite-hosted REE and Zr at Strange Lake, Canada: A reaction path model. Geochimica et Cosmochimica Acta 122, 324–352.

Gysi, A.P., Williams-Jones, A.E., 2015. The thermodynamic properties of bastnäsite-(Ce) and parisite-(Ce). Chemical Geology 392, 87–101.

Gysi, A.P., Williams-Jones, A.E., Harlov, D., 2015. The solubility of xenotime-(Y) and other HREE phosphates (DyPO4, ErPO4 and YbPO4) in aqueous solutions from 100 to 250 °C and p_{sat}. Chemical Geology 401, 83–95.

Jambor, J.L., Roberts, A.C., Grice, J.D., Birkett, T.C., Groat, L.A., Zajac, S., 1998. GERENITE-(Y), $(Ca,Na)_2(Y,REE)_3Si_6O_{18} \cdot 2H_2O$, a new mineral species, and an associated Y-bearing Gadolinite-group mineral, from the Strange Lake peralkaline complex, Quebec-Labrador. Canadian Mineralogist 36, 793–800.

Linnen, R., Keppler, H., 2002. Melt composition control of Zr/Hf fractionation in magmatic processes. Geochimica et Cosmochimica Acta 66, 3293–3301.

Manning, D.A.C., 1981. The effect of fluorine on liquidus phase relationships in the system Qz-Ab-Or with excess water at 1 kb. Contributions to Mineralogy and Petrology 76, 206–215.

Gysi, A.P., Williams-Jones, A.E., Collins, P., 2016b. Lithogeochemical Vectors for Hydrothermal Processes in the Strange Lake Peralkaline Granitic REE-Zr-Nb Deposit. Econ Geol 111, 1241-1276.
DOI:10.2113/econgeo.111.5.1241.

Martin, R., De Vito, C., 2014. The late-stage miniflood of Ca in granitic pegmatites: an open-system acid-reflux model involving plagioclase in the exocontact. Canadian Mineralogist 52, 165–181.

McDonough, W., 1995. The composition of the Earth. Chemical Geology 120, 223–253.

Migdisov, A. A., Williams-Jones, A. E., 2014. Hydrothermal transport and deposition of the rare earth elements by fluorine-bearing aqueous liquids. Mineral Deposita 49, 987–997.

Migdisov, A.A., Williams-Jones, A.E., Wagner, T., 2009. An experimental study of the solubility and speciation of the Rare Earth Elements (III) in fluoride- and chloride-bearing aqueous solutions at temperatures up to 300°C. Geochimica et Cosmochimica Acta 73, 7087-7109.

Migdisov, A.A., Williams-Jones, A.E., Van Hinsberg, V., Salvi, S., 2011. An experimental study of the solubility of baddeleyite (ZrO_2) in fluoride-bearing solutions at elevated temperature. Geochimica et Cosmochimica Acta 75, 7426–7434.

Miller, R., Heaman, L.M.,Birkett, T.C., 1997. U-Pb zircon age of the Strange Lake peralkaline complex: implications for Mesoproterozoic peralkaline magmatism in north-central Labrador. Precambrian Research 81, 67–82.

Miller, R., 1986. Geology of the Strange Lake alkalic complex and the associated Zr-Y-Nb-Be-REE mineralization. Current Research Newfoundland Department of Mines Energy Report 86-1, 11-19.

Miller, R., 1990. The Strange Lake pegmatite-aplite-hosted rare-metal deposit, Labrador. Current Research Newfoundland Department of Mines Energy Report 90-1, 171-182.

Miyawaki, R., Matsubara, S., Yokoyama, K., Okamoto, A., 2007. Hingganite-(Ce) and hingganite-(Y) from Tahara, Hirukawa-mura, Gifu Prefecture, Japan: The description on a new mineral species of the Ce-analogue of hingganite-(Y) with a refinement of the crystal structure of hingganite-(Y). Journal of Mineralogical And Petrological Sciences 102, 1–7.

Nassif, G.J., 1993. The Strange Lake Peralkaline Complex, Québec– Labrador: the hypersolvus–subsolvus granite transition and feldspar mineralogy. Unpublished M.Sc. thesis, McGill Univ. 104.

Petrík, I., Broska, I., Lipka, J., Siman, P., 1995. Granitoid allanite-(Ce): substitution relations, redox conditions and REE distributions (on an example of I-type granitoids, Western Carpathians, Slovakia). Geologica Carpathica 46, 79–94.

Pezzotta, F., Diella, V., Guastoni, A., 1999. Chemical and paragenetic data on gadolinite-group minerals from Baveno and Cuasso al Monte, southern Alps, Italy. American Mineralogist 84, 782–789.

Pillet, D., Bonhomme, M.G., Duthou, J.L., Chenevoy, M., 1989. Chronologie Rb/Sr et K/Ar du granite peralcalin du lac Brisson, Labrador central, Nouveau-Québec. Canadian Journal of Earth Sciences 26, 328–332.

Poitrasson, F., 2002. In situ investigations of allanite hydrothermal alteration: examples from calc-alkaline and anorogenic granites of Corsica (southeast France). Contributions to Mineralogy and Petrology 142, 485–500.

Salvi, S., Williams-Jones, A.E., 1990. The role of hydrothermal processes in the granite-hosted Zr, Y, REE deposit at Strange Lake, Quebec/Labrador: evidence from fluid inclusions. Geochimica et Cosmochimica Acta 54, 2403-2418

Salvi, S., Williams-Jones, A.E., 1992. Reduced orthomagmatic C-O-H-N-NaCl fluids in the Strange Lake rare-metal granitic complex, Quebec/Labrador, Canada. European Journal of Mineralogy 4, 1155–1174.

Salvi, S., Williams-Jones, A.E., 1995. Zirconosilicate phase relations in the Strange Lake (Lac Brisson) pluton, Quebec-Labrador, Canada. American Mineralogist 80, 1031–1040.

Salvi, S., Williams-Jones, A.E., 1996. The role of hydrothermal processes in concentrating high-field strength elements in the Strange Lake peralkaline complex, northeastern Canada. Geochimica et Cosmochimica Acta 60, 1917–1932.

Salvi, S., Williams-Jones, A.E., 1997. Fischer-Tropsch synthesis of hydrocarbons during sub-solidus alteration of the Strange Lake peralkaline granite, Quebec/Labrador, Canada. Geochimica et Cosmochimica Acta 61, 83–99.

Salvi, S., Williams-Jones, A.E., 2006. Alteration, HFSE mineralisation and hydrocarbon formation in peralkaline igneous systems: Insights from the Strange Lake Pluton, Canada. Lithos 91, 19–34.

Salvi, S., Fontan, F., Monchoux, P., Williams-Jones, A.E., Moine, B., 2000. Hydrothermal Mobilization of High Field Strength Elements in Alkaline Igneous Systems: Evidence from the Tamazeght Complex (Morocco). Economic Geology 95, 559–576.

Segalstad, T.V., Larsen, A.O., 1978. Gadolinite-(Ce) from Skien, southwestern Oslo region, Norway. American Mineralogist 63, 188–195.

Siegel, K., Williams-Jones, A.E., 2015. The amphiboles of the REE-enriched Strange Lake peralkaline granitic pluton - fingerprints of magma evolution. Goldschmidt Abstract 2892.

Sheard, E., Williams-Jones, A., Heiligmann, M., 2012. Controls on the Concentration of Zirconium, Niobium, and the Rare Earth Elements in the Thor Lake Rare Metal Deposit, Northwest Territories, Canada. Economic Geology 107, 81–104.

Thomas, R., Davidson, P., Beurlen, H., 2012. The competing models for the origin and internal evolution of granitic pegmatites in the light of melt and fluid inclusion research. Mineralogy and Petrology 106, 55–73.

Tropper, P., Manning, C., 2007. The solubility of fluorite in H_2O and H_2O-NaCl at high pressure and temperature. Geochimica et Cosmochimica Acta 242, 299-306.

Vasyukova, O., Williams-Jones, A.E., 2014. Fluoride–silicate melt immiscibility and its role in REE ore formation: Evidence from the Strange Lake rare metal deposit, Québec-Labrador, Canada. Geochimica et Cosmochimica Acta 139, 110–130.

Vasyukova, O., Williams-Jones, A.E., 2016. The evolution of immiscible silicate and fluoride melts: Implications for REE ore-genesis. Geochimica et Cosmochimica Acta 172, 205-224.

Vigneresse, J.L., 2007. The role of discontinuous magma inputs in felsic magma and ore generation. Ore Geology Reviews 30, 181–216.

Vlach, S., 2012. Structural and compositional variations of hydrothermal epidote-group minerals from a peralkaline granite, Corupá Pluton, Graciosa Province, South Brazil. Anais da Academia Brasileira de Cienccias 84, 407–425.

Williams-Jones, A. E., Migdisov, A. A., Samson, I.M., 2012. Hydrothermal Mobilisation of the Rare Earth Elements - a Tale of "Ceria" and "Yttria." Elements 8, 355–360.

FIGURE CAPTIONS

FIG. 1. A) Geological map of the Strange Lake peralkaline granitic pluton, showing the location of the two pegmatite-rich ore zones (the B Zone and Main Zone). B) A geological map of the B Zone, showing the distribution of the pegmatite spine, the fluorite breccia and the location of drill cores (BZ11176, BZ10027, BZ10078 and BZ11109) and the A-A' section investigated in this study. C) NE-SW section showing the lithological distribution with depth.

FIG. 2. Geochemical model based on bulk rock data, showing the relative concentrations of LREO, HREO and ZrO_2 with depth along a NE-SW profile (section A-A’ in Fig. 1B). Outlines show the location of the pegmatite sheets and squares indicate different domains of metal enrichment (zones 1 to 5). Zone 1: pegmatite spine enriched in LREO, HREO and ZrO_2; zone 2: granite enriched in ZrO_2 with subordinate LREO and HREO; zone 3: granite enriched in ZrO_2, LREO and HREO; zone 4: granite enriched in ZrO_2 and HREO with subordinate LREO; zone 5: granite only enriched in LREO.

FIG. 3. Drill core samples showing the different alteration types that affected the B Zone granites. A) Unaltered subsolvus granite with arfvedsonite phenocrysts and vlasovite (Na-zirconosilicate). B) Relict phenocrysts of hematized arfvedsonite and interstitial ferriallanite-(Ce) and zircon. C) Aegirinized and partly hematized granite with interstitial zircon and fluorite. D) Granite subjected to pervasive Ca-F-metasomatism with a few relict arfvedsonite phenocrysts and interstitial hydrothermal ferriallanite-(Ce), gittinsite (Ca-zirconosilicate) and zircon mineralization. E) Drill core with a highly altered zone representative of a fluid conduit (top) and hematized arfvedsonite phenocrysts with a preserved igneous texture (bottom). Arf: arfvedsonite; Aeg: aegirine; Hem: hematite; Fl: fluorite; Zrn: zircon; Aln-(Ce): ferriallanite-(Ce); Gad-(Y): gadolinite-group minerals.

FIG. 4. Drill core samples illustrating the alteration/mineralization that affected the B Zone pegmatites. A) Border pegmatite with arfvedsonite and K-feldspar phenocrysts. B) Border pegmatite with pseudomorphs after narsarsukite forming a cumulate texture with zirconosilicates, quartz and K-feldspar. C) Border pegmatite with pseudomorphs after elpidite (Na-zirconosilicate), aegirinized/hematized arfvedsonite relicts and K-feldspar. D) Core pegmatite with hydrothermal quartz, fluorite, zircon and bastnäsite-(Ce). E) Strongly mineralized layer in pegmatite with hydrothermal quartz, fluorite and gadolinite-group minerals. Qtz: quartz, Kfs: K-feldspar; Elp: pseudomorphs after elpidite; Bast-(Ce): bastnäsite-(Ce). Other mineral abbreviations are the same as in Fig. 1.

FIG. 5. Backscattered electron images of textures showing evidence of alkali metasomatism, and WDS element X-ray maps. A) Partially albitized K-feldspar phenocryst in granite. B) Replacement of albite lamellae by K-feldspar in a K-feldspar phenocryst of a pegmatite. C-D) Element X-ray maps showing the distribution of K as patches in the phenocryst and Na in albite lamellae relicts. Ab: albite; Kfs: K-feldspar; Qtz: quartz.

FIG. 6. Drill core samples showing textures related to veining and brecciation. A) Barren quartz vein crosscutting a hematized granite. B) Quartz/fluorite vein containing ferriallanite-(Ce), titanite and gadolinite-group minerals crosscutting an aegirinized granite. C) Fluorite vein and veinlets showing colloform zoning. D) Contact of a border pegmatite and granite and micro-breccia filled with hydrothermal fluorite. E) Fluorite/hematite breccia with fragments of gneiss showing evidence of repetitive brecciation.

FIG. 7. Thin section photomicrographs in plain and polarized light showing REE- and Zr-bearing minerals in the granite (A-B) and pegmatite (C-D). A) Primary interstitial

Gysi, A.P., Williams-Jones, A.E., Collins, P., 2016b. Lithogeochemical Vectors for Hydrothermal Processes in the Strange Lake Peralkaline Granitic REE-Zr-Nb Deposit. Econ Geol 111, 1241-1276.
DOI:10.2113/econgeo.111.5.1241.

vlasovite (Na-zirconosilicate) with dark patches of REE-bearing minerals. B) Gittinsite (Ca-zirconosilicate) and quartz at the contact with hydrothermal zircon spherules and fluorite. C) Interstitial ferriallanite-(Ce). D) Spherules of hydrothermal gadolinite-group minerals, fluorite and quartz. Qtz: quartz, Kfs: K-feldspar; Ab: albite; Fl: fluorite; Zrn: zircon; Git: gittinsite; Aln-(Ce): ferriallanite-(Ce); Gad-(Y): gadolinite-group minerals.

FIG. 8. Backscattered electron images showing relicts of primary REE- and Zr-bearing minerals in the granite (A-C) and pegmatite (D-E). D) and F) are pseudomorphs after elpidite and narsarsukite, respectively. Qtz: quartz; Git: gittinsite; Gag-(Y): gagarinite-(Y); Ttn: titanite; Bast-(Ce): bastnäsite-(Ce); Gad-(Y): gadolinite-group minerals.

FIG. 9. Backscattered electron images showing hydrothermal textures involving REE-, Zr- and Ti-bearing minerals in the granite (A-B), pegmatite (C) and in quartz/fluorite veins (D-F). A) Interstitial secondary zircon spherules, gittinsite, ferriallanite-(Ce) and quartz replacing primary K-feldspar. B) Fractures filled with quartz, ferriallanite-(Ce) and gadolinite-group minerals. C) Fractured quartz and an intergrowth of gittinsite and quartz. D) Ferriallanite-(Ce) forming a fibrous intergrowth in a quartz/fluorite vein. E) Quartz and fluorite vein with euhedral titanite crystals that grew on the fluorite. F) Veinlets filled with gadolinite-group minerals and patches of ferriallanite-(Ce) and titanite in hydrothermal quartz.

FIG. 10. Backscattered electron images and WDS element X-ray maps of A) interstitial ferriallanite-(Ce) and a gittinsite intergrowth in granite displaying patches enriched in La and Y, and B) colloform growth of gadolinite-group minerals displaying zoning with cores enriched in the lighter REE (i.e., Dy and Gd) and rims enriched in the heavier REE (i.e., Y and Yb).

FIG. 11. Backscattered electron images and WDS element X-ray maps showing zircon veinlets and a fluorite vein crosscutting an arfvedsonite crystal that has been replaced by aegirine and quartz during aegirinization. This texture provides evidence of low temperature hydrothermal Zr transport during Ca-F-metasomatism (low temperature acidic alteration, IIIb), which occurred after aegirinization/hematization (high temperature acidic alteration, IIIa).

FIG. 12. Mineral paragenesis summarizing the magmatic mineralogy, alteration types, textures and secondary mineralogy interpreted from field relations (Figs. 3-11). See text for details on the different alteration types.

FIG. 13. Bulk rock composition (in wt. %) of HREO, LREO, Nb_2O_5 and ZrO_2 in drill core samples with depth along the NE-SW section (Fig. 1B).

FIG. 14. Mineral chemistry of hydrothermal ferriallanite-(Ce). Symbol shapes are categorized by lithology. Symbol colors correspond to: (f): microfractures; (v) veining;

Gysi, A.P., Williams-Jones, A.E., Collins, P., 2016b. Lithogeochemical Vectors for Hydrothermal Processes in the Strange Lake Peralkaline Granitic REE-Zr-Nb Deposit. Econ Geol 111, 1241-1276.
DOI:10.2113/econgeo.111.5.1241.

(rp/p) mineral replacement and pore space fillings. A) Diagram showing the element substitution mechanisms in epidote-group minerals and the method for estimating $Fe^{3+}/(Fe^{3+}+Fe^{2+})$ of Petrík et al. (1995). B) and C) Diagrams showing element substitution mechanisms involving REE, Ca, Al and Fe. Note that samples of ferriallanite-(Ce) occurring in (f) and (v) have the lowest $Fe^{3+}/(Fe^{3+}+Fe^{2+})$ ratios.

Fig. 15. Mineral chemistry of hydrothermal gadolinite-group minerals. A) Ternary Ca-Si-REE_{tot} diagram in mol % cations for samples in A) granites and B) pegmatites. C) Ca vs. total REE showing a negative correlation of REE with Ca in both pegmatites and granites.

FIG. 16. Chondrite-normalized (McDonough, 1995) REE profiles of gadolinite-group minerals from A) granites and B) pegmatites. C) Gadolinite-group minerals from a variety of localities: Gadolinite-(Y)/Hingganite-(Y) from miarolitic cavities in granophyre from Baveno and Cuasso al Monte, Southern Alps, Italy (Pezzotta et al., 1999); Gadolinite-(Ce) from a syenite pegmatite near Skien, Norway (Segalstad and Larsen, 1978); Hingganite-(Y) from pegmatite at Hirukawa-mura, Japan (Miyawaki et al., 2007); Hingganite-(Ce) and Gerenite-(Y) from pegmatites at Strange Lake (Jambor et al., 1998).

FIG. 17. Ternary Na-Ca-Zr/(Zr+Si) diagram in mol % cations for zirconosilicates in A) granites and B) pegmatites, showing the compositions corresponding to vlasovite, gittinsite, armstrongite and zircon. Shaded areas correspond to data for Strange Lake from Salvi and Williams-Jones (1995). C) and D) Binary plots of HREE vs F and Ca, respectively, in hydrothermal zircon from pegmatites and granites. Note the difference in the correlations for zircon compared to ferriallanite-(Ce) (Fig. 14B) and gadolinite-group minerals (Fig. 15C).

FIG. 18. Chondrite-normalized (McDonough, 1995) REE profiles of hydrothermal zircons from A) granites and B) pegmatites showing LREE enriched patterns in some zircon crystals.

FIG. 19. Compositions of pyrochlore and hydrothermal titanite. A) and B) Fe and F vs. Ti in titanite showing a negative correlation with Ti; the compositions of vein-hosted titanite are closer to that of titanite in the granite than in the pegmatite. C) Total REE vs. Ca showing a negative correlation for pyrochlore, similar to that for hydrothermal ferriallanite-(Ce) and gadolinite-group minerals. D) F vs. Na showing a positive correlation for pyrochlore, indicating that Ca and F may have been decoupled in the pegmatites.

FIG. 20. Lithogeochemical variation diagrams showing trends in bulk rock composition (in wt. %) for different alteration types based on the reactions listed in Table 8. A) Fe_2O_3*/Na_2O vs. CaO/Al_2O_3 showing aegirinized/hematized vs. Ca-F-metasomatized rocks. B) Fe_2O_3*/Na_2O vs. CaO/Na_2O indicating that aegirinization/hematization was overprinted by Ca-F-metasomatism. C) CaO/Na_2O vs. CaO/Al_2O_3 showing trends for Ca-metasomatism (pseudomorphs Na-/Ca-zirconosilicates) and Ca-F-metasomatism

Gysi, A.P., Williams-Jones, A.E., Collins, P., 2016b. Lithogeochemical Vectors for Hydrothermal Processes in the Strange Lake Peralkaline Granitic REE-Zr-Nb Deposit. Econ Geol 111, 1241-1276.
DOI:10.2113/econgeo.111.5.1241.

(hydrothermal zircon spherules, gittinsite, quartz, fluorite and ferriallanite-(Ce)). D-F) Density plots showing an increase of HREO and ZrO_2 with Ca-F-metasomatism (CaO/Al_2O_3); LREO concentration is relatively constant. Fe_2O_3* corresponds to total Fe. Data have been separated (red for high temperature acidic alteration; turquoise for low temperature acidic alteration) based on Fe_2O_3*/Na_2O vs. CaO/Al_2O_3 ratios.

FIG. 21. Schematic model of subsolidus pegmatite evolution illustrating the different stages of acidic alteration (Ca-metasomatism, aegirinization/hematization and Ca-F-metasomatism), the associated REE and Zr mobilization, and the chemical evolution of the three different zircon types. A) the formation of zircon I (LREE-depleted and HREE-enriched REE profiles; red) during Ca-metasomatism and pseudomorphic mineral replacement in a closed system. B) Mobilization of the LREE during high temperature acidic alteration and the formation of zircon II (LREE-enriched REE profiles; blue). C) involved open system Ca-F-metasomatism, mobilization of REE and Zr and the formation of zircon spherules (zircon III) in the granite (LREE-enriched REE profiles; blue). Intermediate zircon compositions (green) indicate complex processes of HREE depletion and LREE enrichment of zircon I.

FIG. 22. A schematic model for the emplacement of the Strange Lake peralkaline granitic pluton and the stages of fluid-rock interaction responsible for the observed alteration types. A) Magmatic stage with the emplacement of the pluton and accumulation of volatiles originating from a deep magma chamber and rising along structural weaknesses (contacts with gneiss and monzonite) towards the roof of the intrusion. Three hydrothermal stages are distinguished in the B Zone: B) alkali metasomatism, C) high temperature acidic alteration and D) low temperature acidic alteration. B) Alkali metasomatic stage with pervasive Na-metasomatism in the granite and K-metasomatism restricted to the pegmatite border. C) Closed system high temperature acidic alteration with a fluid exsolved from the pegmatite core, leading to dissolution of fluorite and bastnäsite-(Ce), enrichment in Ca and F (and LREE), and pseudomorphic mineral replacement reactions (Ca-metasomatism) in the border pegmatite. This stage also involved the formation of an alteration halo around the pegmatite spine, where the fluids had a rock buffered pH. D) Open system low temperature acidic alteration by a HF-HCl-rich fluid (Fluid 1, Ca-depleted by Ca-metasomatism) capable of transporting REE and Zr. This fluid led to the formation of Zr-REE mineralized quartz/fluorite veins due to mixing with a meteoric Ca-bearing fluid (fluid 2). Also shown is the late fluorite breccia indicating a late stage mixing of fluid 1 and fluid 2.

Gysi, A.P., Williams-Jones, A.E., Collins, P., 2016b. Lithogeochemical Vectors for Hydrothermal Processes in the Strange Lake Peralkaline Granitic REE-Zr-Nb Deposit. Econ Geol 111, 1241-1276. DOI:10.2113/econgeo.111.5.1241.

Figure1

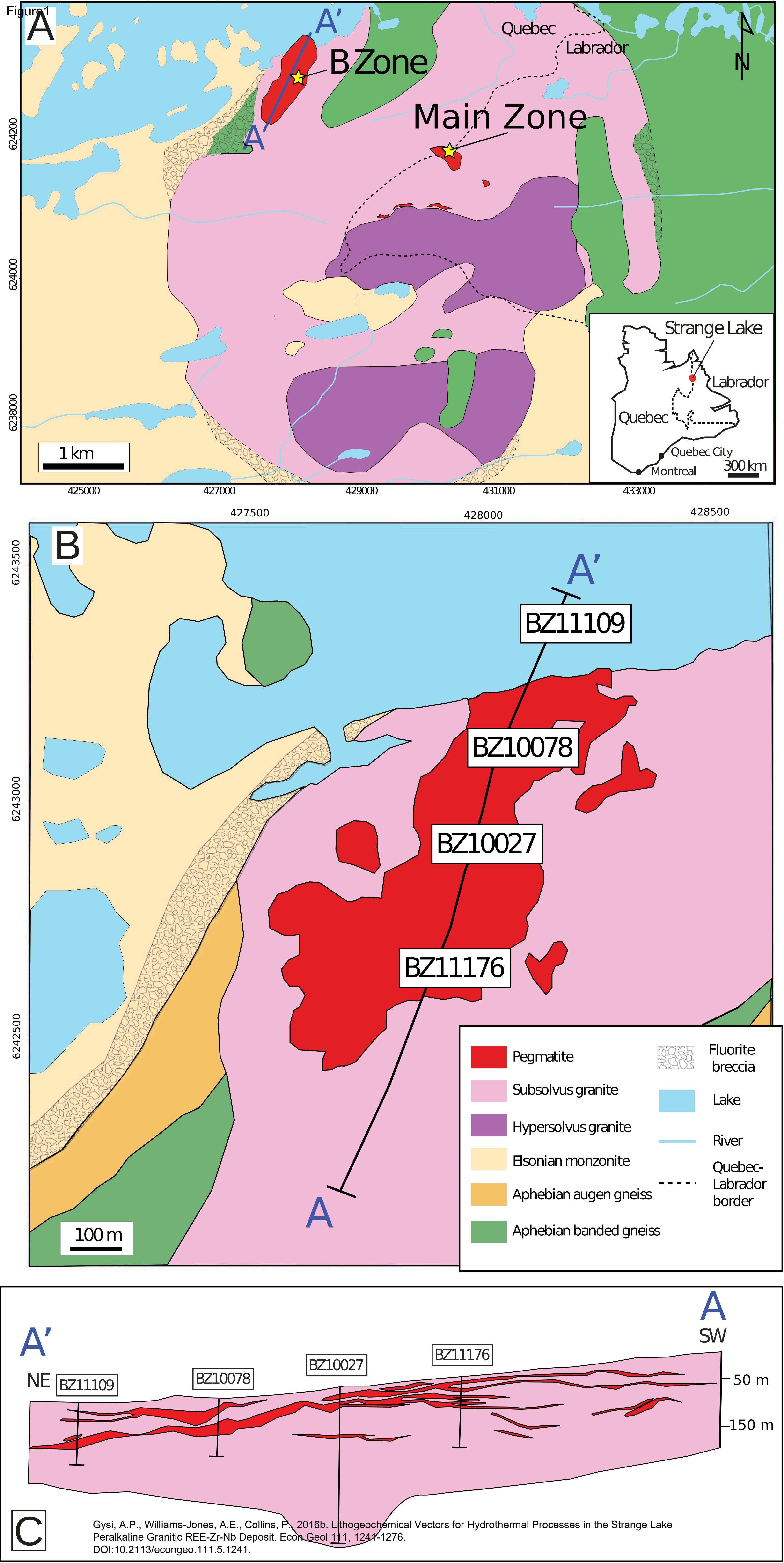

Gysi, A.P., Williams-Jones, A.E., Collins, P., 2016b. Lithogeochemical Vectors for Hydrothermal Processes in the Strange Lake Peralkaline Granitic REE-Zr-Nb Deposit. Econ Geol 111, 1241-1276.
DOI:10.2113/econgeo.111.5.1241.

Figure2

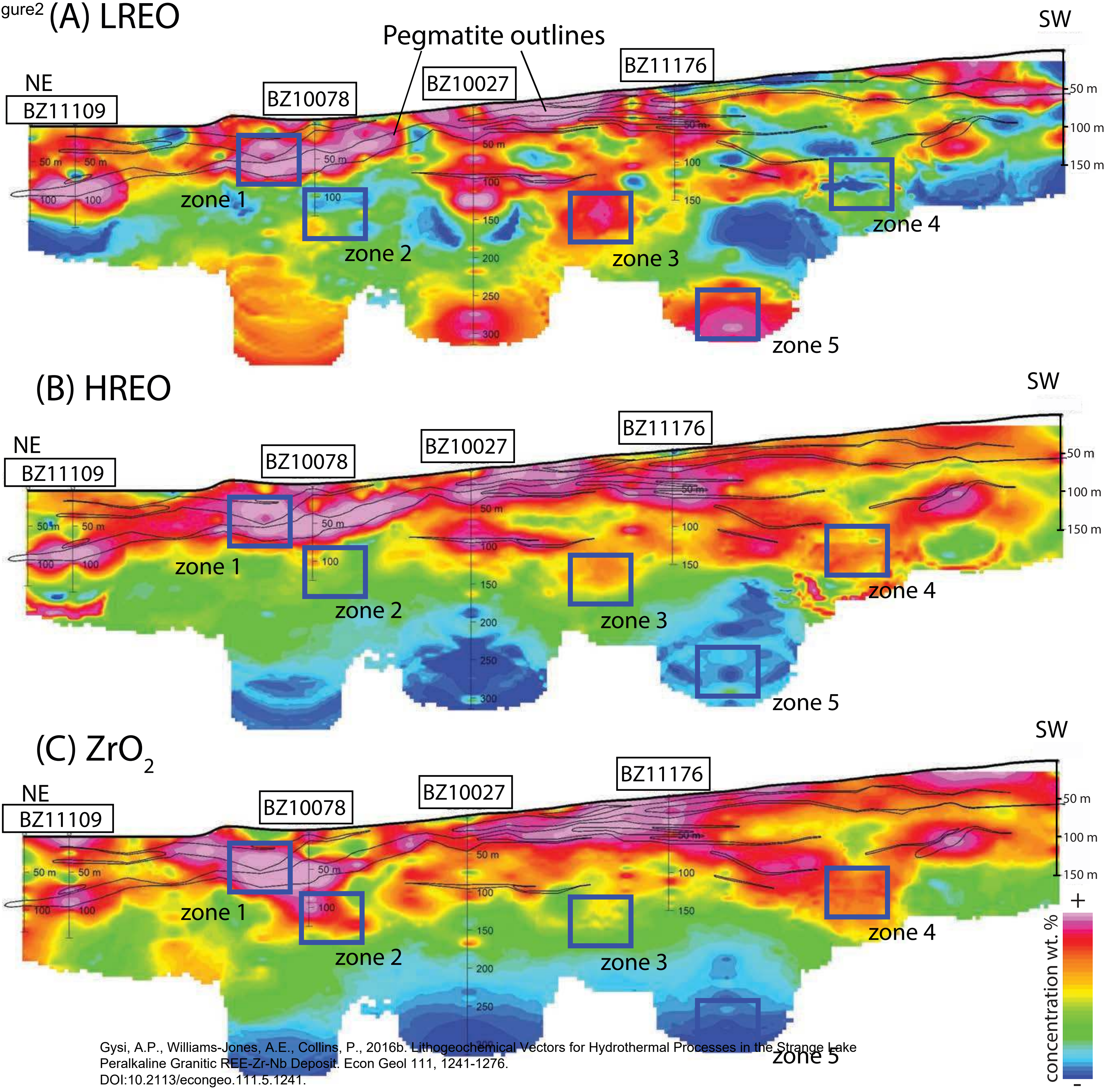

Gysi, A.P., Williams-Jones, A.E., Collins, P., 2016b. Lithogeochemical Vectors for Hydrothermal Processes in the Strange Lake Peralkaline Granitic REE-Zr-Nb Deposit. Econ Geol 111, 1241-1276. DOI:10.2113/econgeo.111.5.1241.

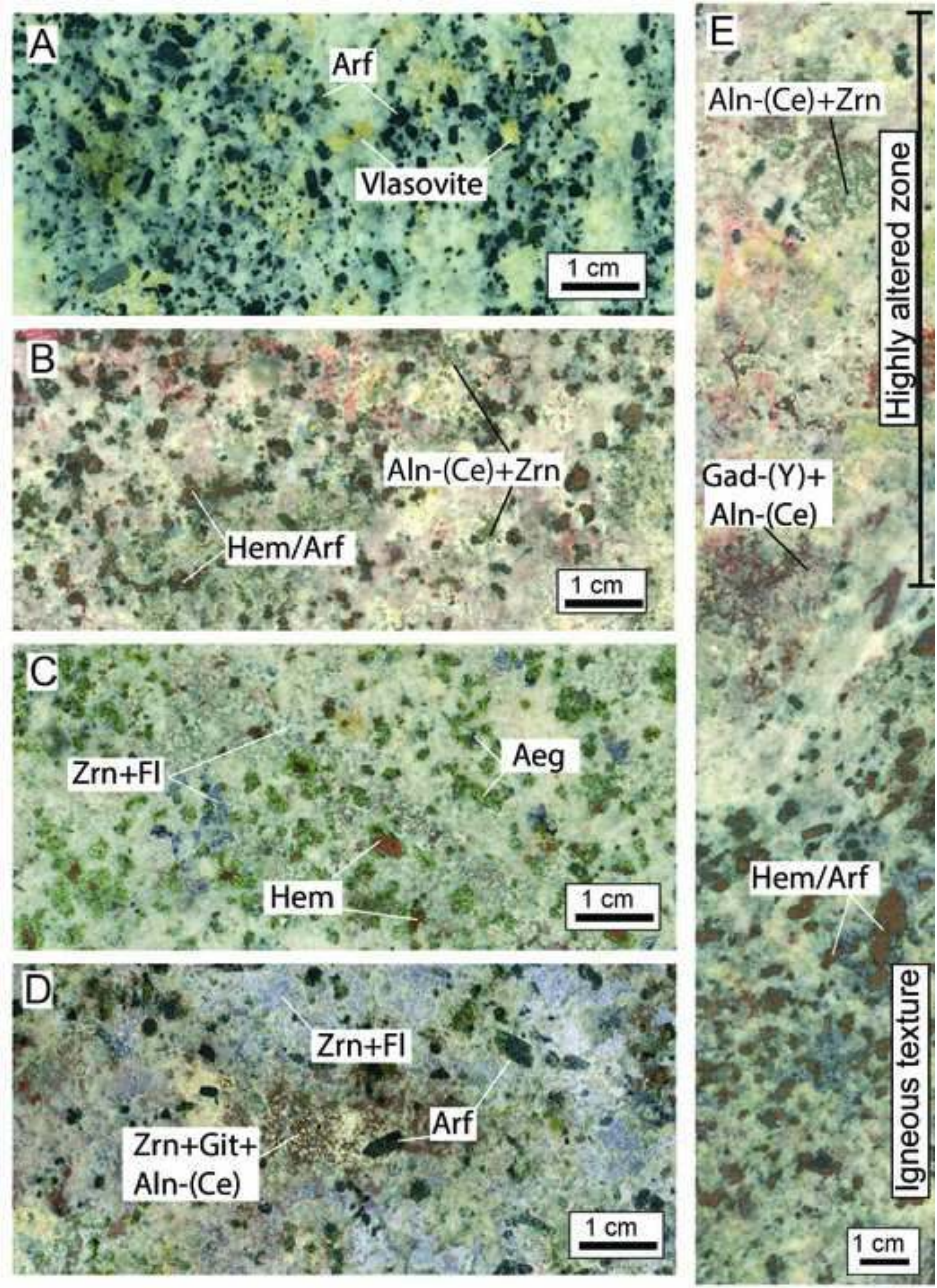

Gysi, A.P., Williams-Jones, A.E., Collins, P., 2016b. Lithogeochemical Vectors for Hydrothermal Processes in the Strange Lake Peralkaline Granitic REE-Zr-Nb Deposit. Econ Geol 111, 1241-1276.
DOI:10.2113/econgeo.111.5.1241.

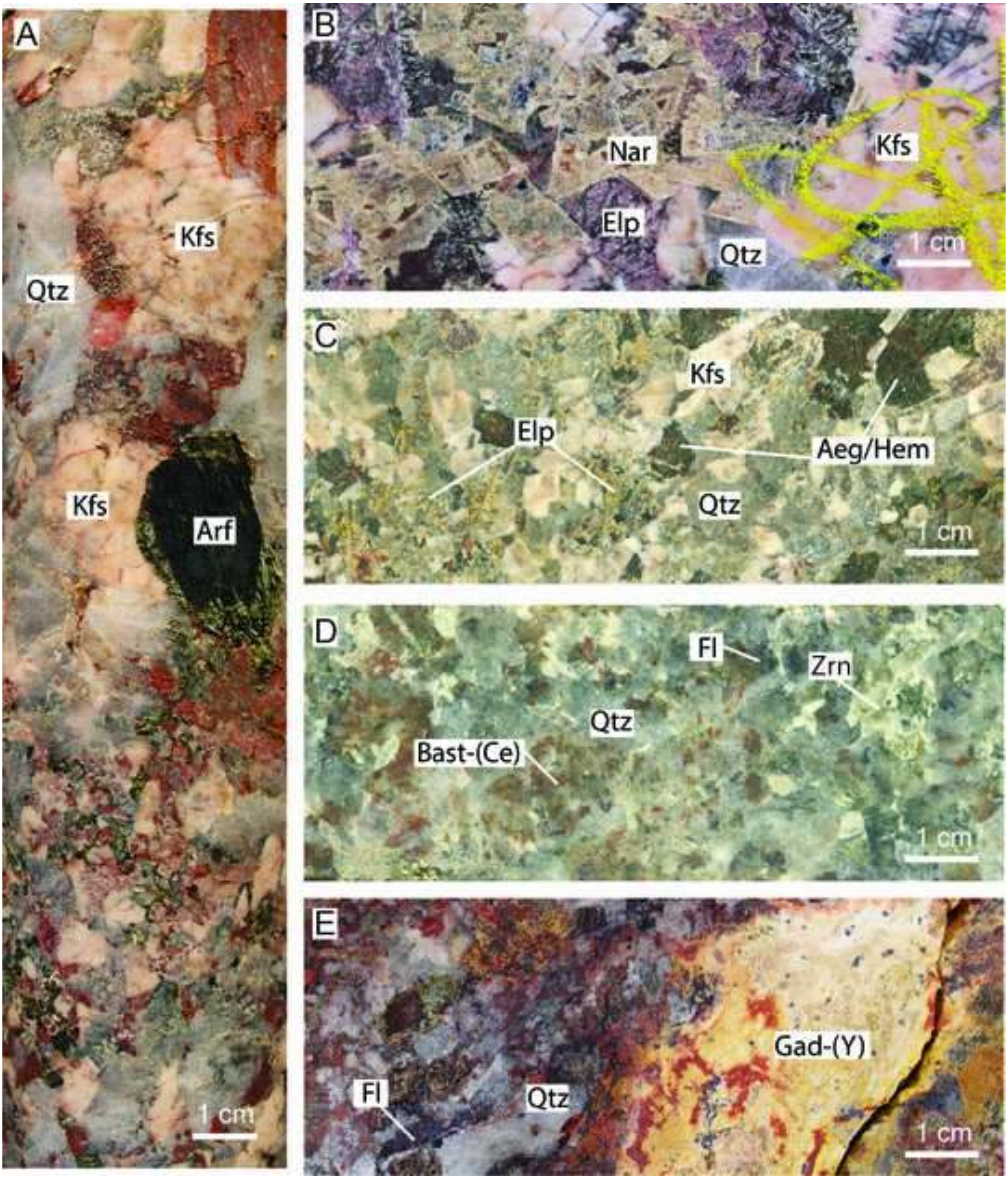

Gysi, A.P., Williams-Jones, A.E., Collins, P., 2016b. Lithogeochemical Vectors for Hydrothermal Processes in the Strange Lake Peralkaline Granitic REE-Zr-Nb Deposit. Econ Geol 111, 1241-1276.
DOI:10.2113/econgeo.111.5.1241.

Figure5

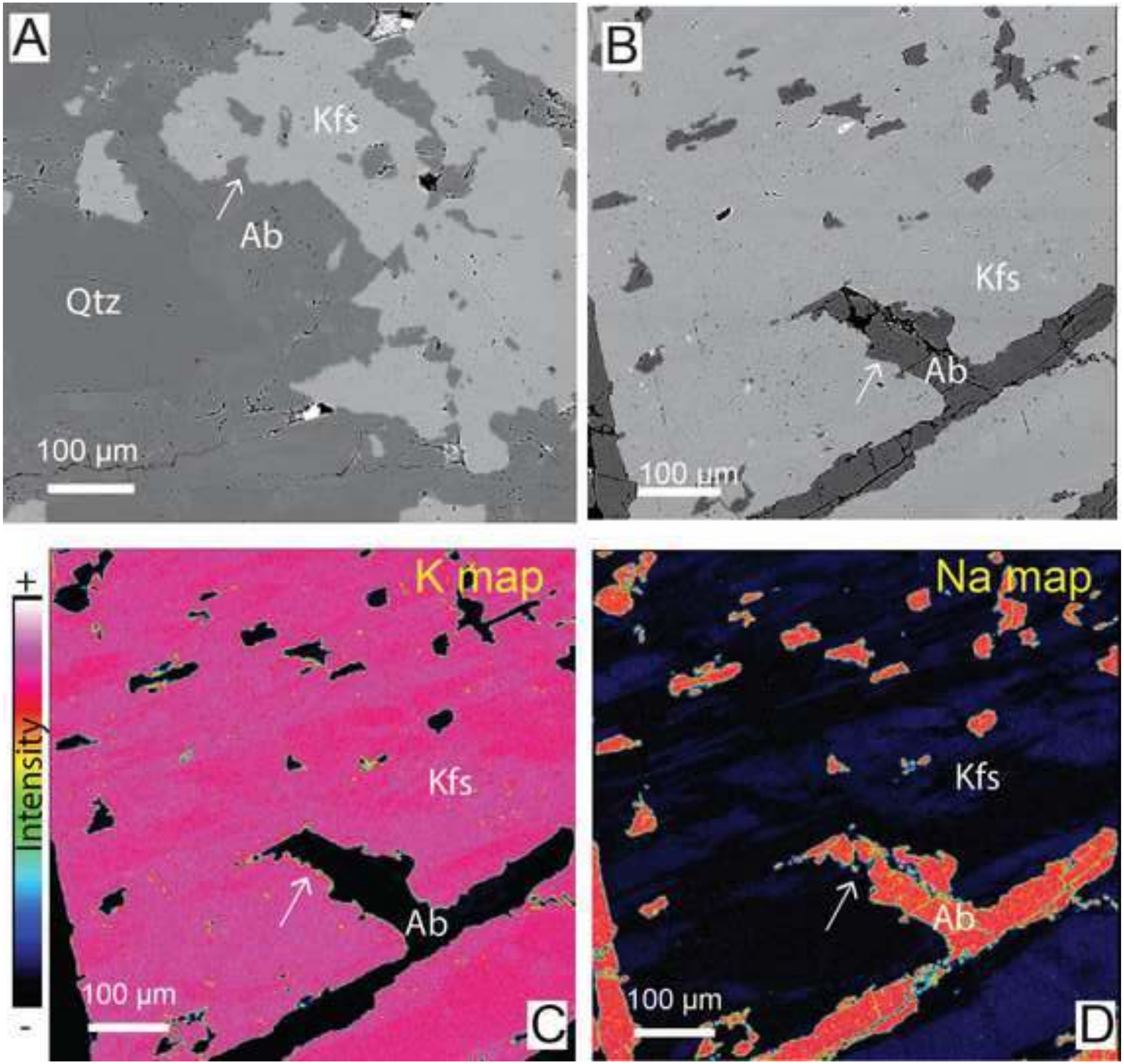

Gysi, A.P., Williams-Jones, A.E., Collins, P., 2016b. Lithogeochemical Vectors for Hydrothermal Processes in the Strange Lake Peralkaline Granitic REE-Zr-Nb Deposit. Econ Geol 111, 1241-1276. DOI:10.2113/econgeo.111.5.1241.

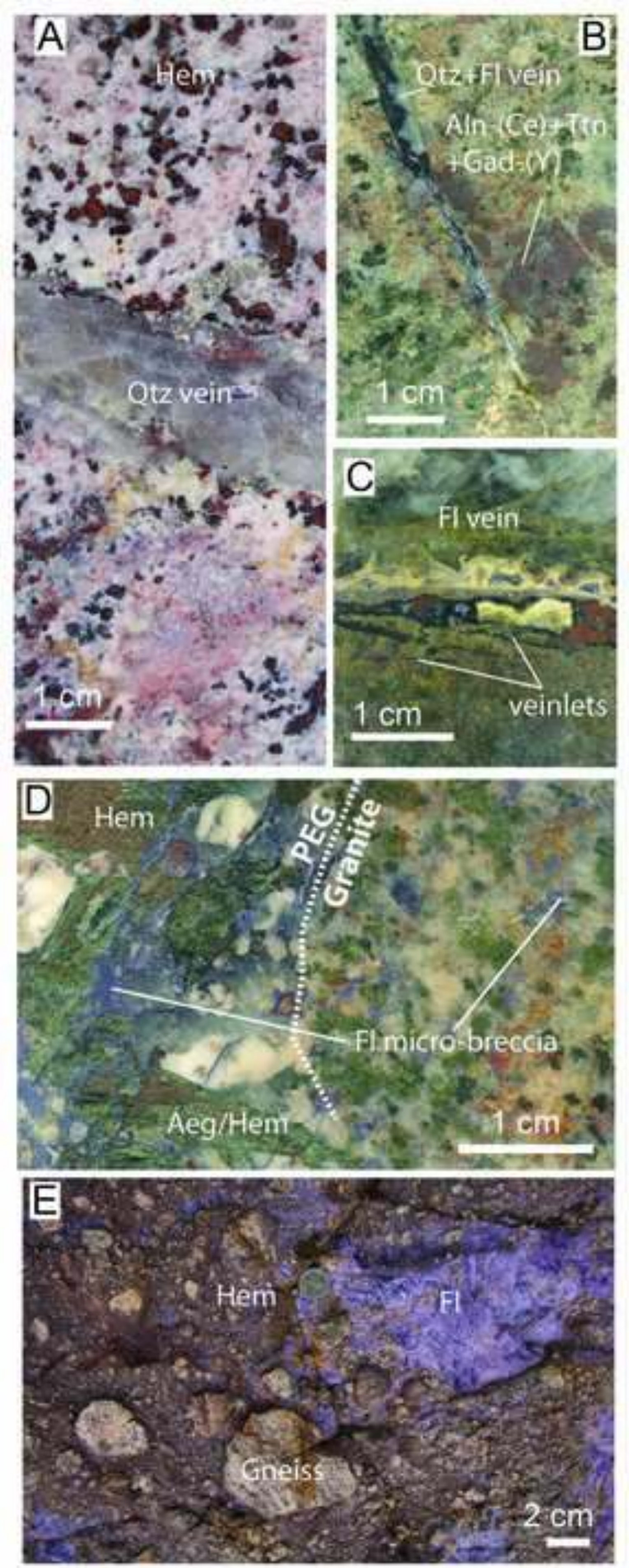

Gysi, A.P., Williams-Jones, A.E., Collins, P., 2016b. Lithogeochemical Vectors for Hydrothermal Processes in the Strange Lake Peralkaline Granitic REE-Zr-Nb Deposit. Econ Geol 111, 1241-1276.
DOI:10.2113/econgeo.111.5.1241.

Figure7

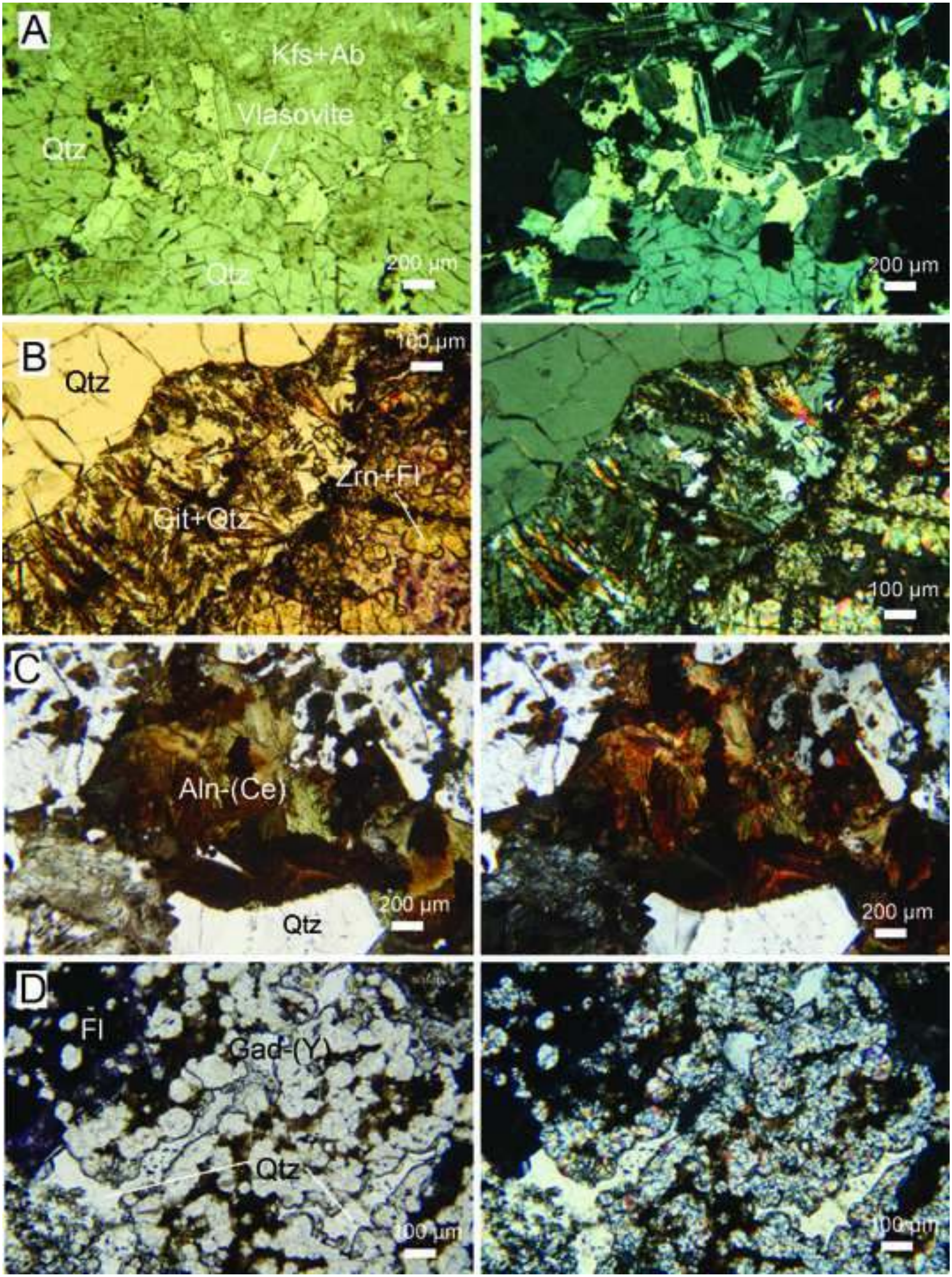

Gysi, A.P., Williams-Jones, A.E., Collins, P., 2016b. Lithogeochemical Vectors for Hydrothermal Processes in the Strange Lake Peralkaline Granitic REE-Zr-Nb Deposit. Econ Geol 111, 1241-1276.
DOI:10.2113/econgeo.111.5.1241.

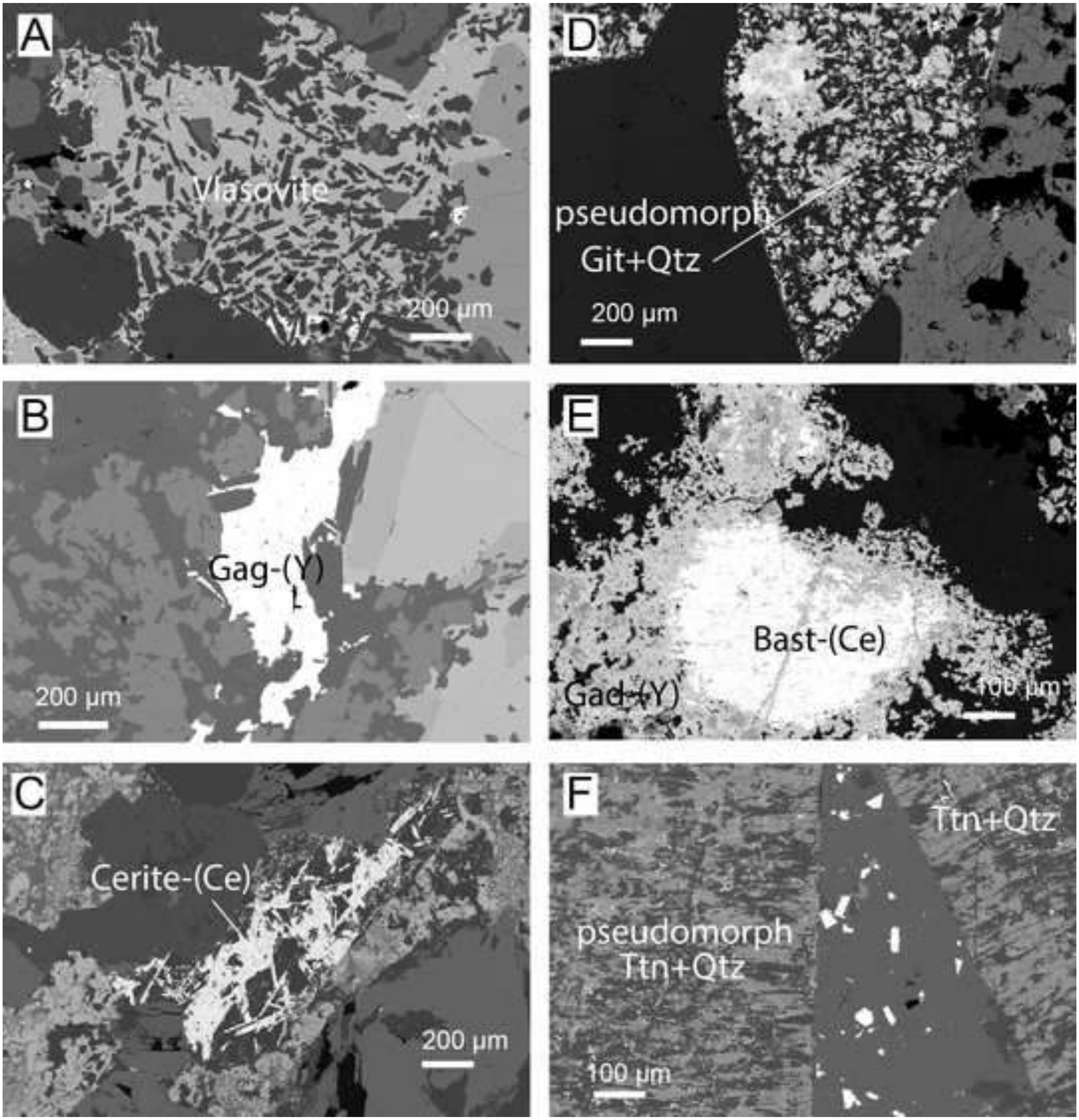

Gysi, A.P., Williams-Jones, A.E., Collins, P., 2016b. Lithogeochemical Vectors for Hydrothermal Processes in the Strange Lake Peralkaline Granitic REE-Zr-Nb Deposit. Econ Geol 111, 1241-1276.
DOI:10.2113/econgeo.111.5.1241.

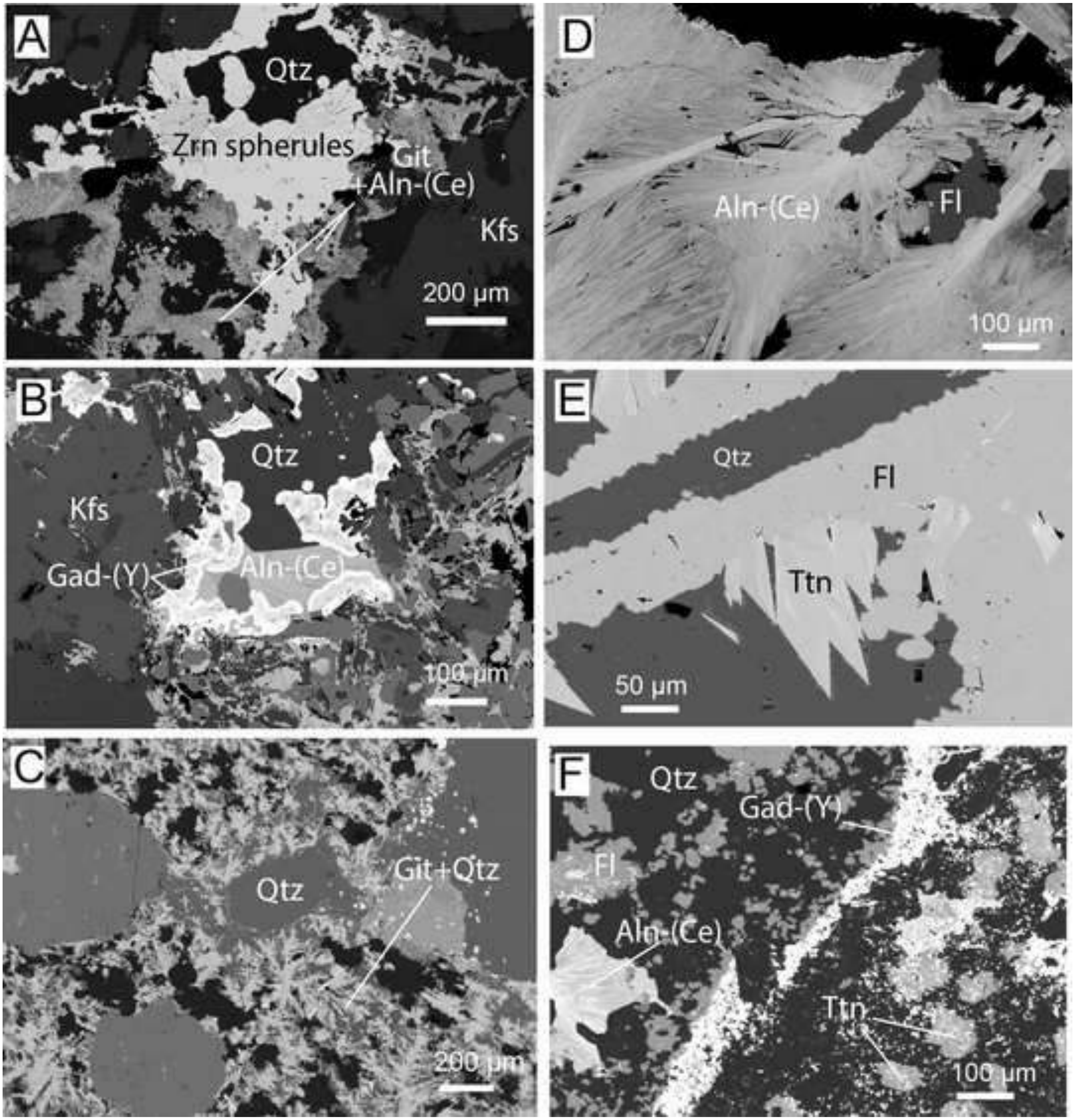

Gysi, A.P., Williams-Jones, A.E., Collins, P., 2016b. Lithogeochemical Vectors for Hydrothermal Processes in the Strange Lake Peralkaline Granitic REE-Zr-Nb Deposit. Econ Geol 111, 1241-1276.
DOI:10.2113/econgeo.111.5.1241.

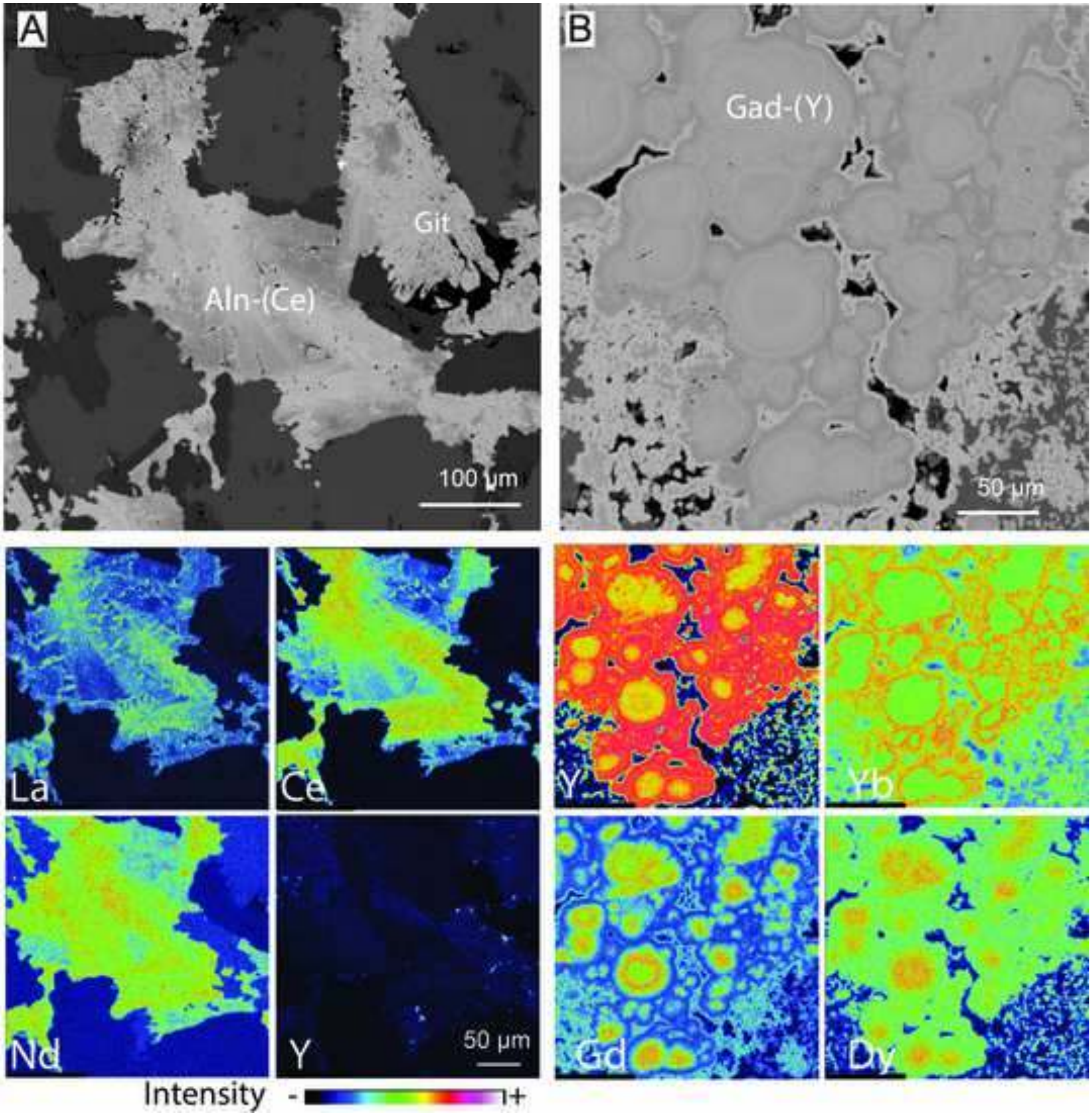

Gysi, A.P., Williams-Jones, A.E., Collins, P., 2016b. Lithogeochemical Vectors for Hydrothermal Processes in the Strange Lake Peralkaline Granitic REE-Zr-Nb Deposit. Econ Geol 111, 1241-1276.
DOI:10.2113/econgeo.111.5.1241.

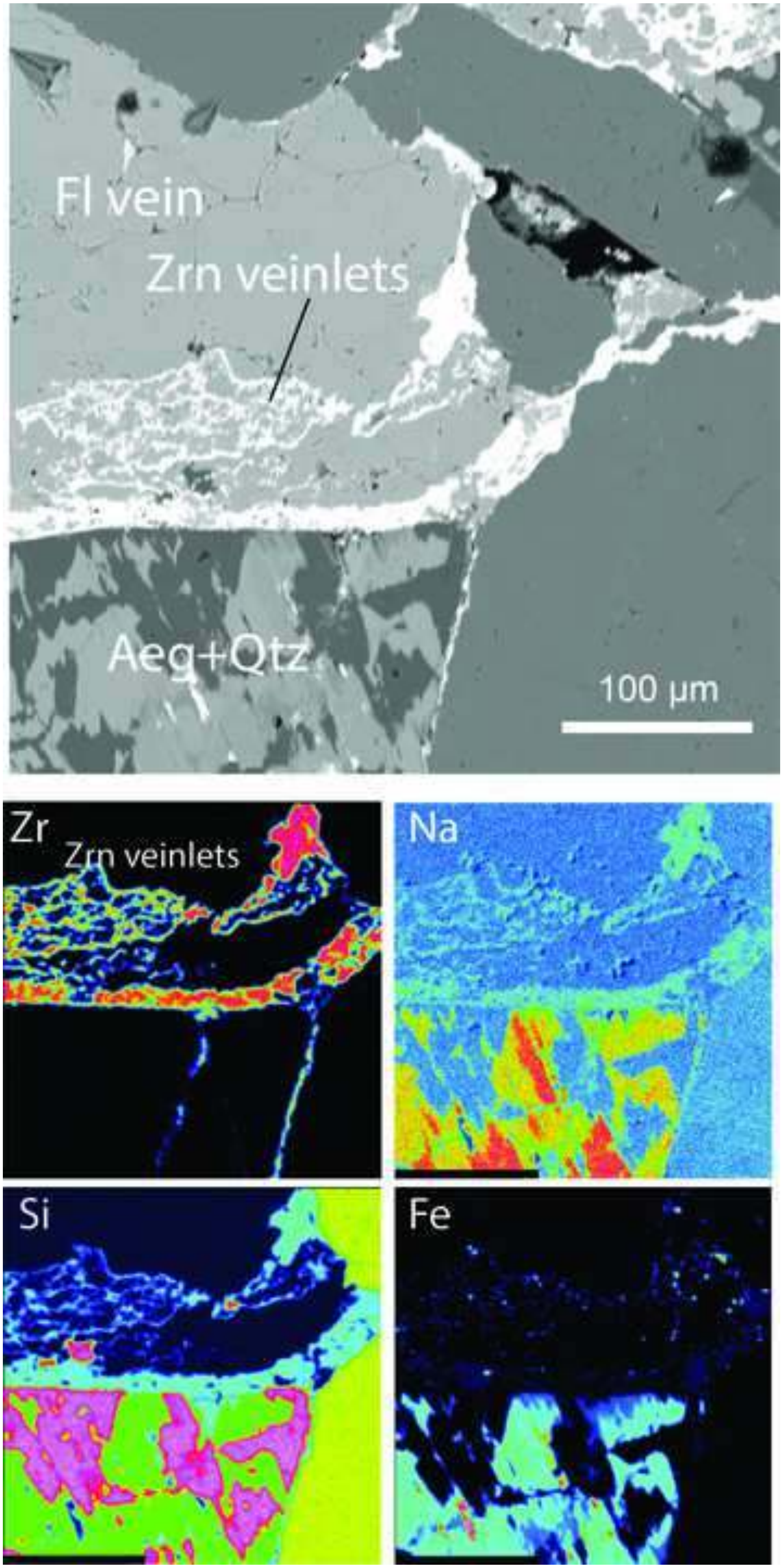

Gysi, A.P., Williams-Jones, A.E., Collins, P., 2016b. Lithogeochemical Vectors for Hydrothermal Processes in the Strange Lake Peralkaline Granitic REE-Zr-Nb Deposit. Econ Geol 111, 1241-1276.
DOI:10.2113/econgeo.111.5.1241.

Figure12

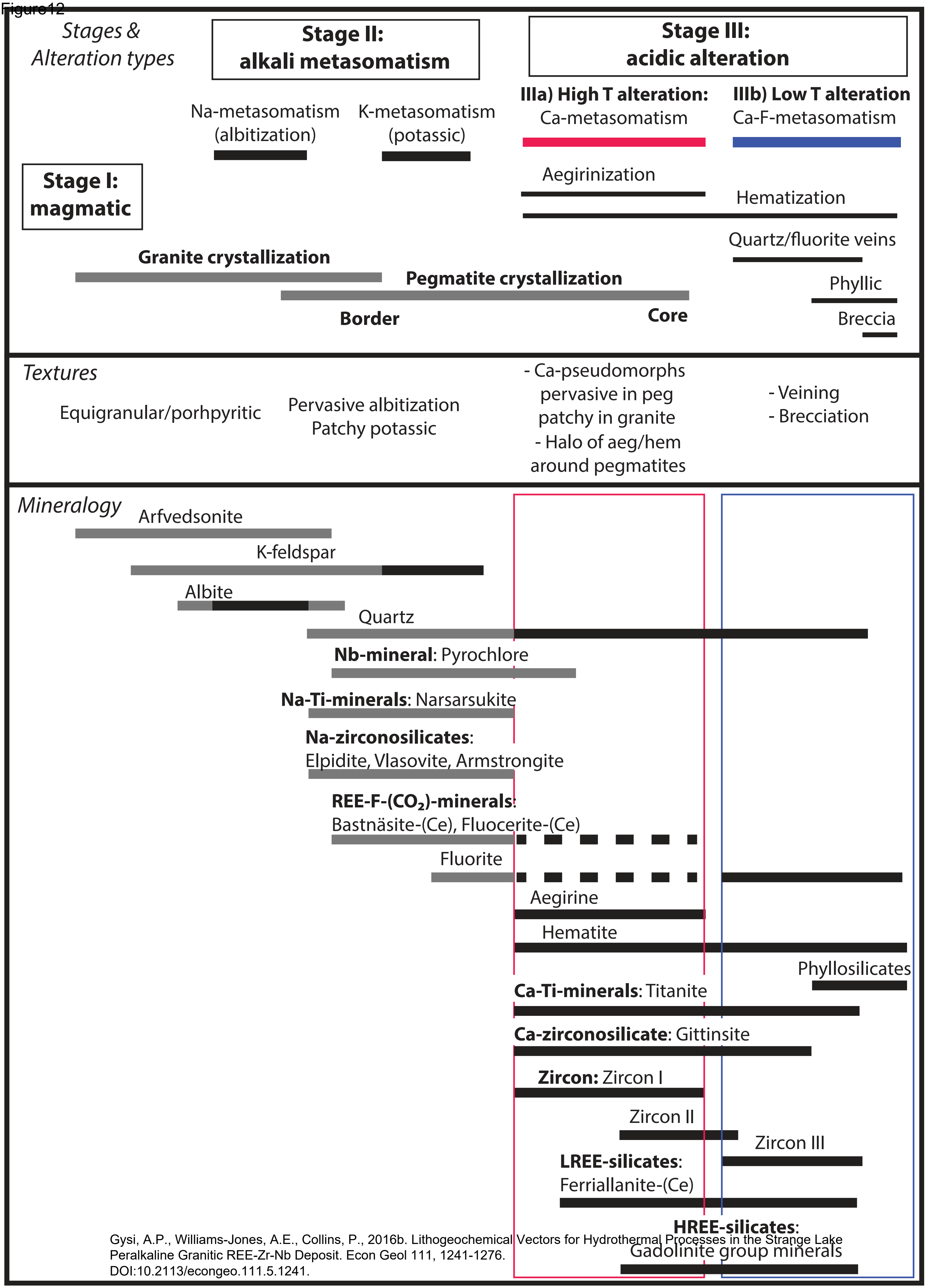

Gysi, A.P., Williams-Jones, A.E., Collins, P., 2016b. Lithogeochemical Vectors for Hydrothermal Processes in the Strange Lake Peralkaline Granitic REE-Zr-Nb Deposit. Econ Geol 111, 1241-1276. DOI:10.2113/econgeo.111.5.1241.

Figure 13

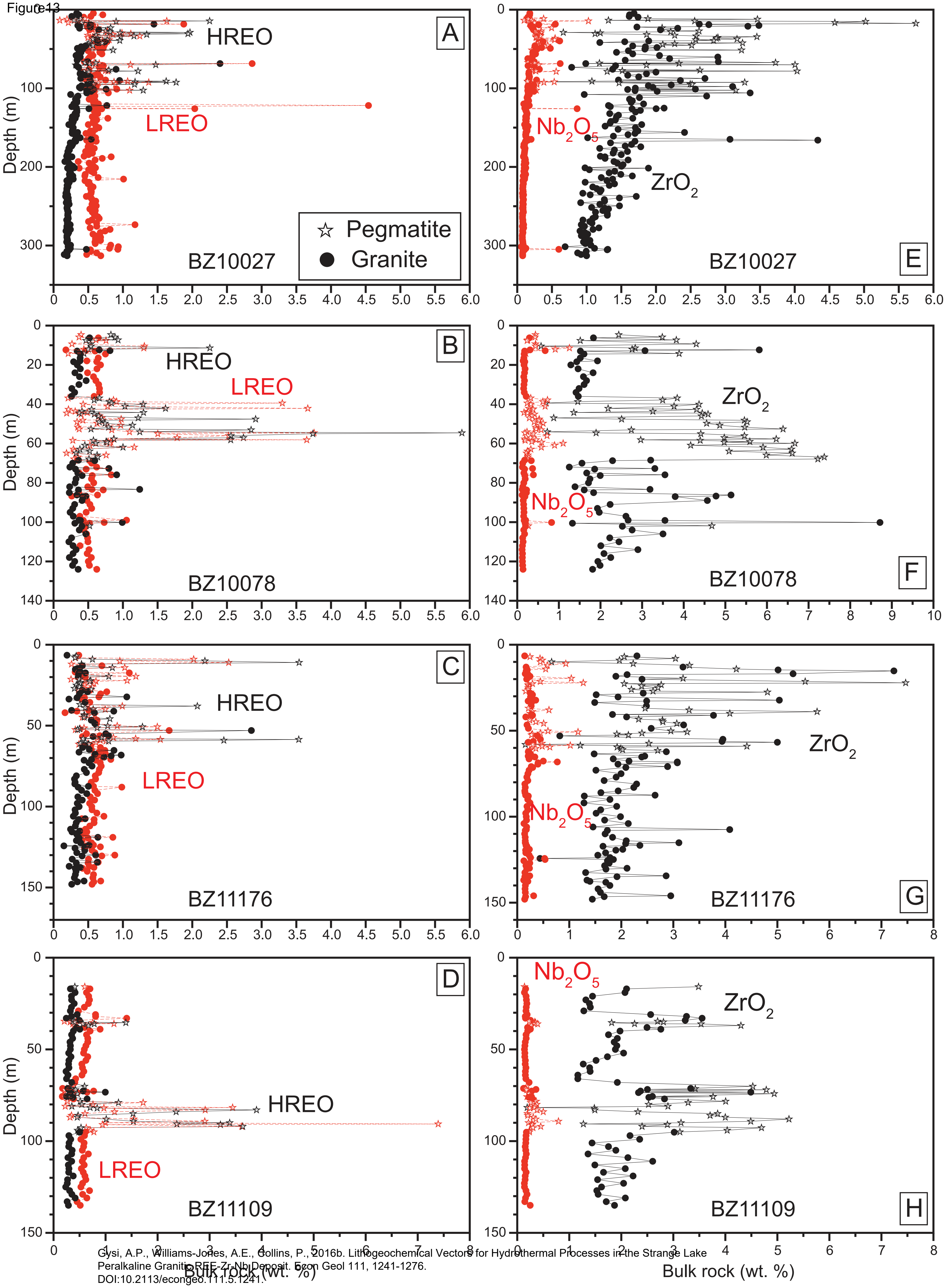

Gysi, A.P., Williams-Jones, A.E., Collins, P., 2016b. Lithogeochemical Vectors for Hydrothermal Processes in the Strange Lake Peralkaline Granitic REE-Zr-Nb Deposit. Econ Geol 111, 1241-1276. DOI:10.2113/econgeo.111.5.1241.

Figure14

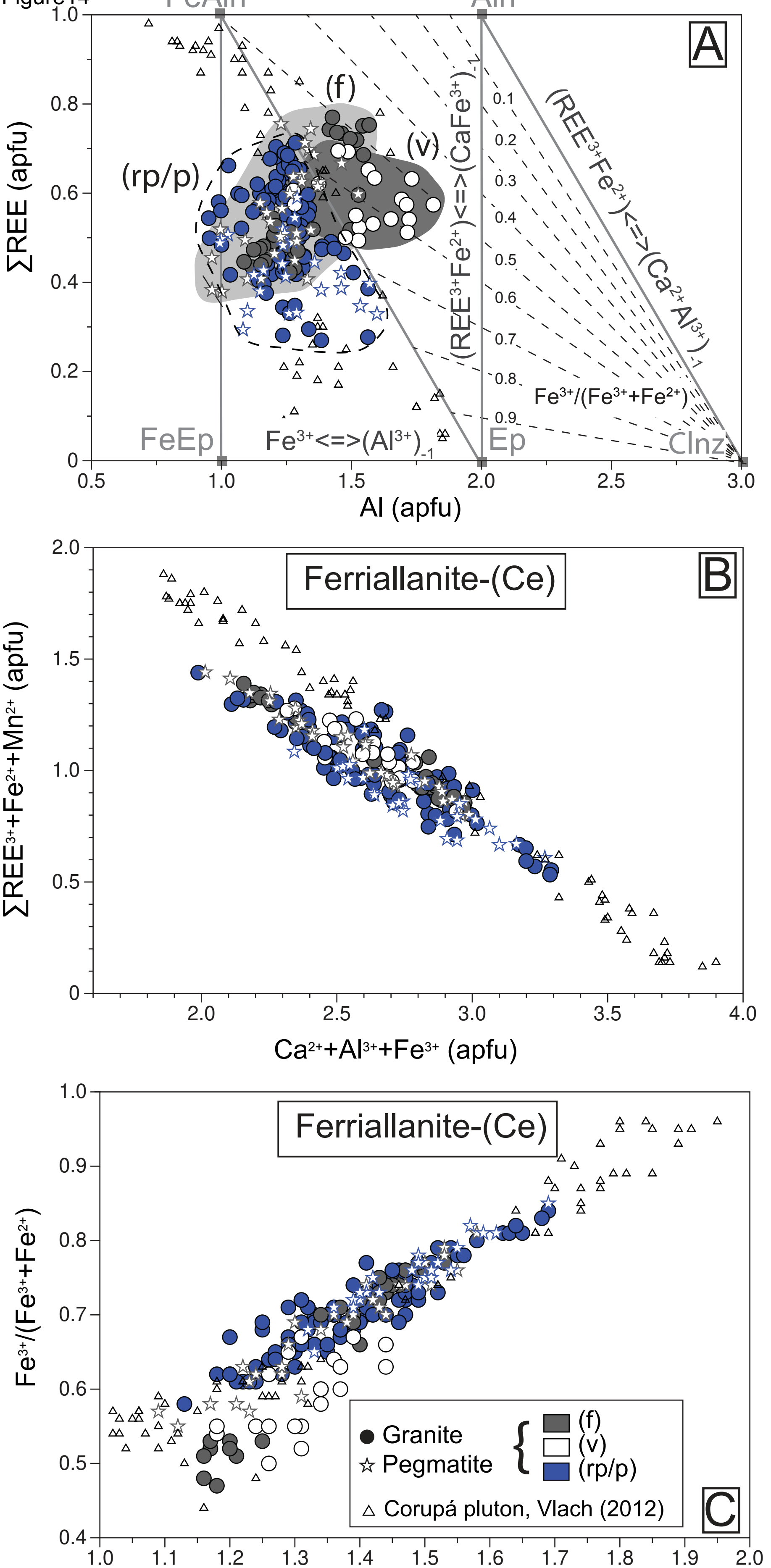

Gysi, A.P., Williams-Jones, A.E., Collins, P., 2016b. Lithogeochemical Vectors
Peralkaline Granitic REE-Zr-Nb Deposit, Econ Geol 111, 1241-1276.
DOI:10.2113/econgeo.111.5.1241.

Figure15

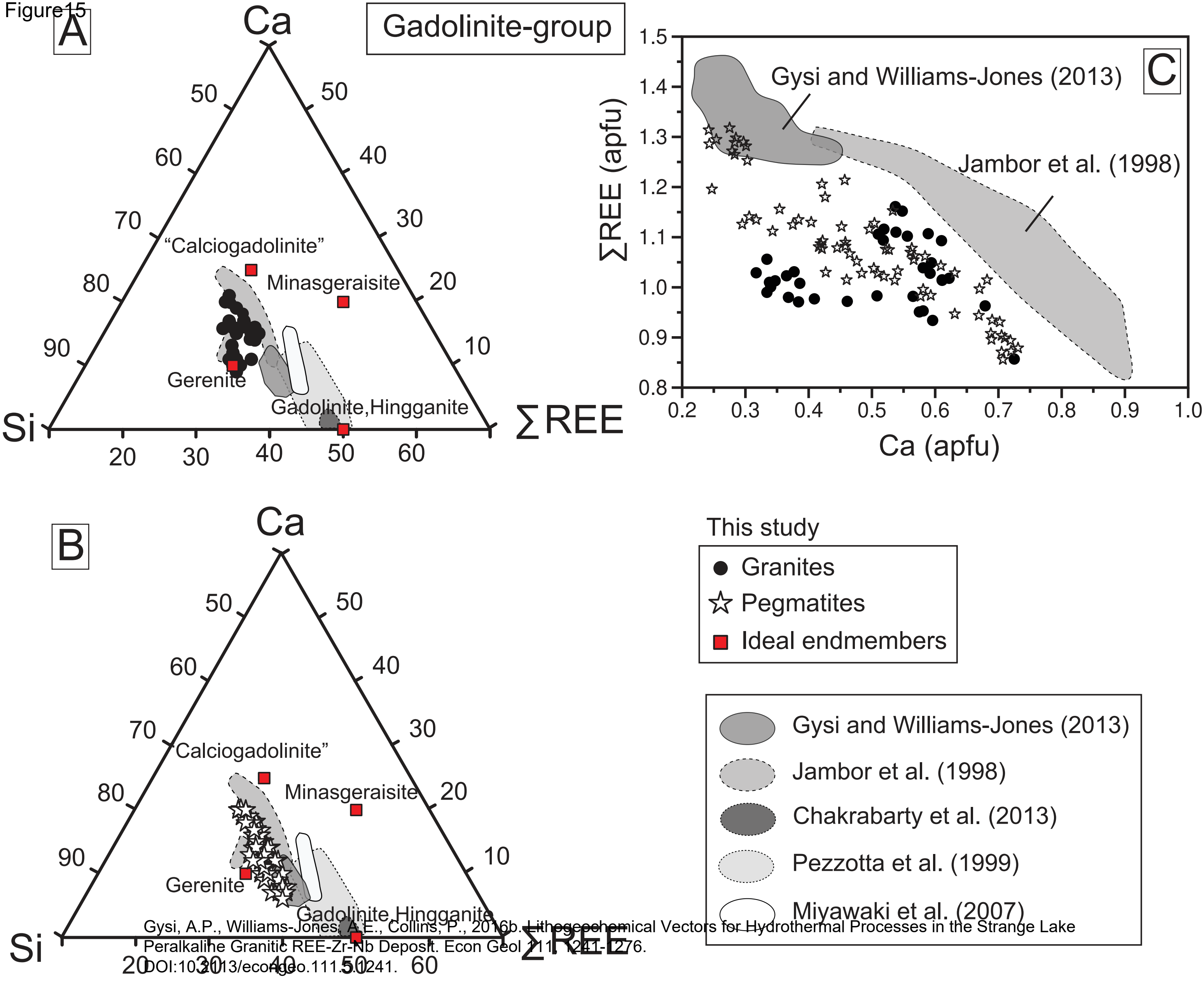

Gysi, A.P., Williams-Jones, A.E., Collins, P., 2016b. Lithogeochemical Vectors for Hydrothermal Processes in the Strange Lake Peralkaline Granitic REE-Zr-Nb Deposit. Econ Geol 111: 1241-1276. DOI:10.2113/econgeo.111.5.1241.

Figure16

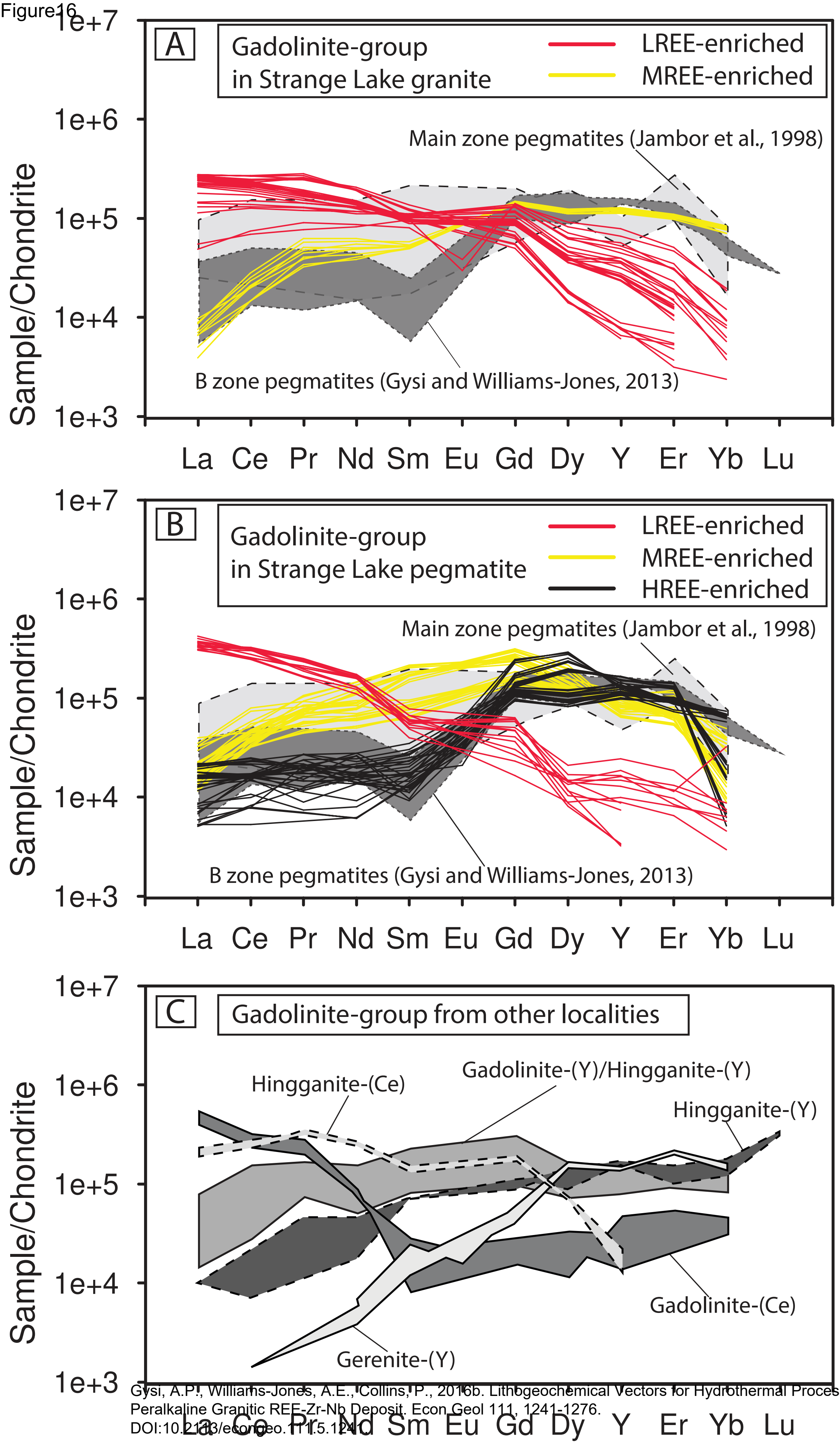

Gysi, A.P., Williams-Jones, A.E., Collins, P., 2016b. Lithogeochemical Vectors for Hydrothermal Processes
Peralkaline Granitic REE-Zr-Nb Deposit. Econ Geol 111, 1241-1276.
DOI:10.2113/econgeo.111.5.1241.

Figure17

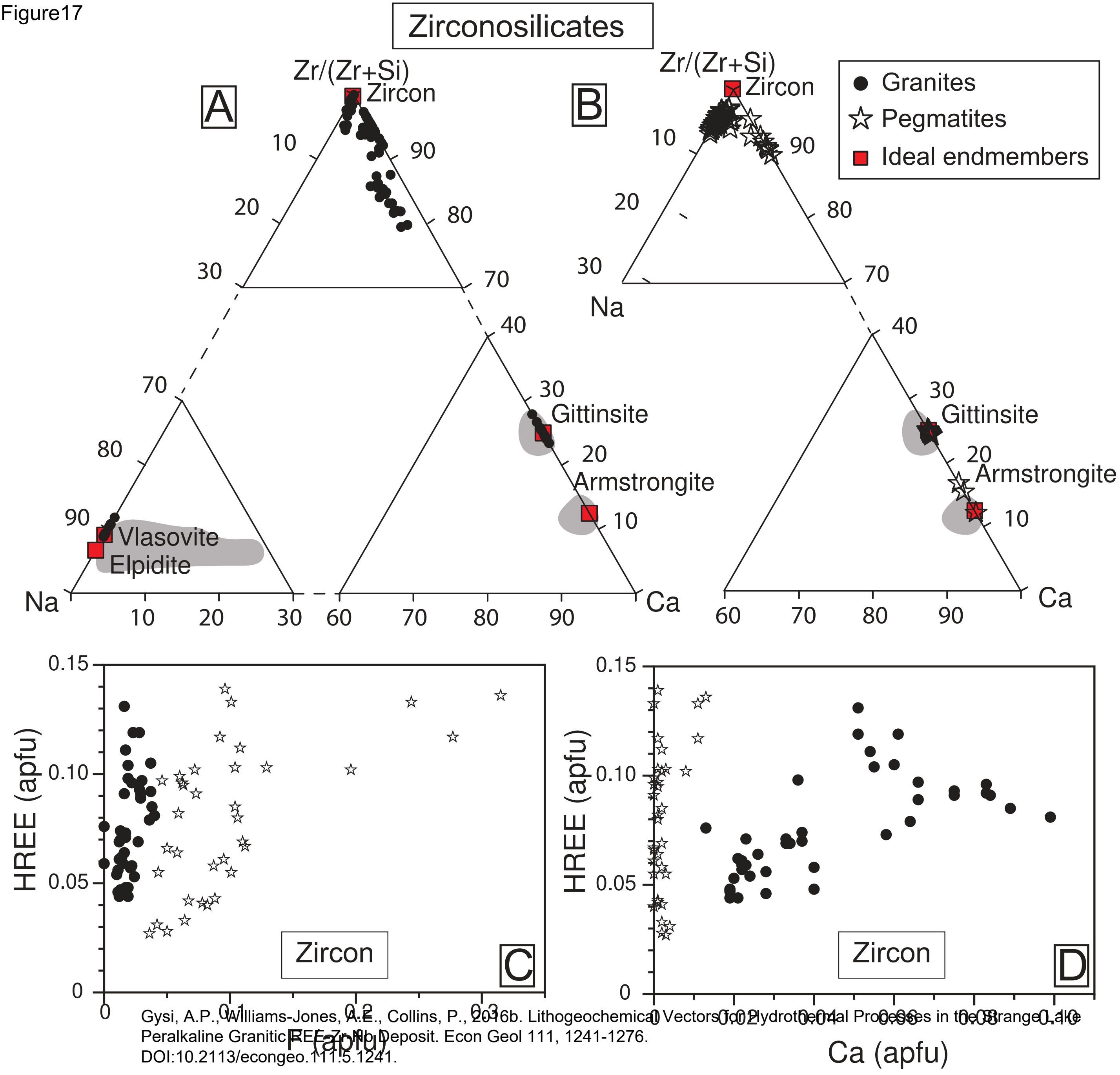

Gysi, A.P., Williams-Jones, A.E., Collins, P., 2016b. Lithogeochemical Vectors for Hydrothermal Processes in the Strange Lake Peralkaline Granitic REE-Zr-Nb Deposit. Econ Geol 111, 1241-1276. DOI:10.2113/econgeo.111.5.1241.

Figure18

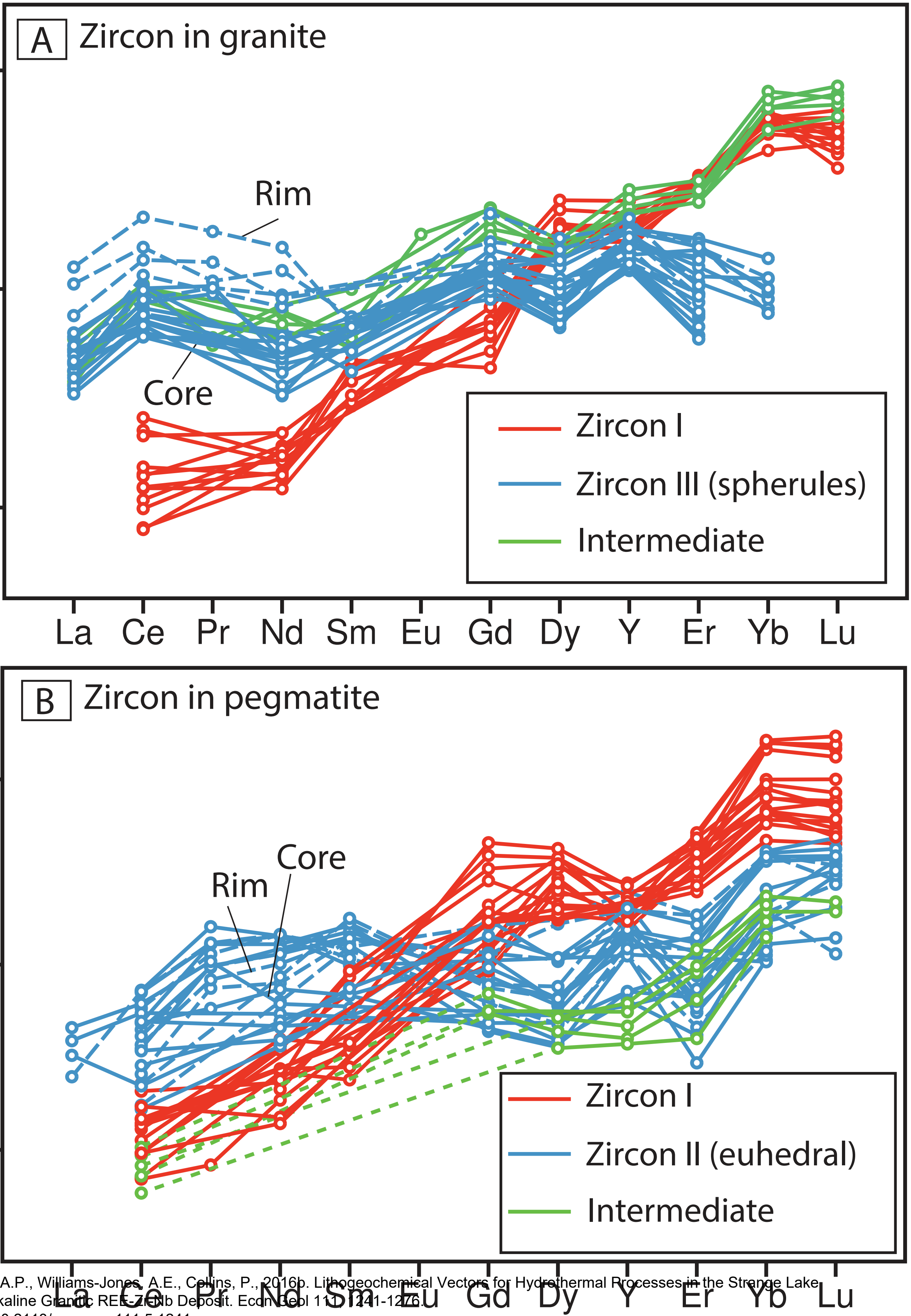

Gysi, A.P., Williams-Jones, A.E., Collins, P., 2016b. Lithogeochemical Vectors for Hydrothermal Processes in the Strange Lake Peralkaline Granitic REE-Zr-Nb Deposit. Econ Geol 111, 1241-1276.
DOI:10.2113/econgeo.111.5.1241.

Figure19

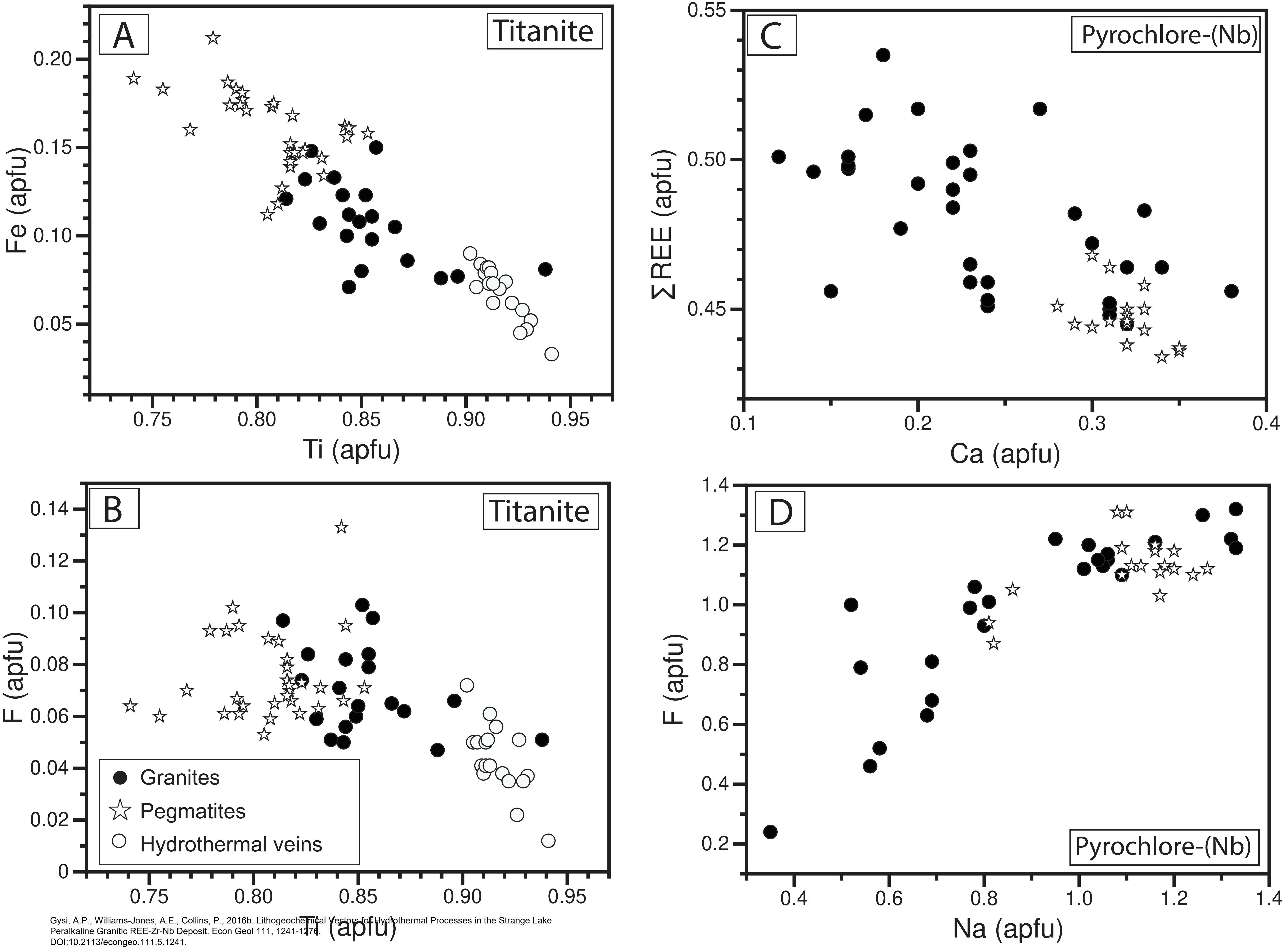

Gysi, A.P., Williams-Jones, A.E., Collins, P., 2016b. Lithogeochemical Vectors for Hydrothermal Processes in the Strange Lake Peralkaline Granitic REE-Zr-Nb Deposit. Econ Geol 111, 1241-1276. DOI:10.2113/econgeo.111.5.1241.

Figure20

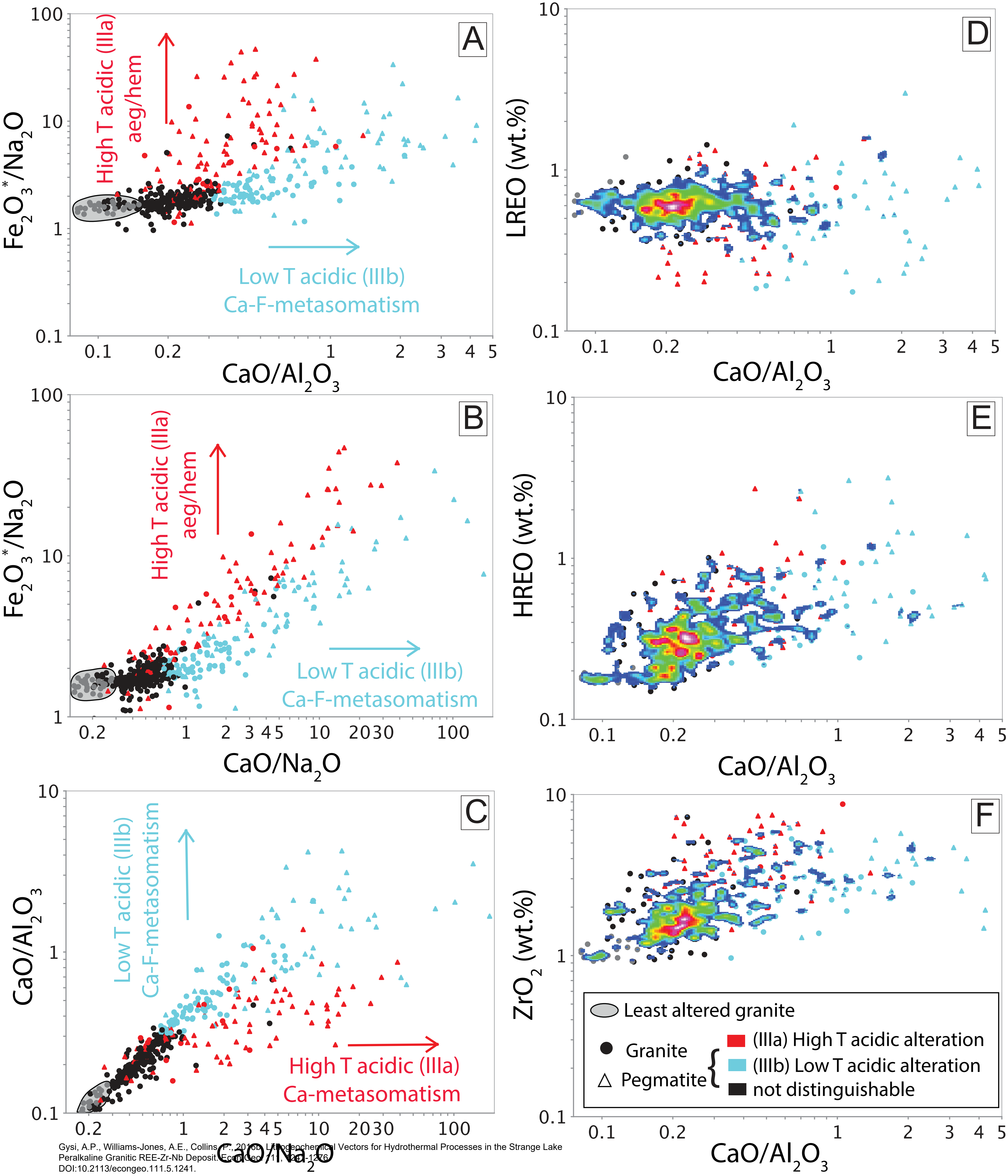

Gysi, A.P., Williams-Jones, A.E., Collins, P., 2016b. Lithogeochemical Vectors for Hydrothermal Processes in the Strange Lake Peralkaline Granitic REE-Zr-Nb Deposit. Econ Geo 111, 1241-1276.
DOI:10.2113/econgeo.111.5.1241.

Figure21

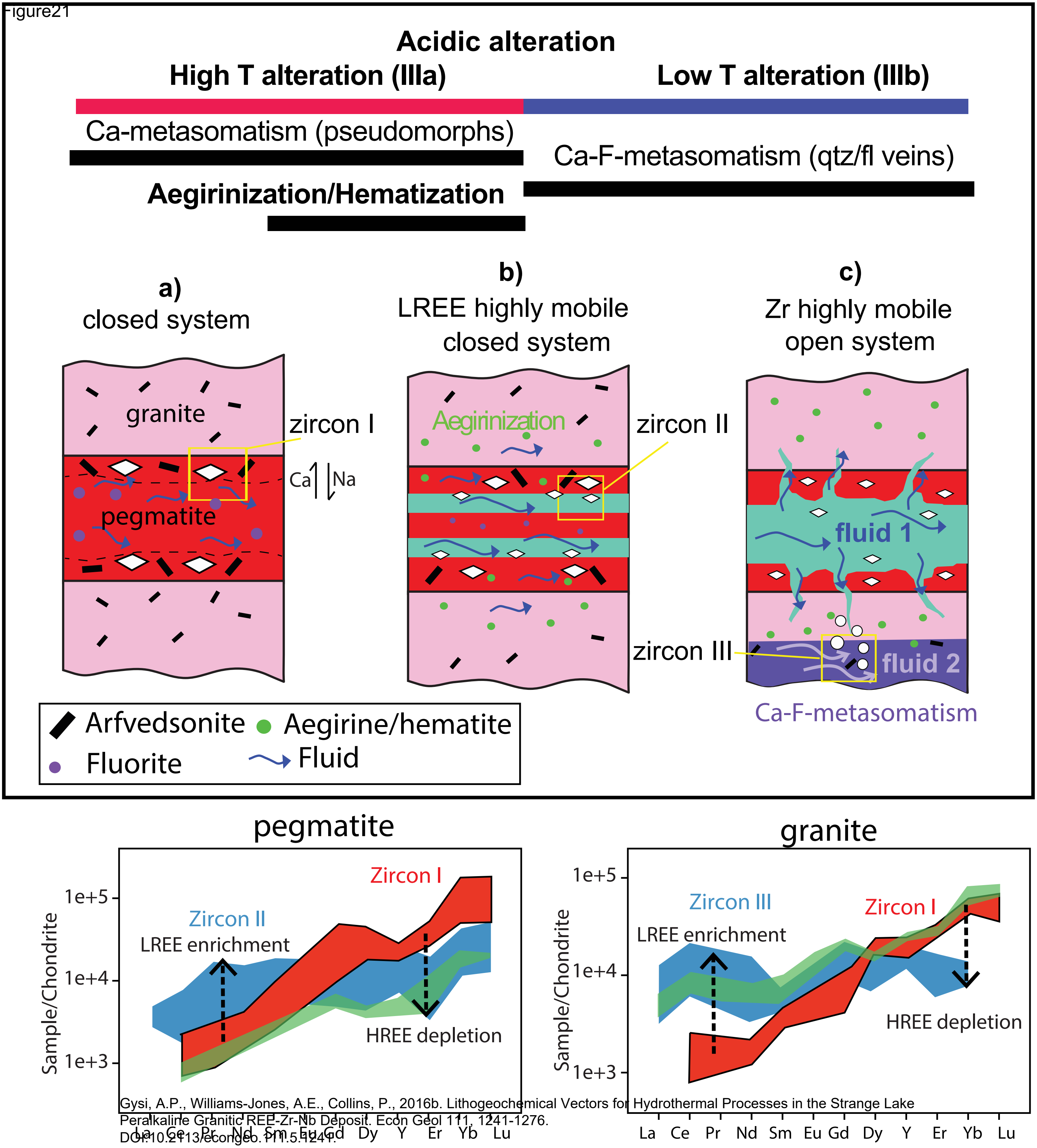

Gysi, A.P., Williams-Jones, A.E., Collins, P., 2016b. Lithogeochemical Vectors for Hydrothermal Processes in the Strange Lake Peralkaline Granitic REE-Zr-Nb Deposit. Econ Geol 111, 1241-1276. DOI:10.2113/econgeo.111.5.1241.

Figure22

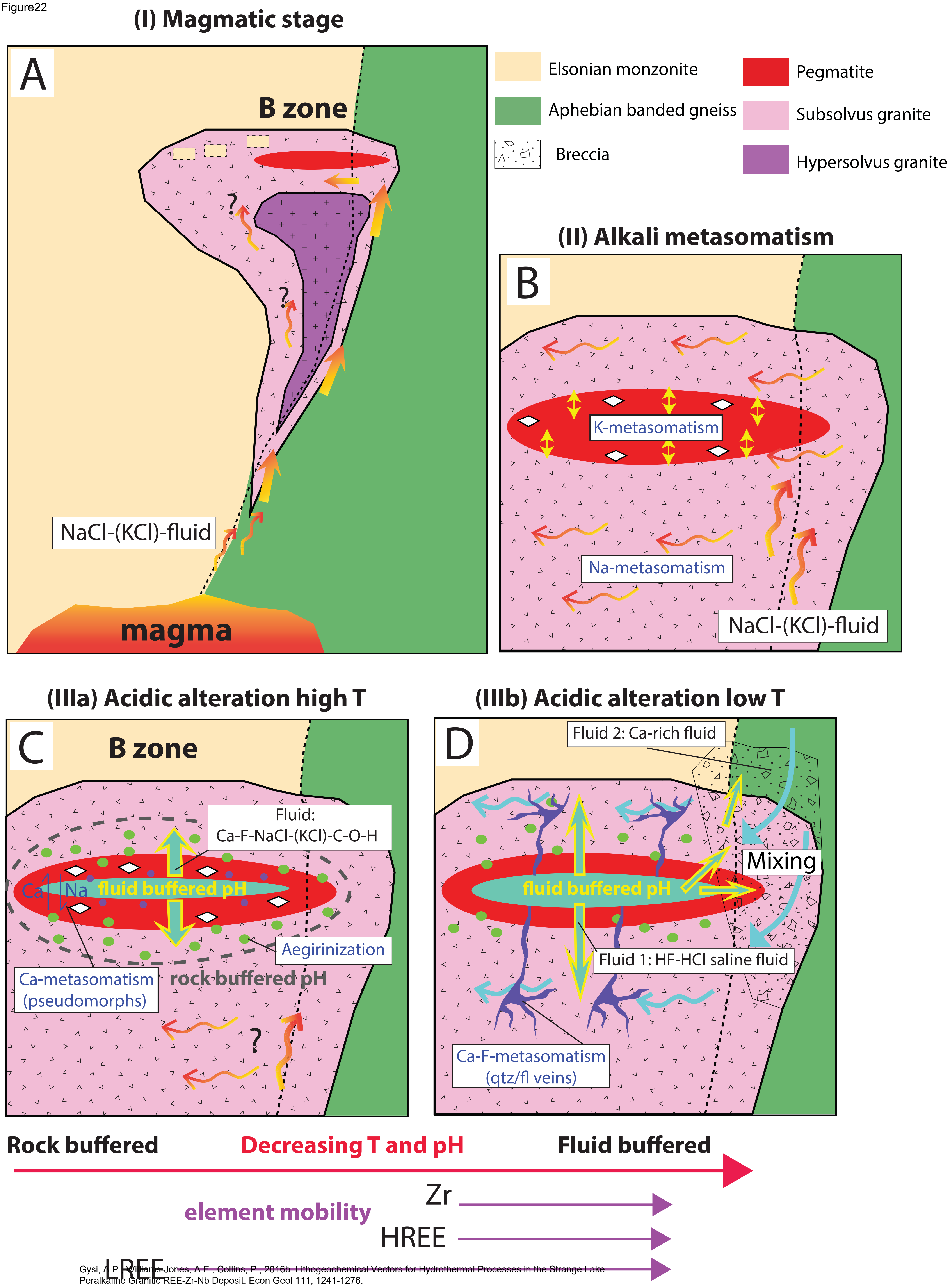

Gysi, A.P., Williams-Jones, A.E., Collins, P., 2016b. Lithogeochemical Vectors for Hydrothermal Processes in the Strange Lake Peralkaline Granitic REE-Zr-Nb Deposit. Econ Geol 111, 1241-1276.
DOI:10.2113/econgeo.111.5.1241.

TABLES

TABLE 1. List of REE/HFSE minerals observed at Strange Lake.

	Ideal formulae	Occurrences
REE-bearing minerals		
REE silicates		
Ferrillanite-(Ce)	$Ca(La,Ce,Nd)AlFe^{2+} Fe^{3+} (Si_2O_7)(SiO_4)O(OH)$	Vein, Gr, Peg
Gadolinite-(Y)	$(Ce,Y)_2Fe^{2+}Be_2Si_2O_{10}$	Vein, Gr, Peg
Gerenite-(Y)	$(Ca,Na)_2Y_3Si_6O_{18} \cdot 2H_2O$	Vein, Peg
Kainosite-(Y)	$Ca_2Y_2(SiO_3)_4(CO_3) \cdot H_2O$	Peg
Cerite-(Ce)	$Ce_9Fe (SiO_4)_6(SiO_3)(OH)_4$	Gr
REE-F-(CO_2)-minerals		
Fluocerite-(Ce)	$(La, Ce, Nd)F_3$	Peg
Bastnäsite-(Ce)	$(La, Ce, Nd)CO_3F$	Peg
Gagarinite-(Y)	$NaCa(Y,Ce)F_6$	Gr
Zr-bearing minerals		
Zircon	$ZrSiO_4$	Vein, Gr, Peg
Gittinsite	$CaZrSi_2O_7$	Vein, Gr, Peg
Elpidite	$Na_2ZrSi_6O_{15} \cdot 3H_2O$	Peg
Vlasovite	$Na_2ZrSi_4O_{11}$	Gr
Nb-bearing minerals		
Pyrochlore-(Nb)	$(Ca,Na)_2(Nb,Ta)_2O_6(OH,F)$	Gr, Peg
Ti-bearing minerals		
Titanite	$CaTiSiO_5$	Vein, Gr, Peg
Narsarsukite	$Na_2(Ti,Fe^{3+})Si_4O_{10}(O,F)$	Peg, Gr

Gr: granite; Peg: pegmatite.

Gysi, A.P., Williams-Jones, A.E., Collins, P., 2016b. Lithogeochemical Vectors for Hydrothermal Processes in the Strange Lake Peralkaline Granitic REE-Zr-Nb Deposit. Econ Geol 111, 1241-1276.
DOI:10.2113/econgeo.111.5.1241.

TABLE 2. Average EMP analyses (in wt. %) of hydrothermal ferriallanite-(Ce) from Strange Lake granites, pegmatites (Peg) and quartz/fluorite veins. Type corresponds to micro-fractures (f), pore space fillings (p), mineral replacement reactions (rp) and veining (v).

Sample	**SL11-59**	2σ	**SL11-62**	2σ	**SL11-55**	2σ	**SL11-60**	2σ	**SL11-155**	2σ	**SL11-148**	2σ	**SL11-154**	2σ	**SL11-158**	2σ
Rock	Granite		Granite		Granite		Granite		Granite		Granite		Granite		Granite	
Type	(p)		(p)		(rp)		(p)		(p)		(f)		(rp)		(rp)	
Nr.	3		5		10		10		15		10		22		26	
SiO_2	31.7	0.7	33.9	0.8	33.0	0.6	32.8	0.7	33.4	1.0	32.6	0.6	33.1	1.9	34.5	1.1
Al_2O_3	11.2	0.6	12.9	2.7	11.5	1.2	11.7	1.6	11.2	2.7	13.8	1.2	11.6	2.5	12.5	1.7
TiO_2	d.l.		0.11	0.12	0.20	0.19	0.23	0.33	0.33	0.54	0.53	0.30	0.37	0.63	0.25	0.21
FeO	20.7	0.4	18.1	3.1	19.6	2.6	20.9	1.8	21.4	3.5	13.7	1.2	19.7	3.2	16.8	4.1
MnO	0.29	0.08	0.52	0.31	0.59	0.40	0.27	0.22	0.37	0.24	0.91	0.34	0.44	0.45	2.20	1.67
CaO	13.4	0.3	15.0	2.0	13.6	1.7	14.3	1.9	15.0	1.6	12.2	1.3	14.7	4.2	14.5	3.0
Na_2O	d.l.		d.l.		d.l.		d.l.		d.l.		d.l.		d.l.		0.60	0.50
F	d.l.		d.l.		d.l.		0.55		0.10	0.04	0.21	0.07	0.13	0.04	0.14	0.08
Y_2O_3	d.l.		d.l.		d.l.		0.32		0.23	0.14			0.24	0.22	0.13	0.16
La_2O_3	6.69	1.45	7.43	2.48	7.92	4.25	5.17	1.31	3.95	1.15	7.34	4.38	4.21	2.95	4.36	2.22
Ce_2O_3	8.66	1.01	6.57	1.50	8.28	1.51	8.21	2.03	8.25	1.89	11.6	1.9	8.27	5.45	8.57	3.22
Pr_2O_3	0.57	0.22	0.24	0.16	0.45	0.24	0.68	0.26	0.60	0.13	0.90	0.60	0.62	0.31	0.84	0.25
Nd_2O_3	1.96	0.68	0.41	0.22	1.01	1.12	1.76	0.92	1.74	0.40	1.54	1.38	2.01	0.76	1.81	0.40
Sm_2O_3	d.l.		d.l.		d.l.		d.l.		0.12	0.03	d.l.		0.19	0.16	0.12	0.03
Eu_2O_3	0.27	0.03	d.l.		0.44	0.06	d.l.		d.l.		d.l.		d.l.		0.13	0.11
Gd_2O_3	d.l.		d.l.		d.l.		d.l.		0.10	0.03	d.l.		0.16	0.09	d.l.	
Total	95.4		95.3		96.2		96.1		96.5		95.3		95.8		96.6	
$^1Fe^{3+}/Fe^{3+}+Fe^{2+}$	0.64		0.71		0.67		0.69		0.73		0.52		0.70		0.71	
$^2REE^{3+}+Fe^{2+}+Mn^{2+}$	1.240		0.899		1.130		1.038		0.948		1.296		0.996		1.014	
$^2Ca^{2+}+Fe^{3+}+Al^{3+}$	2.657		2.724		2.543		2.772		2.800		2.248		2.712		2.509	
^{2}sumREE	0.628		0.476		0.589		0.531		0.488		0.721		0.524		0.501	
$^2Al^{3+}$	1.250		1.347		1.230		1.261		1.184		1.495		1.235		1.283	

The uncertainties (2σ) represent the standard deviation of average mineral analyses with Nr. representing the number of analyzed mineral spots per thin section; (d.l.) below detection limit. The concentrations of K, Dy, Er, and Yb not reported here were all below detection limit.

[1] Fe^{3+} and Fe^{2+} calculated based on the method by Petrik et al. (1995). [2] apfu calculated from mineral formulae based on 3 Si.

Gysi, A.P., Williams-Jones, A.E., Collins, P., 2016b. Lithogeochemical Vectors for Hydrothermal Processes in the Strange Lake Peralkaline Granitic REE-Zr-Nb Deposit. Econ Geol 111, 1241-1276.
DOI:10.2113/econgeo.111.5.1241.

TABLE 2. (Continued)

Sample	**SL11-58**	2σ	**SL12-47**	2σ	**SL12-49**	2σ	**SL11-65**	2σ	**SL11-111**	2σ	**SL11-97**	2σ	**SL11-100**	2σ	**SL11-106**	2σ
Rock	Granite		Qtz/Fl vein		Qtz/Fl vein		Granite		Peg		Peg		Peg		Peg	
Type	(f)		(v)		(v)		(p)		(p)		(f)		(f)		(rp)	
Nr.	18		12		7		5		3		5		9		3	
SiO_2	33.7	0.7	33.8	1.0	33.3	0.8	33.2	0.4	32.4	0.0	33.0	0.4	33.4	0.7	33.5	1.8
Al_2O_3	11.6	1.7	15.7	2.5	13.5	2.4	9.8	1.3	9.2	0.3	11.5	1.6	10.0	1.6	12.1	2.4
TiO_2	0.13	0.12	0.20	0.44	0.33	0.56	0.42	0.38	0.06	0.04	0.07	0.04	0.30	0.26	0.24	0.58
FeO	21.7	2.1	15.6	2.3	17.1	1.6	21.9	3.2	22.0	0.6	19.9	1.1	21.5	2.6	20.4	3.2
MnO	0.37	0.14	0.29	0.18	0.60	0.15	0.23	0.05	0.48	0.13	1.23	0.19	1.53	0.53	0.77	0.47
CaO	15.0	1.4	13.5	1.7	14.1	1.7	13.4	2.1	15.1	0.2	14.8	2.3	15.5	1.7	15.3	3.1
Na_2O	d.l.		d.l.		d.l.		0.17	0.08	d.l.		d.l.		d.l.		d.l.	
F	d.l.		d.l.		d.l.		d.l.		d.l.		d.l.		0.11		d.l.	
Y_2O_3	0.27	0.17	0.13	0.07	0.16	0.12	0.37	0.22	d.l.		d.l.		0.73	0.07	0.12	0.02
La_2O_3	4.79	1.96	7.44	3.48	10.5	3.8	3.42	1.40	2.23	0.26	9.33	2.57	3.60	1.36	4.91	3.66
Ce_2O_3	6.74	1.07	8.98	0.86	5.43	1.09	8.71	1.78	9.21	0.33	4.58	1.78	7.66	1.89	7.37	2.40
Pr_2O_3	0.62	0.20	0.56	0.22	0.23	0.10	0.95	0.21	1.01	0.05	0.16	0.05	0.52	0.08	0.52	0.12
Nd_2O_3	1.88	0.62	1.09	0.69	0.32	0.27	3.00	0.50	2.28	0.06	0.63	0.15	1.48	0.17	1.28	0.45
Sm_2O_3	0.17	0.12	d.l.		d.l.		0.37	0.17	d.l.		d.l.		d.l.		d.l.	
Eu_2O_3	0.12	0.04	0.14	0.04	0.15	0.06	d.l.		d.l.		d.l.		0.11	0.05	d.l.	
Gd_2O_3	0.15	0.09	d.l.		d.l.		0.28	0.11	d.l.		d.l.		0.17	0.02	d.l.	
Total	97.2		97.5		95.5		96.1		94.0		95.0		95.8		96.5	
[1]$Fe^{3+}/Fe^{3+}+Fe^{2+}$	0.73		0.57		0.65		0.71		0.75		0.72		0.77		0.73	
[2]$REE^{3+}+Fe^{2+}+Mn^{2+}$	0.944		1.096		1.056		1.063		0.960		1.003		0.936		0.938	
[2]$Ca^{2+}+Fe^{3+}+Al^{3+}$	2.830		2.612		2.622		2.514		2.782		2.759		2.803		2.856	
[2]sumREE	0.481		0.578		0.554		0.568		0.497		0.491		0.448		0.467	
[2]Al^{3+}	1.215		1.649		1.434		1.040		1.006		1.228		1.057		1.279	

Gysi, A.P., Williams-Jones, A.E., Collins, P., 2016b. Lithogeochemical Vectors for Hydrothermal Processes in the Strange Lake Peralkaline Granitic REE-Zr-Nb Deposit. Econ Geol 111, 1241-1276.
DOI:10.2113/econgeo.111.5.1241.

TABLE 2. (Continued)

Sample	**SL11-104**	2σ	**SL11-170b**	2σ	**SL11-146**	2σ
Rock	Peg		Peg		Peg	
Type	(rp)		(rp)		(p)	
Nr.	5		15		18	
SiO_2	34.4	0.9	34.7	1.1	33.9	0.9
Al_2O_3	12.9	3.6	12.7	3.2	12.7	1.5
TiO_2	0.15	0.31	0.04	0.01	0.12	0.19
FeO	20.6	5.1	17.5	4.1	17.1	2.6
MnO	0.74	0.55	1.73	0.79	1.41	0.80
CaO	16.9	1.6	15.5	1.7	13.4	2.4
Na_2O	d.l.		d.l.		d.l.	
F	d.l.		0.13	0.05	0.15	0.10
Y_2O_3	0.13		0.17	0.20	d.l.	
La_2O_3	2.82	1.31	4.06	1.39	6.66	4.17
Ce_2O_3	5.57	1.08	7.82	2.13	9.38	2.16
Pr_2O_3	0.49	0.14	0.62	0.18	0.97	0.21
Nd_2O_3	1.60	0.57	1.26	0.31	2.13	1.34
Sm_2O_3	0.15	0.15	0.08	0.03	0.13	0.09
Eu_2O_3	d.l.		0.08	0.02	d.l.	
Gd_2O_3	d.l.		0.10	0.03	d.l.	
Total	96.3		96.1		97.9	
[1]$Fe^{3+}/Fe^{3+}+Fe^{2+}$	0.79		0.74		0.63	
[2]$REE^{3+}+Fe^{2+}+Mn^{2+}$	0.696		0.893		1.194	
[2]$Ca^{2+}+Fe^{3+}+Al^{3+}$	3.108		2.666		2.393	
[2]sumREE	0.338		0.442		0.622	
[2]Al^{3+}	1.325		1.290		1.326	

Gysi, A.P., Williams-Jones, A.E., Collins, P., 2016b. Lithogeochemical Vectors for Hydrothermal Processes in the Strange Lake Peralkaline Granitic REE-Zr-Nb Deposit. Econ Geol 111, 1241-1276.
DOI:10.2113/econgeo.111.5.1241.

TABLE 3. Average EMP analyses (in wt. %) of hydrothermal gadolinite-group minerals from Strange Lake granites and pegmatites (Peg). Group corresponds to REE profiles in Fig. 16.

	SL11-151	2σ	**SL11-158**	2σ	**SL11-58a**	2σ	**SL11-58b**	2σ	**SL11-111a**	2σ	**SL11-111b**	2σ	**SL-11-105**	2σ
Rock	Granite		Granite		Granite		Granite		Peg		Peg		Peg	
Group	LREE		MREE		MREE		MREE		LREE		HREE		LREE	
Nr.	6		9		13		7		9		11		4	
SiO_2	31.3	0.4	32.2	1.5	32.3	1.1	32.2	1.0	30.6	1.6	32.7	1.3	30.3	0.6
TiO_2	d.l.		0.04	0.01	0.34	0.09	0.32	0.09	d.l.		0.06	0.03	0.08	0.01
Al_2O_3	0.13	0.22	0.62	0.95	0.19	0.34	0.12	0.09	0.29	0.19	0.06	0.03	0.30	0.66
FeO	0.92	0.19	0.64	0.28	1.36	0.21	2.19	0.55	1.25	4.61	0.60	0.17	2.65	1.06
MnO	0.83	0.06	0.64	0.12	0.09	0.03	0.16	0.08	1.09	0.30	0.59	0.23	0.70	0.06
CaO	8.79	0.41	8.20	0.81	5.52	1.19	9.09	2.33	5.13	2.17	4.23	0.56	7.84	1.14
Na_2O	0.13	0.03	0.21	0.05	1.28	0.34	0.56	0.36	0.63	0.34	0.88	0.16	0.23	0.10
F	0.41	0.13	0.26	0.11	0.41	0.12	0.30	0.08	0.61	1.09	0.28	0.11	0.39	0.06
Y_2O_3	1.47	0.39	24.0	2.3	5.80	2.27	10.9	5.2	1.96	2.82	29.6	6.2	2.95	1.46
La_2O_3	7.33	0.59	0.19	0.10	6.68	1.08	3.20	2.67	9.78	2.09	0.46	0.35	9.27	1.42
Ce_2O_3	18.2	2.0	1.43	0.69	15.3	2.3	8.72	5.38	21.9	3.3	1.32	0.98	18.5	1.7
Pr_2O_3	2.79	0.31	0.49	0.22	1.90	0.25	1.27	0.55	2.39	0.66	0.18	0.14	2.11	0.43
Nd_2O_3	10.2	0.3	2.62	0.84	7.43	0.77	5.81	2.00	8.03	2.40	0.86	0.87	8.02	1.98
Sm_2O_3	1.87	0.44	0.89	0.09	1.63	0.19	1.75	0.38	1.02	0.28	0.21	0.11	0.92	0.41
Eu_2O_3	d.l.		d.l.		d.l.		0.22	0.08	d.l.		0.21	0.09	d.l.	
Gd_2O_3	1.34	0.32	3.26	0.18	2.12	0.38	3.01	0.34	1.18	0.44	3.95	1.99	0.55	0.27
Dy_2O_3	0.45	0.11	3.28	0.28	1.10	0.20	1.93	0.75	0.37	0.23	6.47	2.34	0.36	0.16
Er_2O_3	0.09	0.05	1.89	0.14	0.26	0.12	0.64	0.36	0.20	0.20	2.36	0.24	0.20	0.08
Yb_2O_3	0.04		1.40	0.17	0.11	0.08	0.22	0.19	0.09	0.07	0.27	0.26	0.25	0.46
Total	86.3		82.2		83.9		82.6		86.5		85.1		85.3	
[1]Si (apfu)	2.000		2.000		2.000		2.000		2.000		2.000		2.000	
[1]Σ REE	1.027		1.116		1.005		0.946		1.128		1.287		1.068	
[1]Ca	0.602		0.547		0.366		0.604		0.361		0.277		0.555	

The uncertainties (2σ) represent the standard deviation of average mineral analyses with Nr. representing the number of analyzed mineral spots per thin section; (d.l.) below detection limit. The concentrations of K and Lu not reported here were all below detection limit. [1] apfu calculated from mineral formulae based on 2 Si.

Gysi, A.P., Williams-Jones, A.E., Collins, P., 2016b. Lithogeochemical Vectors for Hydrothermal Processes in the Strange Lake Peralkaline Granitic REE-Zr-Nb Deposit. Econ Geol 111, 1241-1276.
DOI:10.2113/econgeo.111.5.1241.

TABLE 3. (Continued)

	SL-11-100	2σ	**SL-11-104**	2σ	**SL-11-170a**	2σ	**SL-11-170b**	2σ	**SL12-44**	2σ
Rock	Peg		Peg		Peg		Peg		Peg	
Group	MREE		HREE		HREE		MREE		HREE	
Nr.	7		3		10		8		19	
SiO_2	32.5	0.9	31.7	0.4	31.8	2.0	31.6	1.6	33.6	3.5
TiO_2	0.78	0.21	0.58	0.28	0.20	0.08	0.10	0.04	0.10	0.05
Al_2O_3	0.09	0.12	d.l.		0.10	0.07	0.12	0.05	0.07	0.06
FeO	1.03	0.52	0.91	0.51	3.63	5.63	2.70	3.45	3.95	8.85
MnO	0.73	0.10	0.61	0.09	0.45	0.06	0.51	0.06	0.55	0.10
CaO	6.50	1.45	6.95	1.64	8.37	2.75	8.62	3.00	9.42	4.02
Na_2O	0.62	0.20	0.48	0.14	0.44	0.18	0.47	0.19	0.51	0.31
F	0.27	0.09	0.19	0.07	0.22	0.09	0.35	0.05	0.29	0.16
Y_2O_3	17.0	2.0	20.8	3.3	20.9	4.0	14.0	1.7	23.4	5.1
La_2O_3	0.61	0.37	0.99	0.20	0.48	0.21	0.46	0.19	0.35	0.25
Ce_2O_3	3.05	1.44	4.73	2.62	2.91	1.11	2.94	0.65	1.08	0.42
Pr_2O_3	0.92	0.34	0.83	0.42	0.60	0.19	0.81	0.14	0.20	0.11
Nd_2O_3	6.72	1.63	4.37	1.41	3.17	0.68	4.51	0.64	0.96	0.43
Sm_2O_3	3.29	0.56	1.41	0.42	1.31	0.32	2.83	0.34	0.33	0.24
Eu_2O_3	d.l.		d.l.		d.l.		d.l.		d.l.	
Gd_2O_3	5.54	0.60	3.82	0.76	3.50	0.51	6.43	0.97	2.55	0.50
Dy_2O_3	3.72	0.43	3.79	1.32	3.33	0.45	4.87	1.61	2.78	0.68
Er_2O_3	1.23	0.18	2.07	0.26	1.25	0.14	1.21	0.40	1.65	0.25
Yb_2O_3	0.20	0.11	0.65	0.21	0.70	0.18	0.29	0.06	1.20	0.12
Total	84.8		84.9		83.4		82.7		83.0	
^{1}Si (apfu)	2.000		2.000		2.000		2.000		2.000	
$^1\Sigma$ REE	1.091		1.191		1.071		0.996		0.960	
^{1}Ca	0.428		0.471		0.564		0.584		0.600	

Gysi, A.P., Williams-Jones, A.E., Collins, P., 2016b. Lithogeochemical Vectors for Hydrothermal Processes in the Strange Lake Peralkaline Granitic REE-Zr-Nb Deposit. Econ Geol 111, 1241-1276.
DOI:10.2113/econgeo.111.5.1241.

TABLE 4. Average EMP analyses (in wt. %) of Ca- and Na-zirconosilicates from Strange Lake granites and pegmatites (Peg).

	SL11-55	**2σ**	**SL11-59**	**2σ**	**SL11-62**	**2σ**	**SL11-98**	**2σ**	**SL11-104**	**2σ**	**SL11-106**	**2σ**	**SL11-195**	**2σ**	**SL11-17**	**2σ**	**SL11-80**	**2σ**
Rock	Granite		Granite		Granite		Granite		Peg		Peg		Peg		Peg		Granite	
Mineral	Git		Git		Git		Git		Git		Git		Git		Arm		Vla	
Nr.	3		2		2		8		17		6		5		3		29	
SiO_2	40.9	0.7	37.2	2.0	38.9	0.4	38.1	1.9	38.8	3.1	39.1	4.3	40.2	1.6	60.0	7.4	55.3	0.5
TiO_2	d.l.		d.l.		d.l.		0.05	0.02	0.03	0.03	0.09	0.15	0.08	0.10	0.12	0.07	d.l.	
Al_2O_3	d.l.	d.l.	d.l.	d.l.	0.16	-	0.10	0.11	0.08	0.04	0.19	0.29	0.16	0.27	0.70	0.20	d.l.	
FeO	0.12	0.21	3.99	4.05	0.80	0.16	0.26	0.60	0.20	0.15	0.24	0.23	0.49	0.52	0.16	0.03	0.03	0.06
MnO	0.16	0.09	0.30	0.05			0.87	0.20	0.78	0.15	1.04	0.19	0.35	0.29	0.06	0.01	d.l.	
CaO	19.0	0.3	17.6	1.0	18.4	0.1	16.3	1.6	17.2	1.4	17.0	1.7	18.3	0.3	7.26	1.95	d.l.	
Na_2O	d.l.		d.l.		d.l.		d.l.		d.l.		d.l.		d.l.		d.l.		13.6	2.1
K_2O	d.l.		d.l.		d.l.		d.l.		d.l.		d.l.		d.l.		d.l.		0.11	0.18
P_2O_5	d.l.		d.l.		d.l.		0.04	-	d.l.		0.06	-	d.l.		0.05	-	d.l.	
F	d.l.		d.l.		d.l.		0.15	0.09	0.12	0.06	0.06	0.11	0.11	0.04	4.94	0.94	0.16	0.11
HfO_2	1.06	0.20	0.99	0.11	1.23	0.51	1.21	0.29	0.88	0.14	0.90	0.17	1.22	0.22	0.44	0.07	0.69	0.24
ZrO_2	39.8	0.5	37.4	0.8	38.0	1.5	37.0	0.8	36.3	3.6	35.6	4.3	37.8	1.6	19.0	2.9	27.7	1.0
Nb_2O_5	0.11		0.11				0.24	0.26	0.14	0.07	0.46	1.38	0.17	0.13	0.89	0.36	d.l.	
Y_2O_3	d.l.		0.13	0.01	0.13	-	0.72	1.09	0.11	0.05	0.23	0.21	0.14	-	1.42	0.70	d.l.	
La_2O_3	d.l.		d.l.		d.l.		d.l.		0.07	0.02	0.06	-	d.l.		d.l.		d.l.	
Ce_2O_3	d.l.		d.l.		d.l.		0.14	0.23	0.06	0.04	0.19	0.17	d.l.		0.15	0.06	d.l.	
Nd_2O_3	d.l.		d.l.		d.l.		d.l.		d.l.		0.05	0.06	d.l.		0.13	0.04	d.l.	
Sm_2O_3	d.l.		d.l.		d.l.		d.l.		d.l.		d.l.		d.l.		0.08	0.02	d.l.	
Eu_2O_3	d.l.		d.l.		d.l.		0.06	-	0.07	0.02	0.09	0.03	d.l.		d.l.		d.l.	
Gd_2O_3	d.l.		d.l.		d.l.		d.l.		d.l.		d.l.		d.l.		0.17	0.11	d.l.	
Dy_2O_3	d.l.		d.l.		d.l.		0.13	0.15	d.l.		d.l.		d.l.		0.36	0.11	d.l.	
Er_2O_3	d.l.		d.l.		d.l.		0.16	0.16	0.05	-	0.05	0.00	d.l.		0.22	0.09	d.l.	
Yb_2O_3	d.l.		0.18	0.08	d.l.		0.31	0.27	0.19	0.03	0.20	0.06	d.l.		0.25	0.08	d.l.	
Lu_2O_3	d.l.		0.07		d.l.		0.07	0.03	0.06	0.02	0.06	0.01	d.l.		d.l.		d.l.	
Total	101.2		97.9		97.6		95.9		95.1		95.7		99.1		96.4		97.5	

The uncertainties (2σ) represent the standard deviation of average mineral analyses with Nr. representing the number of analyzed mineral spots per thin section; (d.l.) below detection limit. The concentrations of Pr not reported here were all below detection limit.

Gysi, A.P., Williams-Jones, A.E., Collins, P., 2016b. Lithogeochemical Vectors for Hydrothermal Processes in the Strange Lake
Peralkaline Granitic REE-Zr-Nb Deposit. Econ Geol 111, 1241-1276.
DOI:10.2113/econgeo.111.5.1241.

TABLE 5. Average EMP analyses (in wt. %) of zircon from Strange Lake granites and pegmatites (Peg). Groups correspond to Zircon I-III and zircons with intermediate (Inter.) chondrite-normalized REE profiles.

	SL11-119	**2σ**	**SL11-55**	**2σ**	**SL11-59**	**2σ**	**SL11-62**	**2σ**	**SL11-62**	**2σ**	**SL11-60**	**2σ**	**SL11-60**	**2σ**	**SL11-30**	**2σ**
Rock	Granite		Granite		Granite		Granite		Granite		Granite		Granite		Granite	
Mineral	Zrn		Zrn		Zrn		Zrn-core		Zrn-rim		Zrn-core		Zrn-rim		Zrn	
Group	I		III		Inter.		III		III		III		III		I	
Nr	12		3		5		7		3		8		3		15	
SiO_2	29.1	0.9	32.8	0.3	29.6	0.7	32.0	1.0	31.8	0.7	30.8	3.2	31.8	0.7	31.4	1.7
TiO_2	0.05	0.04	0.13	0.01	0.07	0.01	d.l.		d.l.		d.l.		d.l.		0.09	0.02
Al_2O_3	0.09	0.08	0.54	0.09	0.58	0.12	0.73	0.42	0.65	0.21	0.71	0.17	0.45	0.65	0.07	0.02
FeO	0.80	0.59	0.67	0.14	0.87	0.09	1.12	0.86	0.63	0.50	0.48	0.15	0.44	0.72	0.38	0.31
MnO	0.37	0.19	0.07	0.01	0.14	0.02	d.l.		d.l.		d.l.		d.l.		0.09	0.04
CaO	2.03	0.76	0.73	0.14	1.42	0.49	0.81	0.41	1.33	0.63	0.72	0.38	0.62	0.44	0.14	0.14
Na_2O	0.29	0.08	d.l.		0.30	0.13	0.13	0.08	0.09	0.05	0.10	0.03	d.l.		0.17	0.21
P_2O_5	0.39	0.16	0.07	-	d.l.		d.l.		d.l.		d.l.		d.l.		d.l.	
F	0.28	0.13	0.15	0.05	0.18	0.05	0.19	0.10	0.17	0.06	0.14	0.08	0.13	0.05	0.32	0.30
HfO_2	1.09	0.29	1.62	0.18	1.36	0.23	1.58	0.24	1.32	0.29	1.51	0.17	1.47	0.11	1.70	0.77
ZrO_2	51.7	1.7	55.8	1.5	49.5	3.1	54.4	2.0	54.1	3.9	54.3	7.4	56.2	2.3	64.9	1.7
Nb_2O_5	0.33	0.15	0.54	0.13	0.66	0.28	0.31	0.09	0.29	0.18	0.31	0.20	0.27	0.29	0.13	0.03
Y_2O_3	3.74	1.08	3.41	0.31	4.87	1.08	3.41	0.70	3.43	1.39	2.72	0.79	3.57	1.15	0.22	0.15
La_2O_3	d.l.		0.11		0.13	0.06	0.13	0.06	0.18	0.20	0.13	0.04	0.24	0.20	d.l.	
Ce_2O_3	0.10	0.08	0.56	0.05	0.71	0.09	0.66	0.23	0.83	0.56	0.50	0.13	1.05	0.90	0.07	0.02
Pr_2O_3	d.l.		d.l.		0.06	0.01	0.11		0.12		0.10		0.15	0.09	d.l.	
Nd_2O_3	0.09	0.03	0.33	0.02	0.39	0.11	0.25	0.09	0.47	0.33	0.25	0.08	0.60	0.39	d.l.	
Sm_2O_3	0.07	0.02	0.08	0.03	0.12	0.07	d.l.		0.12	0.02	0.10	0.03	0.12	-	d.l.	
Eu_2O_3	d.l.		d.l.		0.12		d.l.		d.l.		d.l.		d.l.		d.l.	
Gd_2O_3	0.17	0.09	0.24	0.07	0.48	0.12	0.30	0.08	0.38	0.25	0.28	0.07	0.29	0.03	d.l.	
Dy_2O_3	0.54	0.16	0.23	0.07	0.43	0.07	0.34	0.11	0.40	0.19	0.25	0.12	0.30	0.15	d.l.	
Er_2O_3	0.56	0.05	0.21	0.04	0.50	0.10	0.29	0.06	0.25	0.14	0.14	0.06	0.17	0.05	d.l.	
Yb_2O_3	1.05	0.22	0.17	0.06	1.25	0.36	0.22	0.09	0.17	0.09	d.l.		d.l.		d.l.	
Lu_2O_3	0.14	0.05	d.l.		0.21	0.05	d.l.		d.l.		d.l.		d.l.		d.l.	
Total	92.9		98.5		93.9		97.0		96.8		93.6		97.9		99.7	

The uncertainties (2σ) represent the standard deviation of average mineral analyses with Nr. representing the number of analyzed mineral spots per thin section; (d.l.) below detection limit. The concentrations of K not reported here were all below detection limit.

Gysi, A.P., Williams-Jones, A.E., Collins, P., 2016b. Lithogeochemical Vectors for Hydrothermal Processes in the Strange Lake Peralkaline Granitic REE-Zr-Nb Deposit. Econ Geol 111, 1241-1276.
DOI:10.2113/econgeo.111.5.1241.

TABLE 5. (Continued)

	SL11-42	**2σ**	**SL11-42**	**2σ**	**SL11-42**	**2σ**	**SL11-9**	**2σ**	**SL11-9**	**2σ**	**SL11-7**	**2σ**	**SL11-7**	**2σ**	**SL11-4**	**2σ**	**SL11-6**	**2σ**
Rock	Peg		Peg		Peg		Peg		Peg		Peg		Peg		Peg		Peg	
Mineral	Zrn		Zrn-core		Zrn-rim		Zrn		Zrn		Zrn		Zrn		Zrn		Zrn	
Group	I		II		II		I		II		II		I		Inter.		I	
Nr	7		5		7		4		4		3		2		5		3	
SiO_2	28.7	3.1	31.2	0.7	31.4	2.3	29.9	1.2	31.0	0.3	30.8	0.1	30.0	0.5	32.9	0.6	31.8	0.2
TiO_2	0.06	0.04	0.07	0.01	0.07	0.02	0.10	0.07	0.24	0.04	0.18	0.06	0.07	0.01	0.16	0.03	0.09	0.00
Al_2O_3	0.30	0.28	0.59	0.11	0.55	0.19	0.53	0.26	0.82	0.18	0.27	0.15	0.10	0.02	0.60	0.12	0.12	0.04
FeO	0.13	0.06	0.25	0.09	0.23	0.11	0.34	0.33	0.55	0.32	0.87	0.86	1.42	2.34	0.51	0.08	0.25	0.14
MnO	0.06	0.07	0.13	0.06	0.11	0.07	0.10	0.09	0.27	0.11	0.11	0.02	0.09	0.05	0.51	0.27	0.10	0.06
CaO	0.21	0.22	0.06	0.03	0.03	0.02	0.04	0.02	0.08	0.04	0.03	-	d.l.		0.10	0.08	0.04	0.01
Na_2O	0.24	0.10	0.44	0.07	0.42	0.14	0.39	0.08	0.28	0.16	0.32	0.12	0.32	0.08	0.32	0.33	0.31	0.04
P_2O_5	0.67	0.80	0.13	0.11	0.15	0.13	d.l.		d.l.		d.l.		d.l.		0.09	0.05	0.56	0.12
F	1.74	1.37	0.91	0.27	0.95	0.27	0.78	0.21	0.47	0.24	0.49	0.15	0.58	0.04	0.49	0.15	0.57	0.17
HfO_2	1.40	0.46	1.50	0.08	1.42	0.25	1.23	0.21	1.37	0.56	1.57	0.58	1.29	0.22	1.58	0.12	1.40	0.46
ZrO_2	53.7	3.6	57.7	1.3	56.4	1.3	53.5	4.1	58.0	0.6	57.7	1.6	55.9	2.3	59.7	1.9	56.8	0.6
Nb_2O_5	0.40	0.24	0.58	0.15	0.51	0.16	0.46	0.21	0.53	0.26	0.13	-	0.12	0.04	0.11	0.02	0.11	0.06
Y_2O_3	3.98	1.76	2.79	1.15	3.52	1.91	4.44	1.36	1.33	0.23	2.83	0.69	4.02	0.19	0.96	0.41	3.97	0.98
La_2O_3	d.l.		d.l.		0.07		d.l.		0.12	0.03	0.09	-	d.l.		d.l.		d.l.	
Ce_2O_3	0.10	0.09	0.39	0.24	0.28	0.28	0.08	0.03	0.38	0.09	0.17	0.13	0.09	0.05	0.06	0.03	0.10	0.06
Pr_2O_3	d.l.		0.13	0.06	0.11	0.05	d.l.		0.09	0.07			d.l.		d.l.		d.l.	
Nd_2O_3	0.15	0.07	0.69	0.14	0.56	0.34	0.15	0.09	0.31	0.12	0.22	0.07	0.13	-	d.l.		0.08	0.01
Sm_2O_3	0.09	0.10	0.23	0.08	0.24	0.09	0.13	0.06	0.12	-	0.11	0.03	d.l.		d.l.		0.07	
Eu_2O_3	d.l.		d.l.		d.l.		d.l.		d.l.		d.l.		d.l.		d.l.		d.l.	
Gd_2O_3	0.33	0.20	0.15	0.09	0.23	0.17	0.84	0.34	0.12	0.02	0.29	0.19	0.41	0.07	0.14	0.04	0.36	0.09
Dy_2O_3	0.85	0.29	0.15	0.07	0.27	0.31	0.96	0.52	0.13	0.04	0.22	0.13	0.50	0.02	0.13	0.04	0.54	0.05
Er_2O_3	0.74	0.30	0.11	0.09	0.19	0.24	0.71	0.36	0.13	0.08	0.24	0.05	0.59	0.14	0.15	0.11	0.57	0.16
Yb_2O_3	2.28	1.50	0.24	0.09	0.41	0.44	1.31	0.73	0.37	0.15	0.72	0.09	1.24	0.03	0.35	0.13	1.24	0.41
Lu_2O_3	0.33	0.24	0.05	0.03	0.07	0.05	0.18	0.10	0.09	0.02	0.12	0.03	0.19	0.06	0.06	0.01	0.16	0.07
Total	96.5		98.6		98.2		96.1		96.8		97.4		97.1		98.8		99.3	

Gysi, A.P., Williams-Jones, A.E., Collins, P., 2016b. Lithogeochemical Vectors for Hydrothermal Processes in the Strange Lake Peralkaline Granitic REE-Zr-Nb Deposit. Econ Geol 111, 1241-1276.
DOI:10.2113/econgeo.111.5.1241.

TABLE 6. Average EMP analyses (in wt. %) of titanite from Strange Lake granites and pegmatites (Peg).

	SL11-155	**2σ**	**SL11-151**	**2σ**	**SL11-106**	**2σ**	**SL11-100**	**2σ**	**SL11-104**	**2σ**	**SL11-131**	**2σ**	**SL12-47**	**2σ**
Rock	Granite		Granite		Peg		Peg		Peg		Peg		Vein	
Mineral	Titanite		Titanite		Titanite		Titanite		Titanite		Titanite		Titanite	
Nr.	10		10		6		18		3		4		18	
SiO_2	30.1	0.8	30.5	0.4	30.4	0.6	29.8	0.9	30.2	0.4	31.9	2.1	30.3	0.6
TiO_2	32.7	3.1	31.5	2.6	30.4	0.8	30.4	1.7	29.6	0.1	27.9	1.1	35.2	1.2
Al_2O_3	0.72	0.29	d.l.		1.12	0.30	0.91	0.37	1.05	0.17	0.19	0.11	d.l.	
FeO	3.48	1.30	3.76	1.85	4.40	0.99	5.43	1.16	6.08	0.51	5.77	0.95	2.33	1.05
MnO	0.05	0.01	0.13	0.32	0.06	0.05	0.10	0.08	0.11	0.09	0.15	0.03	d.l.	
CaO	27.21	0.9	27.5	1.8	26.6	1.3	26.1	1.0	26.5	0.8	24.4	1.0	27.2	1.0
Na_2O	0.21	0.15	0.16	0.12	0.31	0.33	0.17	0.08	0.14	0.14	0.44	0.17	0.29	0.19
K_2O	d.l.		d.l.		d.l.		0.08	0.02	d.l.		d.l.		d.l.	
F	0.60	0.26	0.66	0.34	0.64	0.23	0.71	0.33	0.56	0.05	0.56	0.07	0.40	0.25
Y_2O_3	0.12	0.07	0.40	0.24	0.52	0.22	d.l.		0.62	0.01	0.38	0.08	0.19	0.14
La_2O_3	d.l.		0.17	0.24	0.07		d.l.		d.l.		d.l.		d.l.	
Ce_2O_3	0.19	0.14	0.27	0.28	0.19	0.09	d.l.		0.61	0.16	d.l.		0.16	-
Pr_2O_3	0.07	0.01	0.15	0.19	d.l.		d.l.		0.07	0.03	d.l.		d.l.	
Nd_2O_3	0.13	0.05	0.28	0.28	d.l.		d.l.		0.28	0.10	d.l.		0.10	-
Sm_2O_3	d.l.		d.l.		d.l.		d.l.		0.05	-	d.l.		d.l.	
Eu_2O_3	d.l.		0.17	0.22	d.l.		d.l.		d.l.		d.l.		d.l.	
Gd_2O_3	d.l.		0.08	0.05	d.l.		d.l.		0.08	0.05	d.l.		0.11	-
Dy_2O_3	d.l.		d.l.		d.l.		d.l.		0.06	-	d.l.		d.l.	
Er_2O_3	d.l.		d.l.		d.l.		d.l.		0.07	-	0.09		d.l.	
Yb_2O_3	d.l.		0.07	0.02	0.14	0.09	d.l.		0.17	0.03	0.11	0.08	d.l.	
Total	95.41		94.64		94.77		95.60		96.13		91.81		95.98	

The uncertainties (2σ) represent the standard deviation of average mineral analyses with Nr. representing the number of analyzed mineral spots per thin section; (d.l.) below detection limit. The concentrations of Lu not reported here were all below detection limit.

Gysi, A.P., Williams-Jones, A.E., Collins, P., 2016b. Lithogeochemical Vectors for Hydrothermal Processes in the Strange Lake Peralkaline Granitic REE-Zr-Nb Deposit. Econ Geol 111, 1241-1276.
DOI:10.2113/econgeo.111.5.1241.

TABLE 7. Average EMP analyses (in wt. %) of pyrochlore-(Nb) from Strange Lake granites and pegmatites (Peg).

	SL11-80	**2σ**	**SL11-179**	**2σ**	**SL11-158**	**2σ**	**SL11-9**	**2σ**	**SL11-40**	**2σ**
Rock	Granite		Granite		Granite		Peg		Peg	
Nr.	14		10		10		15		3	
SiO_2	1.19	2.20	0.69	0.72	0.28	0.39	1.15	0.40	1.31	0.13
TiO_2	4.69	2.36	4.51	1.64	2.70	2.07	4.57	0.65	5.47	0.31
FeO	0.35	0.37	0.56	0.40	0.28		d.l.		d.l.	
MnO	0.11	0.15	d.l.		0.06	-	0.05	-	d.l.	
CaO	2.57	1.26	4.56	1.32	3.41	1.36	4.46	0.40	4.98	0.09
Na_2O	6.22	3.90	8.76	3.03	5.90	3.72	8.68	2.41	8.65	0.21
F	4.14	3.01	5.63	1.09	5.15	1.51	5.26	0.90	6.17	0.66
ZrO_2	0.40	0.08	0.27	0.19	0.18		0.33	0.14	0.36	0.07
Nb_2O_5	56.5	5.2	57.6	5.4	61.7	4.4	56.2	1.4	55.3	0.7
Ta_2O_5	2.26	1.91	2.49	1.83	1.94	0.98	3.51	0.35	3.45	0.24
ThO_2	0.20	0.17	d.l.		d.l.		d.l.		d.l.	
UO_2	0.98	1.13	0.20	0.14	0.46	0.49	0.15	0.04	0.13	0.03
Y_2O_3	0.29	0.20	0.17	0.05	0.15	0.07	0.17	0.06	0.18	0.07
La_2O_3	4.39	0.46	4.64	0.62	5.61	1.47	4.24	0.24	4.25	0.18
Ce_2O_3	10.82	0.69	10.75	0.52	11.19	0.59	10.51	0.30	10.32	0.10
Pr_2O_3	1.01	0.15	0.97	0.08	0.90	0.33	0.99	0.10	0.98	0.09
Nd_2O_3	2.33	0.31	2.47	0.15	2.18	1.03	2.47	0.17	2.28	0.06
Sm_2O_3	0.23	0.15	0.19	0.04	0.18	0.07	0.22	0.05	0.20	0.03
Gd_2O_3	0.18	0.12	d.l.		d.l.		0.14	0.02	0.13	
Dy_2O_3	0.24	0.10	d.l.		d.l.		d.l.		d.l.	
Total	99.1		104.4		102.3		103.1		104.2	
O=F	1.7		2.4		2.2		2.2		2.6	
Total	97.4		101.5		100.1		100.9		101.6	

The uncertainties (2σ) represent the standard deviation of average mineral analyses with Nr. representing the number of analyzed mineral spots per thin section; (d.l.) below detection limit. The concentrations of Lu, Yb, Er, Eu, Al and K not reported here were all below detection limit.

Gysi, A.P., Williams-Jones, A.E., Collins, P., 2016b. Lithogeochemical Vectors for Hydrothermal Processes in the Strange Lake Peralkaline Granitic REE-Zr-Nb Deposit. Econ Geol 111, 1241-1276.
DOI:10.2113/econgeo.111.5.1241.

TABLE 8. Link between alteration types and bulk rock chemistry with key lithogeochemical vectors for alteration types related to ore mineralization.

Alteration type	Bulk rock ratios	Controlling reactions
High T acidic alteration (IIIa)		
Aegirinization/hematization		
Arf to Aeg+Hem+Qtz	Fe_2O_3/Na_2O	$Na_3Fe^{2+}{}_4Fe^{3+}Si_8O_{22}(OH)_2 + 2H^+ = NaFe^{3+}Si_2O_6 + 2Fe^{3+}{}_2O_3 + 6SiO_2 + 2Na^+ + 2H_{2(g)}$
Ca-metasomatism (pseudomorphs)		
Elp to Git+Qtz	CaO/Na_2O	$Na_2ZrSi_6O_{15} \bullet 3H_2O + Ca^{2+} = CaZrSi_2O_7 + 4SiO_2 + 2Na^+ + 3H_2O$
Low T acidic alteration (IIIb)		
Ca-F-metasomatism		
Kfs to Git+Qtz	CaO/K_2O, CaO/Al_2O_3	$KAlSi_3O_8 + ZrF_2(OH)_2 + Ca^{2+} = CaZrSi_2O_7 + SiO_2 + K^+ + AlF_2^+ + H_2O$
Aeg to Zrn+Fl+Qtz	CaO/Na_2O	$2NaFe^{3+}Si_2O_6 + ZrF_2(OH)_2 + Ca^{2+} = ZrSiO_4 + Fe^{3+}{}_2O_3 + 3SiO_2 + CaF_2 + 2Na^+ + H_2O$

Gysi, A.P., Williams-Jones, A.E., Collins, P., 2016b. Lithogeochemical Vectors for Hydrothermal Processes in the Strange Lake Peralkaline Granitic REE-Zr-Nb Deposit. Econ Geol 111, 1241-1276.
DOI:10.2113/econgeo.111.5.1241.

APPENDIX

TABLE A1. Electron microprobe standards, count times and detection limits used in this study.

Element	Standard	Crystal	Background (sec)	Counting time (sec)	Detection limit (wt. % oxides)
Si	Diopside	TAP	10	20	0.02
Ti	TiO_2	PETJ	10	20	0.02
Al	Orthoclase	TAP	10	20	0.02
Fe	Fe_2O_3	LIF	10	20	0.02
Mn	Spessartine	LIF	10	20	0.02
Ca	Diopside	PETJ	10	20	0.02
Na	Albite	TAP	10	20	0.09
K	Orthoclase	PETJ	10	20	0.04
P	Apatite	PETJ	10	20	0.03
F	CaF_2	TAP	10-50	20-100	0.08
Zr	Zircon	PETJ	10	20	0.02
Hf	Zircon	LIF	10	20	0.04
Nb	$Na_2Nb_2O_6$	LIF	10	20	0.04
Ta	$K_2Ta_2O_6$	LIF	50	100	0.20
Th	ThO_2	PETJ	50	100	0.03
U	UO_2	PETJ	50	100	0.05
Y	MAC-Y	PETJ	10	20	0.07
La	MAC-La	LIFH	30	60	0.05
Ce	MAC-Ce	LIFH	30	60	0.03
Pr	MAC-Pr	LIFH	30	60	0.06
Nd	MAC-Nd	LIF	50	100	0.06
Sm	MAC-Sm	LIFH	40	80	0.05
Eu	MAC-Eu	LIFH	50	100	0.04
Gd	MAC-Gd	LIFH	25-30	50-60	0.06
Dy	MAC-Dy	LIFH	30	60	0.06
Er	MAC-Er	LIF	40	80	0.04
Yb	MAC-Yb	LIFH	25-30	50-60	0.03
Lu	MAC-Lu	LIF	50	100	0.04

Gysi, A.P., Williams-Jones, A.E., Collins, P., 2016b. Lithogeochemical Vectors for Hydrothermal Processes in the Strange Lake Peralkaline Granitic REE-Zr-Nb Deposit. Econ Geol 111, 1241-1276.
DOI:10.2113/econgeo.111.5.1241.

Supplementary Online materials

Click here to access/download

Electronic Appendix (Excel etc.)

Supplementary Material.xlsx

Gysi, A.P., Williams-Jones, A.E., Collins, P., 2016b. Lithogeochemical Vectors for Hydrothermal Processes in the Strange Lake Peralkaline Granitic REE-Zr-Nb Deposit. Econ Geol 111, 1241-1276.
DOI:10.2113/econgeo.111.5.1241.